REPORT NO. FRA-OR&D
FRA/ORD-78/19

AN INVESTIGATION OF TECHNIQUES FOR VALIDATION OF RAILCAR DYNAMIC ANALYSES

W.J. FALLON, N.K. COOPERRIDER, E.H. LAW

MARCH 1978

INTERIM REPORT

Document is available to the public through the National Technical Information Service; Springfield, Virginia, 22161

Prepared for:
U.S. DEPARTMENT OF TRANSPORTATION
Federal Railroad Administration
Office of Research and Development
Washington, D.C. 20590

NOTICE

This document is disseminated under the sponsorship of the U.S. Department of Transportation in the interest of information exchange. The United States Government assumes no liability for the contents or use thereof.

NOTICE

The United States Government does not endorse products or manufactures. Trade or manufacturer's names appear herein solely because they are considered essential to the object of this report.

1. Report No. DOT-FRA ORD & D - 78/19	2. Government Accession No.
	3. Recipient's Catalog No.
4. Title and Subtitle AN INVESTIGATION OF TECHNIQUES FOR VALIDATION OF RAILCAR DYNAMIC ANALYSES	5. Report Date March 1978
	6. Performing Organization Code
7. Authors W. J. Fallon, Jr., N. K. Cooperrider and E. H. Law	8. Performing Organization Report No.
9. Performing Organization Name and Address Arizona State University, Dept. of Mech. Engrg., Tempe, Arizona 85281 Clemson University, Dept. of Mech. Engrg., Clemson, S.C. 29631	10. Work Unit No. (TRAIS)
	11. Contract or Grant No. DOT-OS-40018
12. Sponsoring Agency Name and Address U.S. Department of Transportation Federal Railroad Administration Washington, D.C.	13. Type of Report and Period Covered Interim
	14. Sponsoring Agency Code FRA-RRD-11

15. Supplementary Notes
Prepared in cooperation with Association of American Railroads Research Center, Chicago, Illinois

16. Abstract

A linear model of the vertical dynamics of a railcar was validated by the application of spectral techniques to experimental data. Track input spectra were computed from test track surface measurements gathered in the TTOP test program. Acceleration measurements of a freight car were used to compute vehicle acceleration spectra in response to the test track. The corresponding response of the linear model was computed from the analytical transfer functions and experimental track input spectra. Validation of the linear model was based upon a comparison of corresponding analytical and experimental vehicle acceleration spectra.

The truck suspension was isolated and analyzed from experimental measurements of corresponding truck and car body accelerations. Spectral functions were employed to evaluate the assumptions of suspension linearity.

17. Key Words rail vehicle dynamics, validation techniques, spectral analysis	18. Distribution Statement Document is available to the public through the National Technical Information Service, Springfield, VA 22151

19. Security Classification (of this report) UNCLASSIFIED	20. Security Classif. (of this page) UNCLASSIFIED	21. No. of Pages 105	22. Price A06 A01

SUMMARY

This report describes one aspect of the rail freight car dynamic analysis validation effort carried out at Clemson and Arizona State Universities. This Freight Car Dynamics research project, sponsored by the Federal Railroad Administration and conducted in cooperation with the Association of American Railroads, has the overall objective of developing realistic and efficient mathematical models and associated solution techniques for freight car lateral dynamic behavior. The specific objective of the effort reported here was to investigate the feasibility of using spectral analysis techniques to validate these dynamic analyses.

Spectral analysis techniques are described in this report. The power spectral density, (PSD), cross spectral density, coherence, and transfer functions are explained. Special considerations for spectral analysis of experimental data, such as sampling, prewhitening, and leakage are discussed. The fast Fourier transform (FFT) and its use in spectral analysis are explained. Computer programs to implement these techniques are given.

The spectral analysis techniques are used to analyze the vertical dynamic behavior of a rail freight car. The experimental data used for this work was obtained from the tests conducted by the Southern Pacific Railroad in the TDOP project sponsored by the Federal Railraod Administration.

A linear theoretical analysis of the vertical dynamics of the rail freight car is presented. Results of the analysis corresponding to the TDOP experimental results are presented.

The validation presented in the report entailed comparison of the theoretical and experimental PSD's. Remarkably good agreement was found between the two.

This effort demonstrated that spectral techniques are effective for the analysis of railroad track irregularities and railroad vehicle response. Validation of theoretical analysis by comparison of PSD's was shown to be feasible.

TABLE OF CONTENTS

LIST OF TABLES

LIST OF FIGURES

LIST OF SYMBOLS

A	matrix of s coefficients for linear model
b	vector of s coefficients for track input
B	matrix of s coefficients for linear model
c	linear damping coefficient (Ch. 5)
c	vector of constant coefficients for track input
C_{FS}, C_{RS}	truck suspension damping, front and rear
C_{FT_1}, C_{RT_1}	rail damping, front wheelset, front and rear trucks
C_{FT_2}, C_{RT_2}	rail damping, rear wheelset, front and rear trucks
C	matrix of constant coefficients for linear model
C_{eq}	equivalent linear damping
d	data window correction factor
D	dry friction
DFT[x]	discrete Fourier transform of x
E[x]	expected value of x
f	frequency
f(t)	general time function (Ch. 6)
f_o	frequency of truck suspension oscillation
f_o	fundamental frequency (Ch. 4)
f_s	sampling frequency
$F_F(t)$,$F_R(t)$	force transmitted to car body, front and rear
$F_{R_d}(t)$	dynamic components of $F_R(t)$

$F_{R_d}(t)$	dynamic force transmitted through nonlinear model of rear suspension
g	gravitational constant
g	matrix of linear equation coefficients (Ch. 6)
g(t), G(s)	transfer function
h	vector of constant coefficients
H(f), H(λ)	transfer function
I	performance index
I_c	moment of inertia, car body
I_{FT}, I_{RT}	moment of inertia, front and rear trucks
IDFT[x]	inverse discrete Fourier transform of x
j	$\sqrt{-1}$
k	time index (Ch. 3)
k	linear spring rate
k_{FS}, k_{RS}	truck suspension spring rate, front and rear
k_{FT_1}, k_{RT_1}	rail spring rate, front wheelset, front and rear trucks
k_{FT_2}, k_{RT_2}	rail spring rate, rear wheelset, front and rear trucks
K	number of spectrum estimates to average
ℓ	general distance term
L	general displacement between inputs (Ch. 2)
L	chord length
L_c	car body length
L_F, L_R	car body c.g. to bolster displacement, front and rear
L_{FT_1}, L_{RT_1}	truck c.g. to front wheelset displacement, front and rear trucks

L_{FT_2}, L_{RT_2}	truck c.g. to rear wheelset displacement, front and rear trucks
L_T	truck wheelbase
M	mass
M_c	car body mass
M_{FT}, M_{RT}	truck mass, front and rear
n	frequency index
n	length of parameter vector (Ch. 6)
n, m	uncorrelated noise (Ch. 3)
N	number of data points
$P_x(f)$, $P_y(f)$	power spectral density function
$P_{xy}(f)$	cross spectral density function
$R_x(\tau)$	autocorrelation function
$R_{xy}(\tau)$	cross correlation function
s	Laplace operator
t	time
t_1, t_2	time integral limits
T, T_2,T_3,T_4	time delays
T	data record length (Ch. 3)
u,u_1,u_2,u_3,u_4	vertical track inputs
u,v	pure (noiseless) signals (Ch. 3)
u_F, u_R	car body input, front and rear
V	velocity
Var[x]	variance of x
w(t)	data window

$w_h(t)$	approximate Hanning window
$w_p(t)$	Parzen window
W	$e^{-j2\pi/N}$
$W(f)$	spectral window
x, $x(t)$	bounce
$x(t), y(t), f(t)$	time functions (Ch. 3)
$\hat{x}(t)$	truncated $x(t)$
$\underline{x}$	state vector
x_c	car body bounce
x_{FT}, x_{RT}	truck bounce, front and rear
X_o	amplitude of suspension oscillation
X_1, X_3	true reference deviation of chord endpoints
X_2	track - midchord deviation
$y(t)$	car body c.g. vertical displacement
$y_o(t)$	measured truck suspension displacement
y_F	vehicle front end response
α	parameter vector
$\gamma^2_{xy}(f)$	ordinary coherence function
Δf	frequency increment
Δt	sample time interval
$\varepsilon(t)$	equation error
ε^2_x	Var $[x]/E^2[x]$
$\theta, \dot{\theta}(t)$	angular displacement
θ_c	car body pitch

θ_{FT}, θ_{RT}	truck pitch, front and rear
λ	wavelength
μ_x	mean of x
σ_x	standard deviation of x
σ_x^2	variance of x
τ	correlation lag time
ω	radian frequency

Chapter 1

INTRODUCTION

Background

The lateral dynamics of rail vehicles has always been a source of concern for railroad operators and users. At present, the lateral dynamic behavior of rail freight cars causes major problems for North American railroads. Vehicle hunting, derailment, wheel and component wear, and lading damage are among the problems associated with freight car lateral dynamics.

The Freight Car Dynamics research project sponsored by the Federal Railroad Administration at Clemson and Arizona State Universities was initiated to develop tools and techniques to solve these freight car problems. The specific objective was to develop realistic and computationally efficient mathematical models and associated solution techniques for the freight car lateral dynamic behavior. It is envisioned that these mathematical models and solution techniques, in the form of digital computer programs, will be used to explore the causes of freight car dynamic problems, and to evaluate solutions for these problems.

Mathematical models of varying complexity have been developed to simulate both the freight vehicle behavior on tangent track, and the dynamics of the vehicle during curve entry and negotiation. A variety of solution techniques ranging from linear system methods to numerical and hybrid integration of nonlinear equations of motion are used to solve the vehicle equations of motion. In order to aid the user of these computer programs, an evaluation of the validity and efficiency

of each of the models and solution techniques is being developed in this project.

This assessment of the validity of the mathematical models entails the comparison of theoretical predictions of vehicle dynamic behavior with experimental results. The experimental data for this effort was provided by field tests conducted by the Association of American Railroads and the Union Pacific Railroad. A description of these tests may be found in Reference [1].

After validation, the models will be supplied to the railroad industry for use in evaluating supplemental devices for improving vehicle dynamics, in studying possible modifications of current freight vehicles, in exploring new design concepts, and in examining current vehicle and track maintenance procedures.

This report deals with one aspect of the validation study to assess the fidelity and applicability of the various rail vehicle lateral dynamic models.

Previous Work

Until recently, experimental and theoretical evaluation of rail car dynamics have gone down separate paths. This lack of interaction can be attributed to the fact that the experimental and analytical work has been done by different groups. Not surprisingly, those organizations, such as the British Rail and Japanese National Railway research groups, that first undertook theoretical rail vehicle dynamic analyses have also been the first to attempt to integrate theoretical and exper-

imental methods. This project has built on their background.

Theoretical model validation may be undertaken at many different levels. At the lowest level, a qualitative correlation is obtained between theoretically predicted trends and experimentally observed behavior. For example, almost all linear stability analyses of rail car lateral dynamics predict that vehicles whose wheelsets have high "effective" conicities will hunt at lower speeds than those with low "effective" conicity wheelsets. This trend agrees with observations of rail vehicle operation.

A great deal of qualitative validation has been done to strengthen confidence in the analytical tools. In stability analyses, the effects of changes in primary yaw and warp stiffness on critical hunting speeds have been qualitatively correlated. In curving analyses, the effects of yaw stiffness and wheelset conicity on lateral to vertical force ratios have also been qualitatively correlated.

The value of qualitatively validated analyses should not be underestimated. Such models are invaluable in making design changes and in devising successful experiments, because they provide information about the sensitivity of the vehicle behavior to parameter changes and also provide a framework for interpreting and understanding the test results.

A second level of validation entails correlation of a single, usually critical, value from the analysis with experimental results. For example, the analytical predictions for the critical speed when hunting begins or the resonant speed for rock and roll behavior would be compared with experimental measurements of the same variable.

Too much validation of this sort is done. This can be quite dangerous because it may lend false confidence to an analytical model. This is particularly true when those model parameters that cannot be measured are varied to obtain agreement between analysis and experiment. This second level of validation is generally of questionable value. It is far better to proceed directly to a full validation of the type described below.

The highest level of validation entails a fairly complete quantitative correlation of analytical and experimental results. A frequently used approach is the direct comparison of experimental and analytical time histories of variables such as acceleration, displacement or force level. Another possibility is the comparison of power spectral density curves. A third possibility for validating stability analyses involves comparing the variation of system damping ratios with speed. The work reported here was carried out to develop the tools and explore the feasibility of using the spectral analysis technique in validating our various mathematical models.

One of the most complete attempts to utilize spectral analysis techniques for validation of rail vehicle dynamic analyses was carried out by the British Railway Research Center for the ORE[2]. The effort reported here involved development of an equivalent capability for carrying out the spectral analysis, and application of the techniques to rail freight car dynamic analyses.

Objective

The specific objective of the effort reported here was to develop the computer programs to carry out the spectral analyses, and to explore the feasibility of using this approach to validate theoretical rail vehicle dynamic analyses. The vertical dynamics of a rail freight car were chosen for application of the spectral analysis techniques due to the availability of track, vehicle and vehicle dynamics data. In this exercise, the error between the theoretical dynamic response and the experimental dynamic response to the track input was minimized.

In addition to this primary objective, this research effort had two secondary objectives. The first was to report some of the results based on analysis of the experimental data. Researchers interested in the dynamics of the freight car should find many of these results to be of interest. The other objective was to investigate the influence of the nonlinear truck suspension on vehicle dynamics. One of the most important sources of nonlinearity in this suspension is dry (coulomb) friction between spring-loaded sliding components. The feasibility of modeling this nonlinearity with quasi-linear elements was studied.

Approach

The track, vehicle and vehicle dynamics data gathered by the Southern Pacific Railroad in the TDOP test program[3] were used for this exploration of model validation techniques. The modeling of the vertical dynamics of this rail freight car is described in the following chapter. Sufficient background to understand the spectral analysis techniques used in this study is provided in Chapter 3. The experimental

results pertinent to this work are described in Chapter 4 and the validation effort reported in Chapter 5. Our conclusions and recommendations for future work are provided in the final chapter.

Much of the work reported here was also published as a Master's Thesis of William J. Fallon at Arizona State University[4]. The computer programs that carry out the spectral analysis operations are described in a spearate document[5].

Chapter 2

SYSTEM MODELING

Introduction

As mentioned in Chapter 1, this study focused on the North American freight car. The specific car used to provide the experimental data used in this study* was a Southern Pacific Railroad mechanical refreigerator car similar to the box car pictured in Fig. 2-1. The body is a box type with a refrigeration unit mounted at one end. Both front and rear trucks are nominally identical and are basically configured as illustrated in Fig. 2-2. The car body rests on the centerplate of the bolster which, in turn, is supported at each end through coil springs mounted in the sideframes. The axles are mounted in roller bearings and the sideframes are seated on the bearing adapter housings allowing essentially no axle-sideframe relative vertical motion.

Linear Model

The system model was initially formulated as a linear lumped parameter model and the equations written under the following assumptions:

---

* The experimental test data used in this report was obtained in the "Truck Design Optimization Project" conducted by the Southern Pacific Railroad under sponsorship of the Federal Railroad Administration.

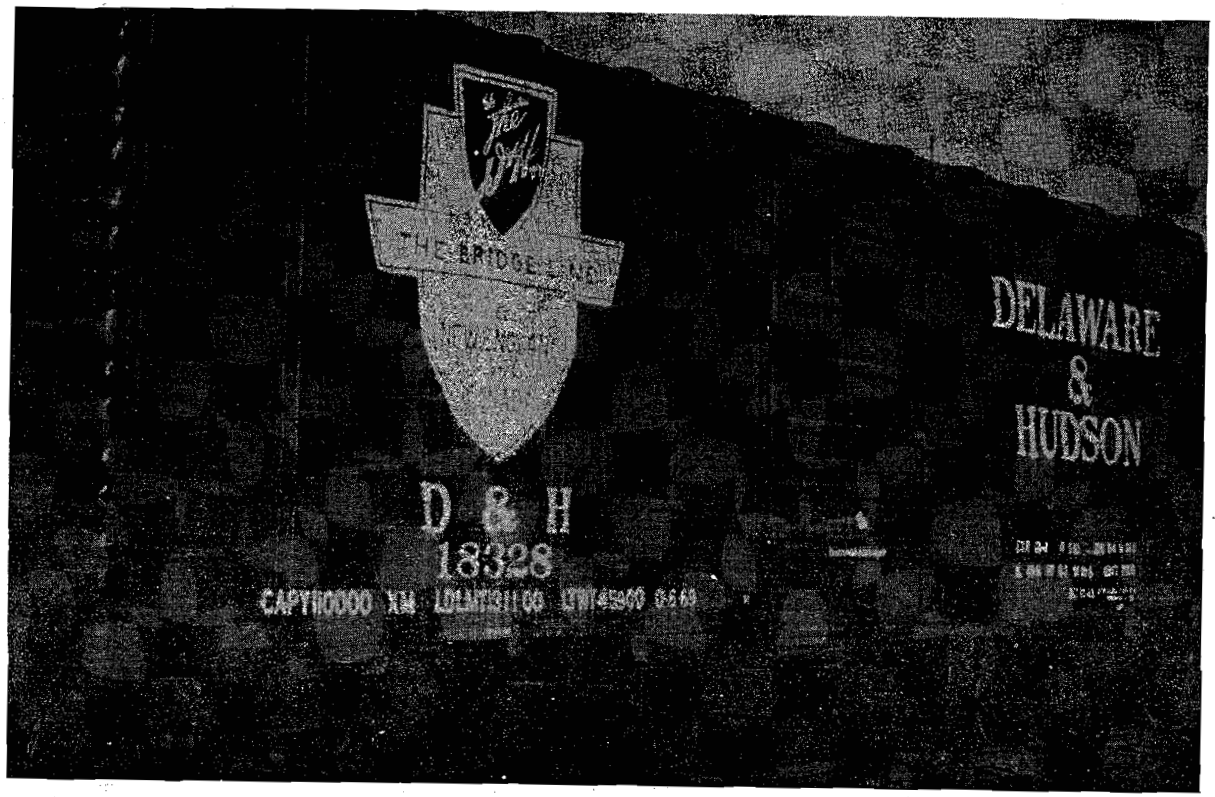

Figure 2-1 Typical Freight Car

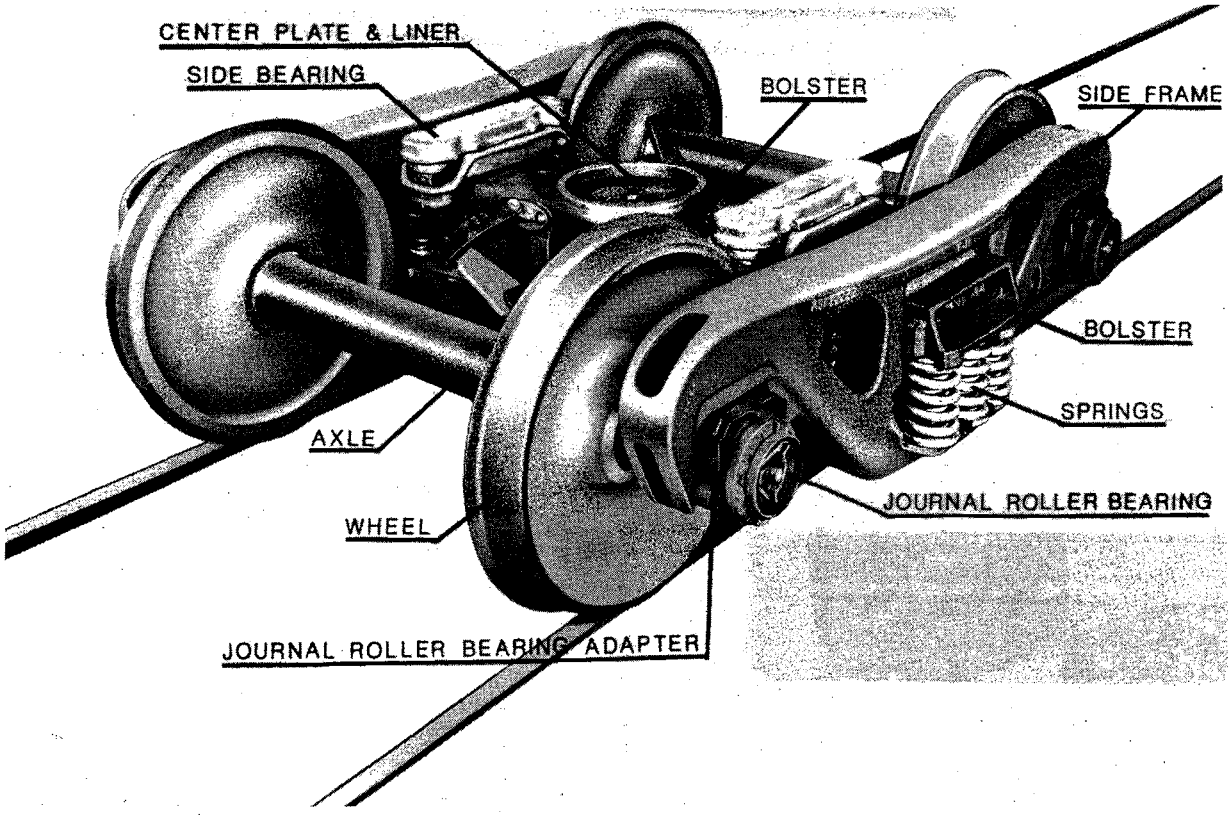

Figure 2-2 Typical Freight Car Truck

(1) rigid car body

(2) linear suspension elements

(3) symmetry about a vertical plane passing through the geometric centerline of the vehicle

(4) small angular displacements.

In addition, it is assumed that any resonant frequencies associated with dynamics not included in the model are sufficiently high to not affect the system response in the frequency range of interest. This would apply, for example, to car body-bolster or axle-sideframe relative vibrations. This assumption also implies that the truck wheels and rail act essentially as a single mass. Therefore, the effective mass of the track structure can be lumped with the associated truck masses. The flexibility of the track structure can then be modeled as a parallel combination of a linear spring and damper. From this viewpoint, then, the input to the vehicle is a motion input due to roadbed irregularities acting through the rail elements. This approach has been used with apparent success by Ahlbeck et.al.[6].

The assumptions of symmetry and linearity allow the vertical motions to be considered independent, or uncoupled, from the lateral and rolling motions. Under these restrictions the vertical motions of the vehicle may be described in terms of the six degree-of-freedom model illustrated in Fig. 2-3. The state of the system may be completely defined in terms of the 12 independent state variables defined as bounce, bounce rate, pitch and pitch rate of the car body and two

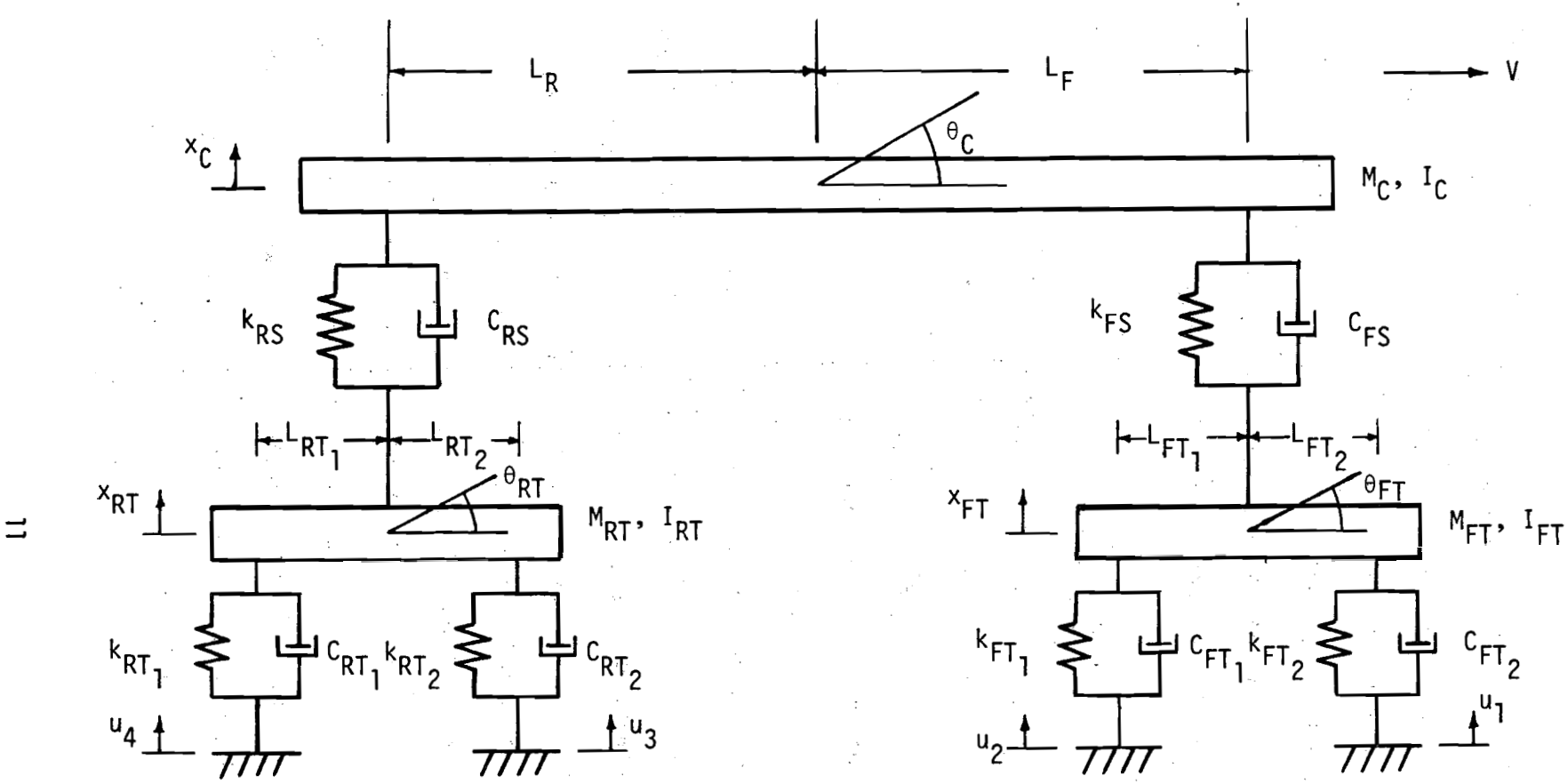

Figure 2-3 Linear 6 DOF Model of the Freight Car Vertical Dynamics

trucks. The equations of motion may be written in a straightforward fashion as six second-order differential equations. The complete set of equations appears in Fig. 2-4.

It may be noted at this point that the four separate inputs to the system may be viewed as a single input with appropriate time delays. In terms of the Laplace transforms of the inputs this viewpoint may be expressed as

$$u_1(s) = u(s)$$
$$u_2(s) = u(s)e^{-sT_2}$$
$$u_3(s) = u(s)e^{-sT_3}$$

and

$$u_4(s) = u(s)e^{-sT_4} . \qquad (2\text{-}1)$$

The general time delay, T, may be expressed as

$$T = L/V \qquad (2\text{-}2)$$

where L is the physical distance between the two inputs and V is the velocity of the vehicle. This approach is useful since it allows the system to be analyzed as a single input-single output system.

The input to the system is essentially a random process (although there are probably some deterministic components) and hence must be described in terms of its statistics. This leads to a characterization of the input in terms of its power spectral density, (PSD), which is discussed in detail in the next chapter. The PSD characterizes the input in the frequency domain, which is valuable since the model equations are most conveniently handled in the frequency domain. Taking the Laplace transform of the equations

CAR BODY EQUATIONS

$$M_c \ddot{x}_c + k_{RS} (x_c - x_{RT} - L_R \theta_c) + C_{RS} (\dot{x}_c - \dot{x}_{RT} - L_R \dot{\theta}_c)$$

$$+ k_{FS} (x_c - x_{FT} + L_F \theta_c) + C_{FS} (\dot{x}_c - \dot{x}_{FT} + L_F \dot{\theta}_c) = 0$$

$$I_c \ddot{\theta}_c - L_R \{k_{RS} (x_c - x_{RT} - L_R \theta_c) + C_{RS} (\dot{x}_c - \dot{x}_{RT} - L_R \dot{\theta}_c)\}$$

$$+ L_F \{k_{FS} (x_c - x_{FT} + L_F \theta_c) + C_{FS} (\dot{x}_c - \dot{x}_{FT} + L_F \dot{\theta}_c)\} = 0$$

FRONT TRUCK EQUATIONS

$$M_{FT} \ddot{x}_{FT} + k_{FT_1} (x_{FT} - u_2 - L_{FT_1} \theta_{FT}) + C_{FT_1} (\dot{x}_{FT} - \dot{u}_2 - L_{FT_1} \dot{\theta}_{FT})$$

$$+ k_{FT_2} (x_{FT} - u_1 + L_{FT_2} \theta_{FT}) + C_{FT_2} (\dot{x}_{FT} - \dot{u}_1 + L_{FT_2} \dot{\theta}_{FT})$$

$$- k_{FS} (x_c - x_{FT} + L_F \theta_c) - C_{FS} (\dot{x}_c - \dot{x}_{FT} + L_F \dot{\theta}_c) = 0$$

$$I_{FT} \ddot{\theta}_{FT} - L_{FT_1} \{k_{FT_1} (x_{FT} - u_2 - L_{FT_1} \theta_{FT}) + C_{FT_1} (\dot{x}_{FT} - \dot{u}_2 - L_{FT_1} \dot{\theta}_{FT})\}$$

$$+ L_{FT_2} \{k_{FT_2} (x_{FT} - u_1 + L_{FT_2} \theta_{FT}) + C_{FT_2} (\dot{x}_{FT} - \dot{u}_1 + L_{FT_2} \dot{\theta}_{FT})\} = 0$$

REAR TRUCK EQUATIONS

$$M_{RT} \ddot{x}_{RT} + k_{RT_1} (x_{RT} - u_4 - L_{RT_1} \theta_{RT}) + C_{RT_1} (\dot{x}_{RT} - \dot{u}_4 - L_{RT_1} \dot{\theta}_{RT})$$

$$+ k_{RT_2} (x_{RT} - u_3 + L_{RT_2} \theta_{RT}) + C_{RT_2} (\dot{x}_{RT} - \dot{u}_3 + L_{RT_2} \dot{\theta}_{RT})$$

$$- k_{R_S} (x_c - x_{RT} - L_R \theta_c) - C_{RS} (\dot{x}_c - \dot{x}_{RT} - L_R \dot{\theta}_c) = 0$$

$$I_{RT} \ddot{\theta}_{RT} - L_{RT_1} \{k_{RT_1} (x_{RT} - u_4 - L_{RT_1} \theta_{RT}) + C_{RT_1} (\dot{x}_{RT} - \dot{u}_4 - L_{RT_1} \dot{\theta}_{RT})\}$$

$$+ L_{RT_2} \{k_{RT_2} (x_{RT} - u_3 + L_{RT_2} \theta_{RT}) + C_{RT_2} (\dot{x}_{RT} - \dot{u}_3 + L_{RT_2} \dot{\theta}_{RT}\} = 0$$

Figure 2-4 Linear Equations of Motion for the 6 DOF Model

in Fig. 2-4 yields a set of linear equations of the form

$$\{[A]s^2 + [B]s + [C]\}\ \underline{x}(s) = \{\underline{b}(s)s + \underline{c}(s)\}\ u(s) \qquad (2\text{-}3)$$

where the square brackets designate a square matrix and the underscore designates a vector. The particular elements are expressed in the expanded form of (2-3) shown in Fig. 2-5.

The frequency response of the system may be computed by employing the substitution variable $s = j\omega$ and solving the associated set of complex linear simultaneous equations for each of the desired values of frequency. This is easily implemented on a digital computer and is essentially the technique employed in [7] for the digital computation of frequency response. The linear simulation program utilizes a modified version of the frequency response subroutine found in [7]. This program incorporates a complex input as defined by (2-3).

Some sample transfer functions are shown in Fig. 2-6, 7, and 8. These computations were performed using the model baseline parameter values listed in Table 5-1 and a vehicle speed of 100 ft/sec. The magnitude of the system response is displayed in terms of the vertical displacement of the car body, e.g., pitch angle of the car body, and vertical displacement of the car body centered over the front truck. This last response variable is a linear combination of the first two response variables. It is interesting to note the filtering effect of the trucks and car body due to combined bounce and pitch motions. At certain frequencies this transfer function magnitude "drops out" and the phase abruptly shifts 180°. The nature of this phenomena is discussed in Appendix B. The car body c.g. sees a drop out at 1.1 Hz

$$A = \begin{bmatrix} M_c & 0 & 0 & 0 & 0 & 0 \\ 0 & I_c & 0 & 0 & 0 & 0 \\ 0 & 0 & M_{RT} & 0 & 0 & 0 \\ 0 & 0 & 0 & I_{RT} & 0 & 0 \\ 0 & 0 & 0 & 0 & M_{FT} & 0 \\ 0 & 0 & 0 & 0 & 0 & I_{FT} \end{bmatrix} \qquad \underline{X}(s) = \begin{bmatrix} X_c(s) \\ \theta_c(s) \\ X_{RT}(s) \\ \theta_{RT}(s) \\ X_{FT}(s) \\ \theta_{FT}(s) \end{bmatrix}$$

$$B = \begin{bmatrix} C_{RS} + C_{FS} & C_{FS}L_F - C_{RS}L_R & -k_{RS} & 0 & -k_{FS} & 0 \\ C_{FS}L_F - C_{RS}L_R & C_{FS}L_F^2 - C_{RS}L_R^2 & k_{RS}L_R & 0 & -k_{FS}L_F & 0 \\ -C_{RS} & C_{RS}L_R & k_{RS} + k_{RT_1} + k_{RT_2} & k_{RT_2}L_{RT_2} - k_{RT_1}L_{RT_1} & 0 & 0 \\ 0 & 0 & k_{RT_2}L_{RT_2} - k_{RT_1}L_{RT_1} & k_{RT_2}L_{RT_2}^2 - k_{RT_1}L_{RT_1}^2 & 0 & 0 \\ -C_{FS} & -C_{FS}L_F & 0 & 0 & k_{FT_1} + k_{FT_2} + k_{FS} & k_{FT_2}L_{FT_2} - k_{FT_1}L_{FT_1} \\ 0 & 0 & 0 & 0 & k_{FT_2}L_{FT_2} - k_{FT_1}L_{FT_1} & k_{FT_2}L_{FT_2}^2 - k_{FT_1}L_{FT_1}^2 \end{bmatrix}$$

$$C = \begin{bmatrix} k_{RS} + k_{FS} & k_{FS}L_F - k_{RS}L_R & -k_{RS} & 0 & -k_{FS} & 0 \\ k_{FS}L_F - k_{RS}L_R & k_{FS}L_F^2 + k_{RS}L_R^2 & k_{RS}L_R & 0 & -k_{FS}L_F & 0 \\ -k_{RS} & k_{RS}L_R & k_{RS} + k_{RT_1} + k_{RT_2} & k_{RT_2}L_{RT_2} - k_{RT_1}L_{RT_1} & 0 & 0 \\ 0 & 0 & k_{RT_2}L_{RT_2} - k_{RT_1}L_{RT_1} & k_{RT_2}L_{RT_2}^2 - k_{RT_1}L_{RT_1}^2 & 0 & 0 \\ -k_{FS} & -k_{FS}L_F & 0 & 0 & k_{FT_1} + k_{FT_2} + k_{FS} & k_{FT_2}L_{FT_2} - k_{FT_1}L_{FT_1} \\ 0 & 0 & 0 & 0 & k_{FT_2}L_{FT_2} - k_{FT_1}L_{FT_1} & k_{FT_2}L_{FT_2}^2 + k_{FT_1}L_{FT_1}^2 \end{bmatrix}$$

$$\underline{b}(s) = \begin{bmatrix} 0 \\ 0 \\ C_{RT_1}e^{-ST_4} + C_{RT_2}e^{-ST_3} \\ -C_{RT_1}L_{RT_1}e^{-ST_4} + C_{RT_2}L_{RT_2}e^{-ST_3} \\ C_{FT_1}e^{-ST_2} + C_{FT_2} \\ -C_{FT_1}L_{FT_1}e^{-ST_2} + C_{FT_2}L_{FT_2} \end{bmatrix} \qquad \underline{c}(s) = \begin{bmatrix} 0 \\ 0 \\ k_{RT_1}e^{-ST_4} + k_{RT_2}e^{-ST_3} \\ -k_{RT_1}L_{RT_1}e^{-ST_4} + k_{RT_2}L_{RT_2}e^{-ST_3} \\ k_{FT_1}e^{-ST_2} + k_{FT_2} \\ -k_{FT_1}L_{FT_1}e^{-ST_2} + k_{FT_2}L_{FT_2} \end{bmatrix}$$

Figure 2-5 Coefficient Matrices and Vectors for the Laplace Transform of the Linear Equations

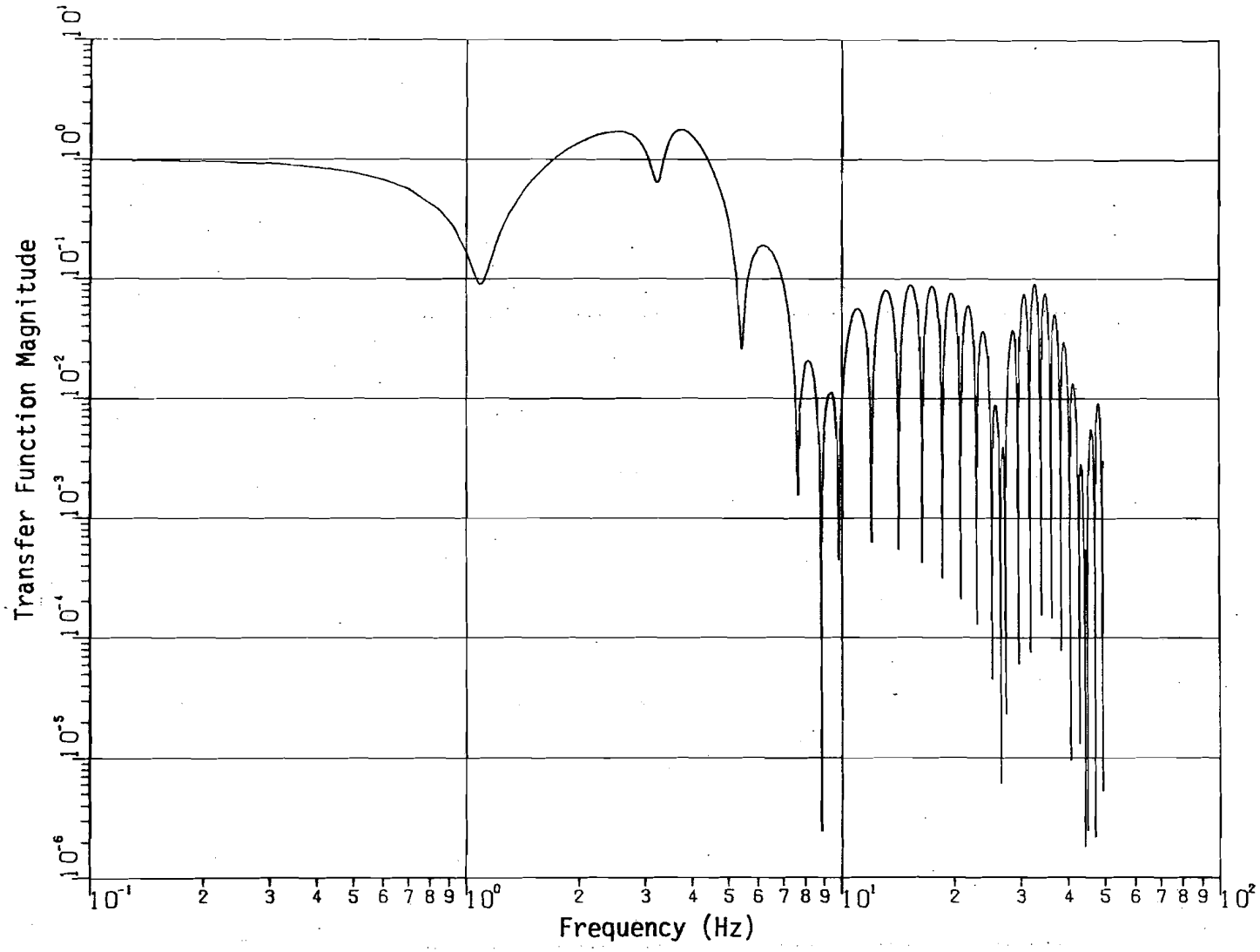

Figure 2-6 Sample Car Body C.G. Transfer Function Magnitude

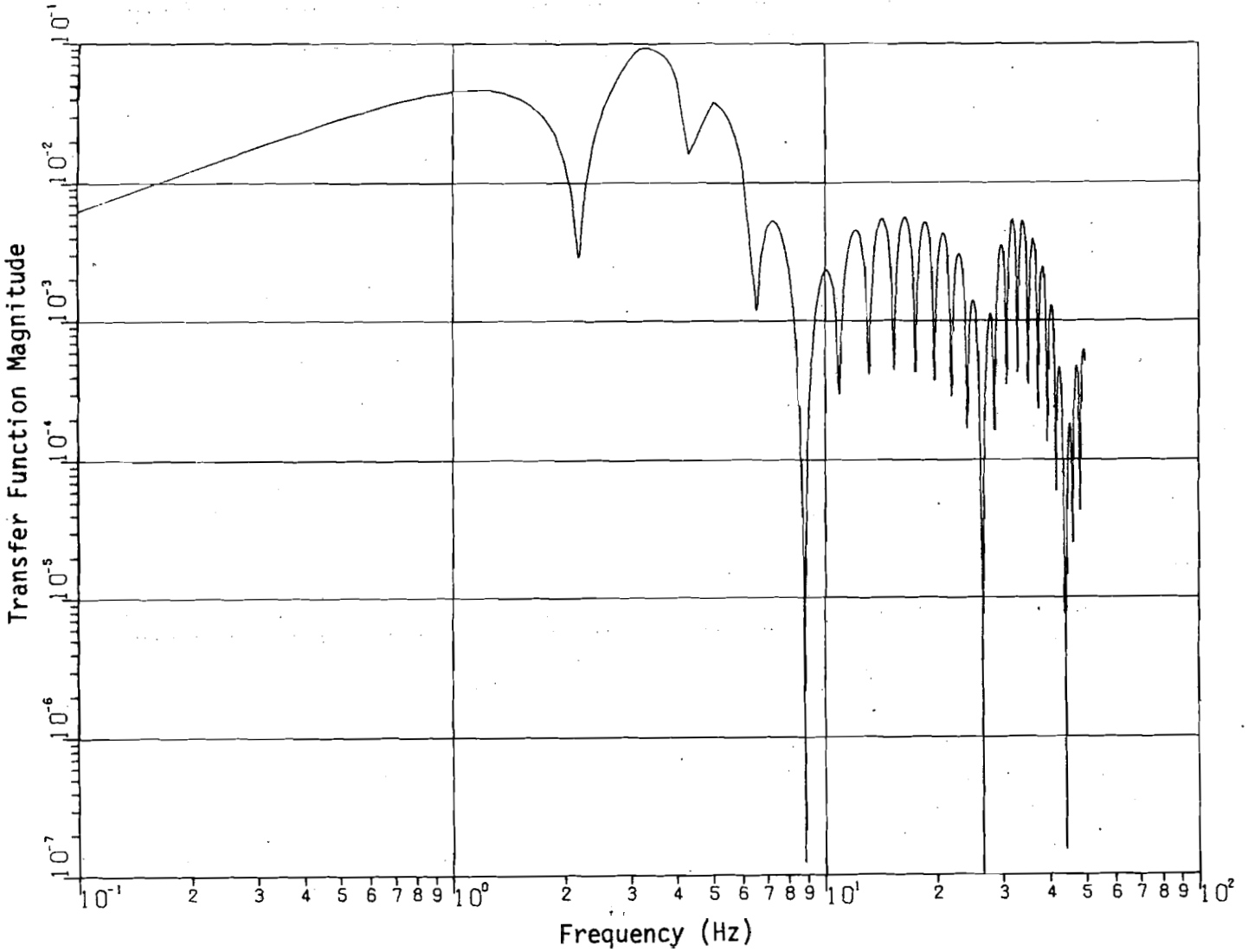

Figure 2-7 Sample Car Body Pitch Transfer Function Magnitude

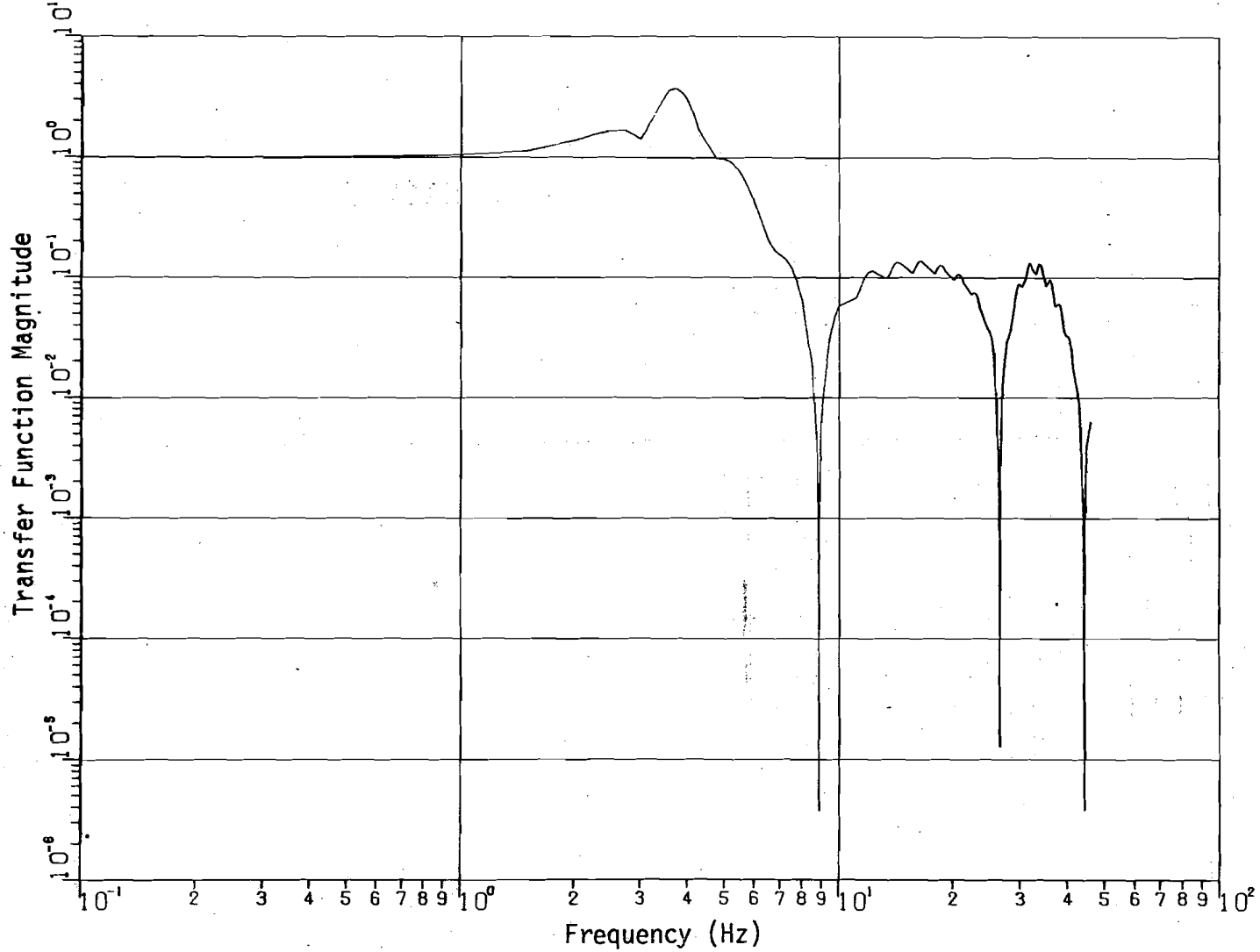

Figure 2-8 Sample Car Body Front End Transfer Function Magnitude

due to pitching of the car body and at 8.8 Hz due to pitching of the trucks and at the odd harmonic associated with these two fundamental frequencies. The corresponding fundamental frequencies for the pitch transfer function are 2.2 Hz and 8.3 Hz. The combined effects of these dropouts result in the jagged appearance of the transfer function for displacement of the front end of the vehicle. Also note that the break frequencies associated with the truck suspension are between 3 Hz and 4 Hz for both pitch and bounce and the second order roll off can be observed in both transfer functions.

Nonlinear Considerations

The freight car, like most physical systems, contains nonlinear elements. In the normal regime of operation, the truck suspension is the primary source of nonlinear effects. This suspension is represented schematically in Fig. 2-9. The spring loaded wedges

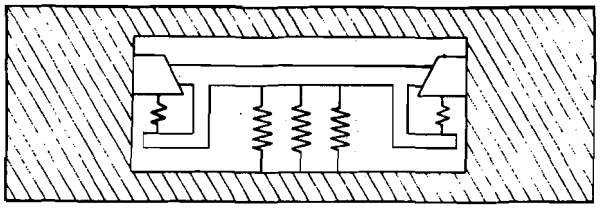

Figure 2-9 Schematic of the Freight Car Truck Suspension

(called friction snubbers) provide damping primarily through sliding (coulomb) friction. The most common approach to modeling this suspension is to use an "equivalent" linear model based on assumptions

about the nature of the suspension dynamics. A nonlinear model and an "equivalent" linear model are illustrated in Fig. 2-10 where D is the constant sliding friction force and C_{eq} is the "equivalent"

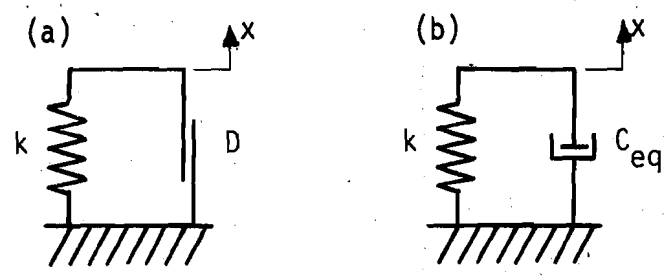

Figure 2-10 (a) Nonlinear Truck Suspension Model
(b) Linear Truck Suspension Model

viscous damping. A common approach to determining C_{eq} is to assume a sinusoidal motion through the suspension of amplitude X_o and frequency f_o. C_{eq} can then be chosen such that the two models are matched in terms of energy dissipated per cycle, i.e.,

$$2\ C_{eq}\ f_o\ X_o^2\ \pi^2 = 4\ D\ X_o, \tag{2-4}$$

which yields

$$C_{eq} = \frac{2\ D}{f_o\ \pi^2\ X_o} \tag{2-5}$$

This approach to equivalent linearization is equivalent in operation to the describing function approach. The describing function technique requires an assumption about the response of the system followed by an analysis of the conditions necessary to maintain this response. The purpose of this technique is to obtain a linear function

that describes the response of the nonlinearity for the assumed mode of response. This technique is quite useful for dealing with systems that exhibit self oscillations, where the assumed mode of response is then some type of sinusoidal motion.

Any linear model, however, has shortcomings in that it cannot accurately portray the dynamics of a nonlinear system. In this case, the effects of dry friction are ignored. At relatively low force levels, the dry friction will keep the suspension "bound up" and cause it to pass the dynamics of the truck directly through to the car body. In addition, this "sticking" can affect the symmetry of the system and lead to coupling of the roll and vertical motions of the vehicle.

However, a linear approach is quite often a practical "first cut" at a problem. This approach is taken in this study. The expression in (2-5) is used to compute an equivalent viscous damping for the linear model. The friction force level used in this computation is extracted from reference [8]. This reference contains the results of extensive laboratory tests of trucks similar to those used in the field tests that provided data for this study. This computation is discussed in Chapter 5 where the particular vehicle parameters are summarized.

Chapter 3

SPECTRAL TECHNIQUES

Introduction

The response of a railway vehicle to a track input is essentially random in nature. Therefore, a statistical approach is dictated for the analysis of the vehicle response data. The experimental time history data must be processed to yield statistically stable functions that provide specific information about the system response in a concise and useful format.

Spectral functions such as the power spectral density (PSD) and cross spectral density are frequency domain functions that satisfy this need. The PSD displays the frequency distribution of the signal strength and yields such information as the mean squared value of the system response in any frequency band. Any strong modal response will then be readily apparent in the PSD of the response signal. The cross spectral density is a complex frequency domain function that yields information such as the phase relationship between two signals. These two functions may be combined to yield such information as the coherence of two signals and a linear transfer function that may relate two signals.

These spectral functions can only be estimated based on finite time history records of data. The digital computer coupled with the

Fast Fourier Transform (FFT) algorithm provide the necessary tools to compute PSD's from such data records. Estimation of the PSD function, as developed in this chapter, requires computation of the discrete Fourier transform (DFT), a task that, until the advent of the FFT, was intractable for all practical purposes.

The FFT has had considerable impact in the area of digital computational techniques. Straightforward computation of an N-point discrete Fourier transform requires a computation time proportional to N^2. However, in 1965 Cooley and Tukey [9] published an algorithm for the machine computation of the DFT that yields a computation time proportional to $N \log_2 N$. The computational savings, expressed as the ratio $N/\log_2 N$, reveals the FFT to be 100 times faster for a 1000 point transform. While significant work had been published dating back over the previous 50 years, it was not until the Cooley-Tukey algorithm was published that the practical implications began to be realized. Since that time, an enormous amount of literature has been published relating to the FFT algorithm. A brief discussion of the FFT along with a Fortran coded routine that uses the successive doubling method is presented in [10]. A rather detailed but intuitively pleasing development of the FFT is given in [11]. In addition, the entire June, 1967 issue of IEEE Transactions on Audio and Electroacoustics is devoted to the FFT. A thorough treatment of the Fourier transform and the FFT can be found in [12].

The remaining portions of this chapter are primarily devoted to development of the spectral functions needed for analysis of the

experimental data. However, these sections are preceded by a brief discussion of the FFT, since the results are needed in developing discrete approximation expressions for the spectral functions. Finally, a number of computational considerations that must be reviewed in any practical application of spectral techniques are presented. Much of the material in this chapter may be found in greater detail in [12, 13].

The FFT and the Discrete Fourier Transform

The Fourier transform pair for a continuous function is defined as

$$X(f) = \int_{-\infty}^{\infty} x(t)\, e^{-j2\pi ft}\, dt \qquad (3\text{-}1)$$

and

$$x(t) = \int_{-\infty}^{\infty} X(f)\, e^{j2\pi ft}\, df\ . \qquad (3\text{-}2)$$

If the signal x(t) is in sampled form, as is often the case, an approximate expression for (3-1) is

$$X(n\Delta f) = \Delta t \sum_{k=0}^{N-1} x(k\Delta t)\, e^{-j2\pi n\Delta f k\Delta t} \qquad (3\text{-}3)$$

where N is the number of sample values of x(t). The sampling frequency, $\frac{1}{\Delta t}$, determines the time record length, T, defined as $N\Delta t$. The frequency increment, Δf, is determined by the sampling frequency and record length, i.e., $\Delta f = 1/N\Delta t$.

For notational convenience let the variables n and k index

frequency and time respectively as arguments of the function. Also let

$$W = e^{-j2\pi/N} \tag{3-4}$$

and note that W assumes a unique complex value once the value of N is chosen. Now (3-3) may be written

$$X(n) = \Delta t \sum_{k=0}^{N-1} x(k)\, W^{nk} . \tag{3-5}$$

In a similar fashion (3-2) may be approximated by

$$x(k) = \Delta f \sum_{n=0}^{N-1} X(n)\, W^{-nk} . \tag{3-6}$$

Equations (3-5) and (3-6) are related to the Discrete Fourier Transform and the Inverse Discrete Fourier Transform by the definitions

$$DFT[x(k)] = \sum_{k=0}^{N-1} x(k)\, W^{nk} \tag{3-7}$$

and

$$IDFT[X(n)] = \frac{1}{N} \sum_{n=0}^{N-1} X(n)\, W^{-nk} . \tag{3-8}$$

Note the similarity of the transform pair. The computations differ only in the sign of the exponent of W. Also, note that W^{nk} is periodic with period N. As detailed in [11], the essence of the FFT algorithm is to take advantage of this cyclic nature of W to efficiently compute the transform in either direction.

Spectral Functions

The power spectral density function, as previously mentioned,

describes the spectral distribution of power in a signal. The PSD, however, is normally defined in terms of the autocorrelation function.

The autocorrelation function describes the dependence of a signal on itself delayed in time. For an ergodic random process the autocorrelation is defined as

$$R_x(\tau) = \lim_{T\to\infty} \frac{1}{T} \int_0^T x(t)\, x(t+\tau)\, dt \quad . \tag{3-9}$$

$R_x(\tau)$ is an even function and can be useful in determining the existence of periodicities, or deterministic components, in a signal. For example, if $x(t)$ were purely random in nature, then $R_x(\tau)$ would quickly approach zero as the lag time, τ, increased from zero. However, the existence of a periodic component in $x(t)$ would cause $R_x(\tau)$ to exhibit a persistent oscillation.

The power spectral density is defined as the Fourier transform of the autocorrelation, i.e.

$$P_x(f) = \int_{-\infty}^{\infty} R_x(\tau) e^{-j2\pi f\tau}\, d\tau \quad . \tag{3-10}$$

Now, the autocorrelation function defined in (3-9) may be estimated based upon a finite record of $x(t)$ of length T. This estimate takes the form

$$\hat{R}_x(\tau) = \frac{1}{T} \int_0^T x(t)\, x(t+\tau)\, d\tau \tag{3-11}$$

where the overscript designates an estimate. Note that the correlation integral is quite similar in form to the familiar convolution integral. In fact, it can be shown (see [12], pp. 66-68) that the

Fourier transform of (3-11), i.e., an estimate of the power spectral density function, is given by

$$\hat{P}_x(f) = \frac{1}{T} X(f) X^*(f) \tag{3-12}$$

where the * indicates the complex conjugate. Equation (3-12) is often employed as an alternate "practical" definition of the power spectrum. Note that the power spectrum is a real valued function and that integration over any frequency band yields the mean squared value of the signal in that band. In fact, for zero mean data the variance is given by

$$\sigma_x^2 = \int_{-\infty}^{\infty} P_x(f)\, df. \tag{3-13}$$

A discrete approximation to (3-12) may now be made by employing (3-5), yielding

$$P_x(n) = \Delta f \, |X(n)|^2 . \tag{3-14}$$

Thus, an approximate expression for the estimation of power spectra has been developed that may be realized computationally utilizing a digital computer.

The cross spectral density is another spectral function that yields the phase relationship between two signals. In the study of linear systems, phase relationship is a critical piece of information that is conspicuously absent in the individual power spectra of the signals. In a manner completely analogous to the power

spectral density, the cross spectral density is defined in terms of the cross correlation function.

The cross correlation function is defined by

$$R_{xy}(\tau) = \lim_{T\to\infty} \frac{1}{T} \int_0^T x(t)\, y(t+\tau)\, dt \,. \qquad (3\text{-}15)$$

An example of the usefulness of the cross correlation is the identification of a pure time delay in a system. If $x(t)$ represents the input to a pure time delay while $y(t)$ represents the output, a spike in $R_{xy}(\tau)$ would clearly indicate correlation at the value of τ corresponding to the time delay.

The cross spectral density is defined as the Fourier transform of the cross correlation function. A development analagous to the PSD development yields an estimate to the cross spectrum given by

$$\hat{P}_{xy}(f) = \frac{1}{T} X(f)\, Y^*(f) \qquad (3\text{-}16)$$

Again, employing (3-5) yields the discrete approximation to (3-16)

$$\hat{P}_{xy}(n) = \Delta f\, X(n)\, Y^*(n) \,, \qquad (3\text{-}17)$$

an expression that may be efficiently computed on the digital computer.

Transfer Function

The utility of the spectral functions in the study of a linear plant can now be examined. A linear, time invariant, single input-

single output system is represented in Fig. 3-1.

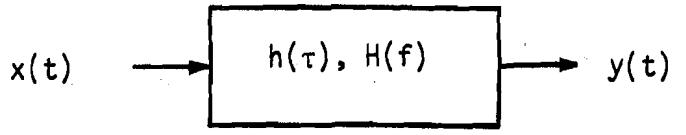

Figure 3-1 Linear Single Input - Single Output System Block Diagram

The system output spectrum is related to the input spectrum by the relationship

$$P_y(f) = |H(f)|^2 P_x(f) . \qquad (3\text{-}18)$$

Note from equation (3-14) that the power spectrum contains no phase information. Hence, only the magnitude of the transfer function can be characterized by the input and output spectra. However, examination of the cross spectrum reveals the important fact that the phase relationship between the input and output has been retained. In fact, the input output relationship may be characterized by

$$P_{xy}(f) = H(f) P_x(f) . \qquad (3\text{-}19)$$

Hence, knowledge of the cross spectrum as well as the input spectrum completely characterizes the system of Fig. 3-1.

Coherence

For two signals, x(t) and y(t), the ordinary coherence function is defined as

$$\gamma^2_{xy}(f) = \frac{|P_{xy}(f)|^2}{P_x(f)\, P_y(f)} \qquad (3\text{-}20)$$

where the value of the coherence function is limited by

$$0 \leq \gamma_{xy}^2 (f) \leq 1 \quad . \tag{3-21}$$

The coherence is a very practical tool that can aid in determining the relationship of two signals. A coherence value of one indicates complete correlation between two signals while zero coherence indicates complete independence of the two signals. For example, consider the system represented in Fig. 3-1. The coherence is given by

$$\gamma_{xy}^2(f) = \frac{|H(f)\, P_x(f)|^2}{|H(f)|^2\, |P_x(f)|^2} = 1. \tag{3-22}$$

The coherence function has many practical applications. For instance, if two signals are known to be completely correlated but their measured values are contaminated with uncorrelated noise, it can be shown (see [13], pp. 142-143) that

$$\gamma_{xy}^2(f) = \frac{\gamma_{uv}^2(f)}{1 + \frac{P_n(f)}{P_u(f)} + \frac{P_m(f)}{P_v(f)} + \frac{P_n(f)\, P_m(f)}{P_u(f)\, P_v(f)}} < \gamma_{uv}^2(f) \tag{3-23}$$

where $x = u + n$ and $y = v + m$, n and m representing the uncorrelated noise. Hence, the coherence can be viewed as an estimate of the noise contamination in the measurements.

However, caution must be employed in interpreting coherence. For example, consider the situation shown in Fig. 3-2. If the ordinary coherence is computed for measured values of the signals y(t) and z(t),

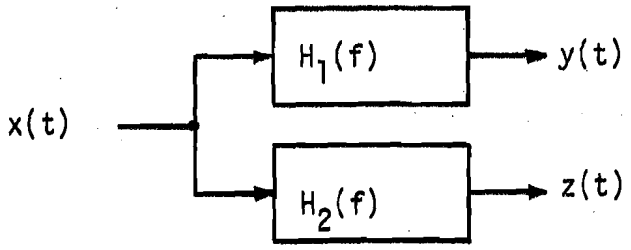

Figure 3-2 Independent Linear Plants With a Common Input

a very high value may well result and lead to a conclusion that some causal relationship exists between y(t) and z(t). Clearly, y(t) and z(t) are only indirectly related via the input x(t) that led to the high coherence. Hence, physical insight must not be overlooked as an indispensable analysis tool.

Computational Considerations

Sampling

One of the most basic considerations in dealing with sampled data is the sampling rate. The continuous signal must be sampled at a rate high enough to retain all the essential information in the signal. Consider the situation illustrated in Fig. 3-3.

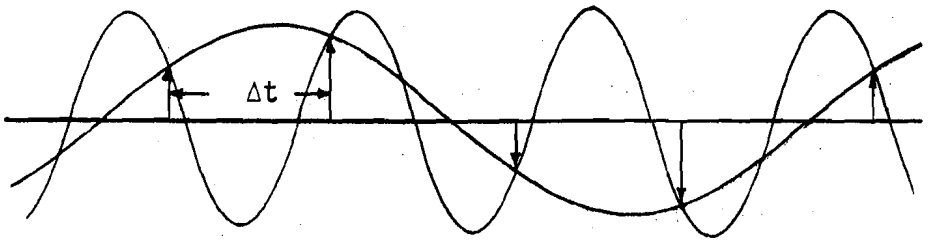

Figure 3-3 Two Harmonically Related Signals Sampled Every Δt Seconds

Clearly, if higher frequency components exist in the signal, they will be indistinguishable from lower frequency components. Another way to view this situation is to note that the effect of sampling is to produce a sampled spectrum that is periodic at the sampling frequency, i.e.,

$$X(n) = X(n + if_s),\ i = 0, 1, 2 \ldots \qquad (3\text{-}24)$$

where $f_s = 1/\Delta t$. If the reproductions of the sampled spectrum are not spaced sufficiently they will overlap. Hence higher frequency information will be "aliased" back into the lower frequency region of the spectrum. This leads to the statement of the Nyquist sampling theorem, i.e., the data must be sampled at a rate at least twice that of the highest frequency component in the signal.

From a practical standpoint, then, care must be taken to remove, via filtering, all components in the signal greater than the Nyquist folding frequency, defined as half the sampling frequency, prior to sampling.

Prewhitening

The concept of "prewhitening" essentially is to treat the raw data in such a way as to remove those components that are relatively strong and would thus contribute to distortion of the spectrum estimate. The resultant spectrum estimate, based on the prewhitened data, would ideally then be "recolored" in some fashion to account for the effects of the strong components. From a practical standpoint, this presents some difficult problems. However, certain types of components are common in experimental data and may be accounted for with a

fair amount of ease.

Experimental data often contains very low frequency components. For example, if not properly nulled, an electrical transducer may contain a DC bias in its output. Such components in the measured signal contaminate measurement of the true process and would result in a low frequency peak in the resultant spectrum estimate, completely obscuring the true low frequency spectrum. Therefore, it is advisable to remove such low frequency trends in the data as a preliminary step in the data processing procedure. For the purposes of this study a bias and linear trend were removed from sample data records prior to spectrum estimate computations.

Leakage

Leakage is the term applied to spreading of spectral components into neighboring frequencies in the spectrum estimate. This phenomena is a result of truncation of data into finite records. For example, consider the infinite signal $x(t)$ and its truncated form $\hat{x}(t)$ defined by

$$\hat{x}(t) = w(t)\, x(t) \tag{3-25}$$

where

$$w(t) = \begin{cases} 1 & 0 \leq t \leq T \\ 0 & \text{Otherwise} \end{cases} . \tag{3-26}$$

$w(t)$ is referred to as a spectral "window" in its general form in equation (3-25). The definition of $w(t)$ in (3-26) is often referred to as the "boxcar" window.

Now, the process defined in (3-25) is equivalent to convolving x(t) and w(t) in the frequency domain, i.e.,

$$\hat{X}(f) = W(f) * X(f) \ . \tag{3-27}$$

For the boxcar window

$$W(f) = \int_0^T e^{-j2\pi ft} \, dt \tag{3-28}$$

which yields

$$|W(f)| = T \, \frac{\sin(\pi fT)}{\pi fT} \ . \tag{3-29}$$

Fig. 3-4 illustrates the form of (3-29).

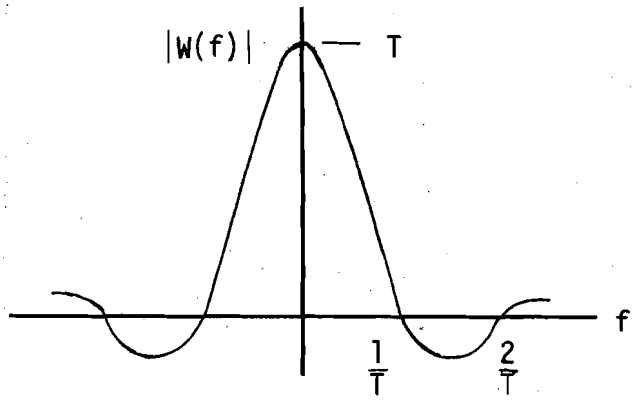

Figure 3-4 The Boxcar Spectral Window

Performing the convolution indicated by (3-27) causes leakage due to the relatively large side lobes of W(f). This leakage effect can be reduced by application of alternate spectral windows. Welch, in [14], suggests an approximate "hanning" window, defined in (3-30), or the Parzen window, defined in (3-31) where

$$w_h(t) = \begin{cases} 1 - \left| \dfrac{t - \frac{T}{2}}{T} \right|^2 & 0 \le t \le T \\ 0 & \text{Otherwise} \end{cases} \tag{3-30}$$

and

$$w_p(t) = \begin{cases} 1 - \left| \frac{t - \frac{T}{2}}{T} \right| & 0 \leq t \leq T \\ 0 & \text{Otherwise} \end{cases} \quad . \tag{3-31}$$

Both of these windows exhibit much smaller side lobes than the box-car window. Hence, use of either window will aid leakage suppression. More complicated windows utilizing trigonometric functions have been suggested, but the ease of computation make (3-30) and (3-31) attractive.

Leakage may not be a serious problem if the spectrum is relatively slowly changing. However, if the spectrum contains a strong peak, leakage may seriously obscure information in the vicinity of the peak.

Finally, using (3-5) and (3-14) and applying an appropriate window yields the following formula for a power spectrum estimate:

$$\hat{P}_x(n) = \frac{\Delta t}{Nd} \left| \sum_{k=0}^{N-1} x(k)\, w(k)\, W^{nk} \right|^2 \tag{3-32}$$

where

$$d = \frac{1}{N} \sum_{k=0}^{N-1} w(k)^2 \tag{3-33}$$

is necessary to compensate for the attenuation of the signal due to application of the window.

Statistical Considerations

The formula of (3-14) represents an estimate of the power spectrum based on a single finite record of data. Now, error is

introduced by the truncation of data (i.e., leakage) as previously discussed. However, serious consideration must also be given to the statistical variability of the estimate. Several techniques have been suggested for reducing this statistical variability (see [13, 14, 15]. In [14] Welch suggests computing individual estimates using possibly overlapping data records and averaging the results point by point. This yields the formula

$$\hat{P}_x(n) = \frac{1}{K} \sum_{i=1}^{K} \hat{P}_{x_i}(n) \tag{3-34}$$

where $\hat{P}_{x_i}(n)$ is computed using (3-32) and represents the spectrum estimate based on the i^{th} data record.

Welch derives an uncertainty relationship that relates the variance of the estimate to the expected value under the assumption that the process is Gaussian. For non-overlapping data records this uncertainty relationship may be expressed as

$$\varepsilon^2 = \frac{\text{Var}\{\hat{P}_x(f)\}}{E^2[\hat{P}_x(f)]} = \frac{1}{K} \tag{3-35}$$

where K represents the number of individual estimates averaged. Richards, in [R1], derives an equivalent expression that may be written as

$$\sigma_{P_x} = \frac{\mu_{P_x}}{\sqrt{K}} \tag{3-36}$$

where μ_{P_x} and σ_{P_x} are the mean and standard deviation, respectively, of the spectrum of the signal. Note that this relationship assumes

a Gaussian distribution of the data. However, it has been suggested as a useful rule of thumb in general. For example, if 25 individual estimates are averaged the resulting spectrum estimate is within 20% of the true value at a 67% confidence level. This rule, along with the fact that the frequency resolution is dictated by the record length, i.e., $\Delta f = 1/T$, reveals the tradeoff between stability and resolution for a fixed amount of data.

Conclusions

The expressions that have been developed in this chapter have been incorporated into a general purpose data processing computer program. The details of this program, including input and output formats, are presented in [5]. This program was used to generate the experimental results that are presented in this report, such as RMS values, PSD's, cross spectral densities, coherence and transfer functions.

The next chapter describes the field tests and presents the experimental results. These results include track input spectra and corresponding vehicle response spectra as well as truck suspension response. The track input spectra are used as input to the linear model in Chapter 5 for purposes of model validation.

Chapter 4

EXPERIMENTAL RESULTS

Introduction

This chapter documents experimental results of track geometry and freight car vertical response measurements. The data reduction process is briefly described, followed by presentation and discussion of the results of the track geometry measurements. Representative test vehicle vertical response results are presented in the final section. Additional results are presented in the next chapter where corresponding analytical results are generated using the linear model for purposes of comparison and model validation.

The field tests that provided the experimental data examined in this report were conducted under the auspices of the U. S. Department of Transportation. This test program, a joint government industry project called the Freight Car Truck Design Optimization Project (TDOP), was conducted by the Southern Pacific Transportation Co.. This set of field tests actually comprises the first phase of a projected four phase program.

The test vehicle was a Southern Pacific refrigerator car equipped with ASF 70-ton trucks. As suggested by the project title, the truck dynamics were of prime interest and therefore the trucks were fitted with the bulk of the instrumentation. This instrumentation

consisted primarily of linear accelerometers and displacement transducers for the purpose of monitoring lateral and vertical acceleration and relative displacements of various truck components. However, the car body was also fitted with accelerometers at either end in order to monitor lateral and vertical car body accelerations. In order to obtain data representative of vehicle response across a broad range of operating conditions several different test configurations were employed. These different configurations involved the use of worn as well as new truck components, empty as well as fully loaded vehicles, and different types of track. A more detailed description of the TDOP program and associated field tests is contained in [3].

The data from this test program, along with detailed documentation, has been made available to the public through the National Technical Information Service. Selected portions of this data, in the form of digitized magnetic tapes, were obtained through NIIS. This selected data represents track geometry measurements for the various sections of test track as well as the vehicle response measurements for a single nominal truck configuration under empty and fully loaded conditions.

Data Processing and Reduction

The raw experimental data examined in this report was initially received in the form of "stranger" magnetic tapes. The term "stranger" implies that the tape formats are foreign to the UNIVAC 1110 computer

system at Arizona State University where all programming and data processing tasks were performed. Therefore, translation programs were written to read these tapes, reformat the data for UNIVAC compatibility, and store the data in UNIVAC disc files. Utilizing these translation programs, selected channels of track geometry and vehicle response measurements were read from tape, converted to engineering units, and stored in separate disc data files for fast access. In many cases these data files had to be combined to obtain the desired variable. For example, the vertical acceleration of the car body front and rear were linearly combined to yield the acceleration of the car body center of gravity.

The data reduction task was accomplished through the use of the general purpose data reduction program described in [5]. All of the experimental results presented in this chapter and the next were generated through the use of this program.

Track Geometry

In order to analytically compute the response of a system, not only must a transfer function be computed but the input to the system must be adequately described. The track irregularity constitutes the input to the system under consideration. This input may be modeled by a mathematical expression or computed from actual measurements. In the next chapter the expression in equation (3-18) is used to compute the PSD of the model response based upon the PSD

of the input. In order to minimize the error associated with the analytical response, it is highly desirable to compute the input spectrum based on measurements of the specific portion of test track over which the vehicle response is measured. For this reason, the track geometry data is very important.

The vehicle response examined in this report represents the response over two specific portions of tangent test track: one section of continuous welded rail (CWR) and one section of jointed rail. The CWR section is a part of the S.P. Oakland-Ogden eastbound mainline (mileposts 42.5 to 47.3) and the jointed rail is a section of the S.P. Shelleville branch line (mileposts 50.2 to 55.0). A U.S. Department of Transportation (DOT) track geometry measurement vehicle was used to measure track geometry parameters including alignment, crosslevel, and surface irregularities.

The track geometry measurement of interest in analyzing the vertical vehicle response is the vertical irregularity of the track centerline, taken to be the mean of the right and left surface deviations. An ideal measurement system would, without error, measure these deviations relative to an arbitrary reference characterized by a "very long" wavelength. By "very long" it is meant that the reference deviates from a straight line so slowly that, if the track corresponded perfectly, the vertical dynamics of the vehicle would in no way be excited. However, from a practical standpoint, such a system is not easily or economically realized.

A common alternative is to employ a "chordal offset" technique where the deviation of the rail is measured relative to the midpoint of a chord traveling along the rail. This is the technique employed in the DOT track geometry vehicle. In order to obtain a more realistic measurement of the "true" surface irregularities, the results must be compensated to account for the effects of this midchord offset measurement system. In Appendix A it is shown that the midchord offset measurement system can be characterized by the following "chordal transfer function":

$$H(\lambda) = 1 - \cos\left(\frac{\pi L}{\lambda}\right) \qquad (4\text{-}1)$$

or, equivalently, in terms of spatial frequency,

$$H(f) = 1 - \cos(\pi L f) \qquad (4\text{-}2)$$

where L is the length of the chord. This transfer function is defined as the ratio of the midchord deviation to the "true" deviation. Note the fact that, when the chordal measurement system is used, information is lost at the fundamental frequency corresponding to a wavelength of half the chord length and at all the harmonics, i.e.,

$$H(f) = 0 \quad \text{at} \quad f = \frac{2n}{L}, \; n = 0, 1, 2 \ldots \quad . \qquad (4\text{-}3)$$

The DOT track measurement vehicle used in the TDOP test samples at a constant interval of approximately 2.42 feet and uses a 14.5 foot chord for surface measurements. The surface spectra based on this data may be compensated by employing the relationship

$$P_c(f) = \frac{P(f)}{|H(f)|^2} \qquad (4\text{-}4)$$

where P(f) is the spectrum based on the chordal measurement data. Note that the compensated spectrum will exhibit peaks in the areas of the frequencies noted in (4-3). These peaks merely indicate where information was lost by using the chordal system. Note the range limitations of the resultant spectrum. Long wavelengths are limited by measurement resolution while short wavelengths are limited by the Nyquist sampling theorem. Under these limitations the range of the compensated spectrum is restricted to frequencies with corresponding wavelengths of about 5 feet (twice 2.42 feet) to about 100 feet. Finally, note that no information exists near the frequency corresponding to a 7.25 foot wavelength (half the chord length).

The experimental track spectrum reported here consists of the original uncompensated spectra as well as the spectra compensated via the relationships of (4-2) and (4-4). The original and compensated PSD's of the left surface irregularities are displayed in Fig. 4-1 through Fig. 4-4 for the CWR and jointed rail test sections. Parallel results are shown in Fig. 4-5 through Fig. 4-8 for the track centerline, computed as the mean of the right and left surface measurements. The centerline spectra are compensated exactly as the left surface spectra based on the assumption that the left and right chords are of equal length and that a chord passing through the midchord points is perpendicular to the track centerline. The two compensated centerline spectra constitute the input to the linear

model of the freight car which is the topic of the next chapter. The right surface spectra are not shown because, as expected, they are quite similar to the corresponding left surface spectra.

All the compensated spectra shown in these figures appear to exhibit a simple exponential relationship to wavelength in the range of about 10 to 100 feet (f = 0.01 to 0.1). This general characteristic has been reported many times and appears to hold consistently for track of widely varying type and condition. The results reported here fall quite agreeably within both the ranges of PSD's reported in references [6] and [16]. Both of these references report a range of vertical spectra for several different samples of track and limit their results to wavelengths between approximately 10 and 100 feet.

A salient feature of the track spectra reported here is the existence of pronounced peaks, particularly in the jointed rail spectra. The peaks correspond to the fundamental frequency corresponding to the standard 39 foot rail and all of its harmonics. This phenomena, considered in some depth in reference [17], is a result of the fact that as rail becomes "service bent" it tends to assume low points at the joints. This is primarily characteristic of jointed rail but also appears in continuous welded rail. This periodic characteristic of the track has often been modeled as a rectified sine wave for analytical purposes. A curious point is the appearance of side lobes on the peaks in the jointed rail left surface

spectrum. These peaks may be the result of some "ballast memory" as described in reference [17]. Ballast memory refers to periodicities in the roadbed ballast that are eventually reflected in the track irregularities. A final point worth noting is that the peaks in the centerline spectra are significantly less pronounced than in the corresponding left surface. This is due to the fact that in the U.S. the rail is laid in an offset fashion such that a joint in the left rail corresponds to the midpoint of the right rail. This tends to cancel the periodic vertical irregularity reflected at the centerline.

Table 4-1 contains a summary of the RMS deviations for the four separate measurements. The values in this table represent the positive square root of the integral of the corresponding uncompensated PSD's over the entire frequency range shown in the figures. Note that these values are based on the original chordal

Table 4-1. RMS Values of Four Track Surface Measurements

MEASUREMENT	RMS VALUE (IN.)
Left Surface, CWR	.043
Centerline, CWR	.039
Left Surface, Jointed	.099
Centerline, Jointed	.0833

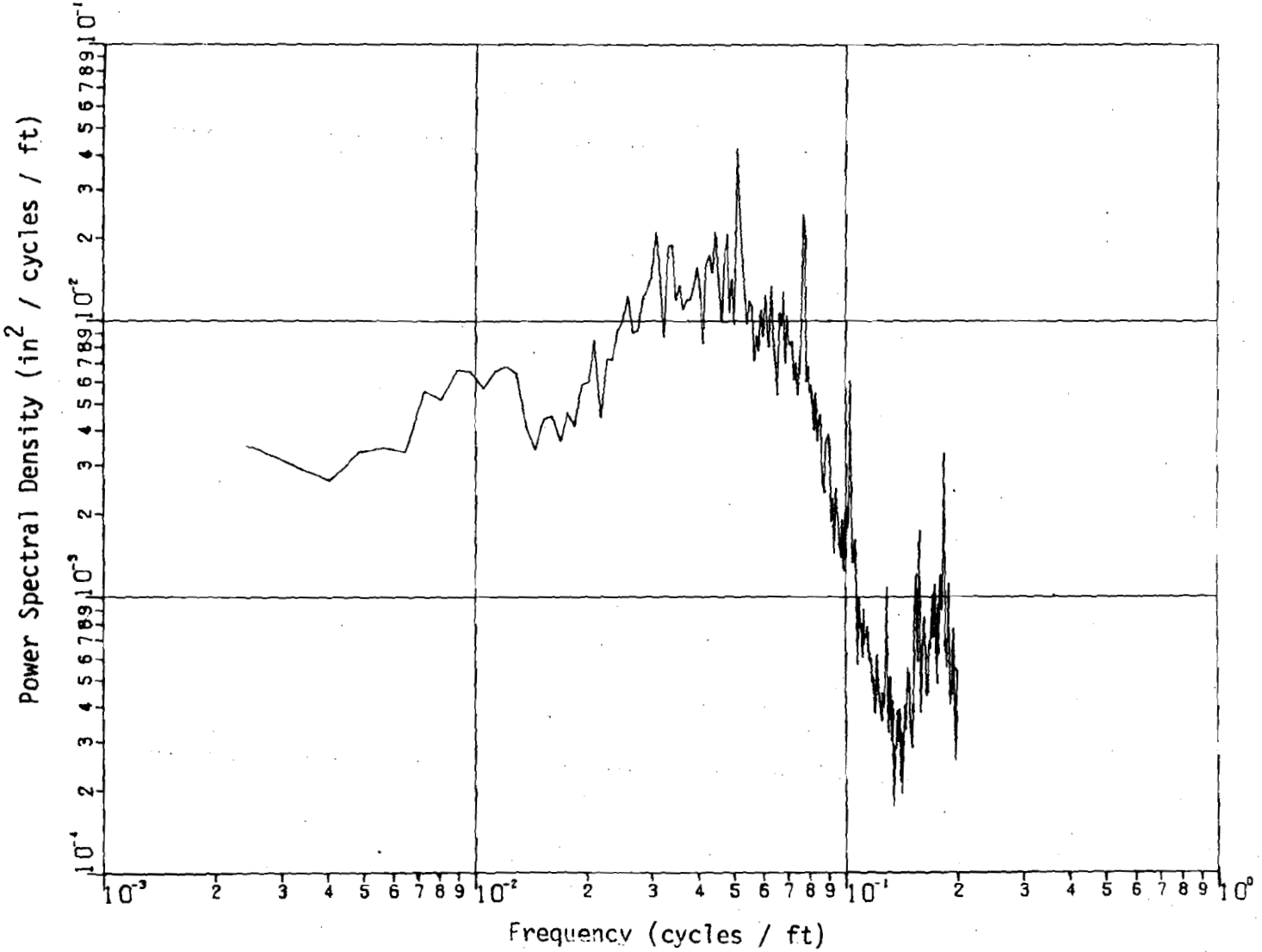

Figure 4-1 Uncompensated PSD of the Left Surface Measurement, CWR

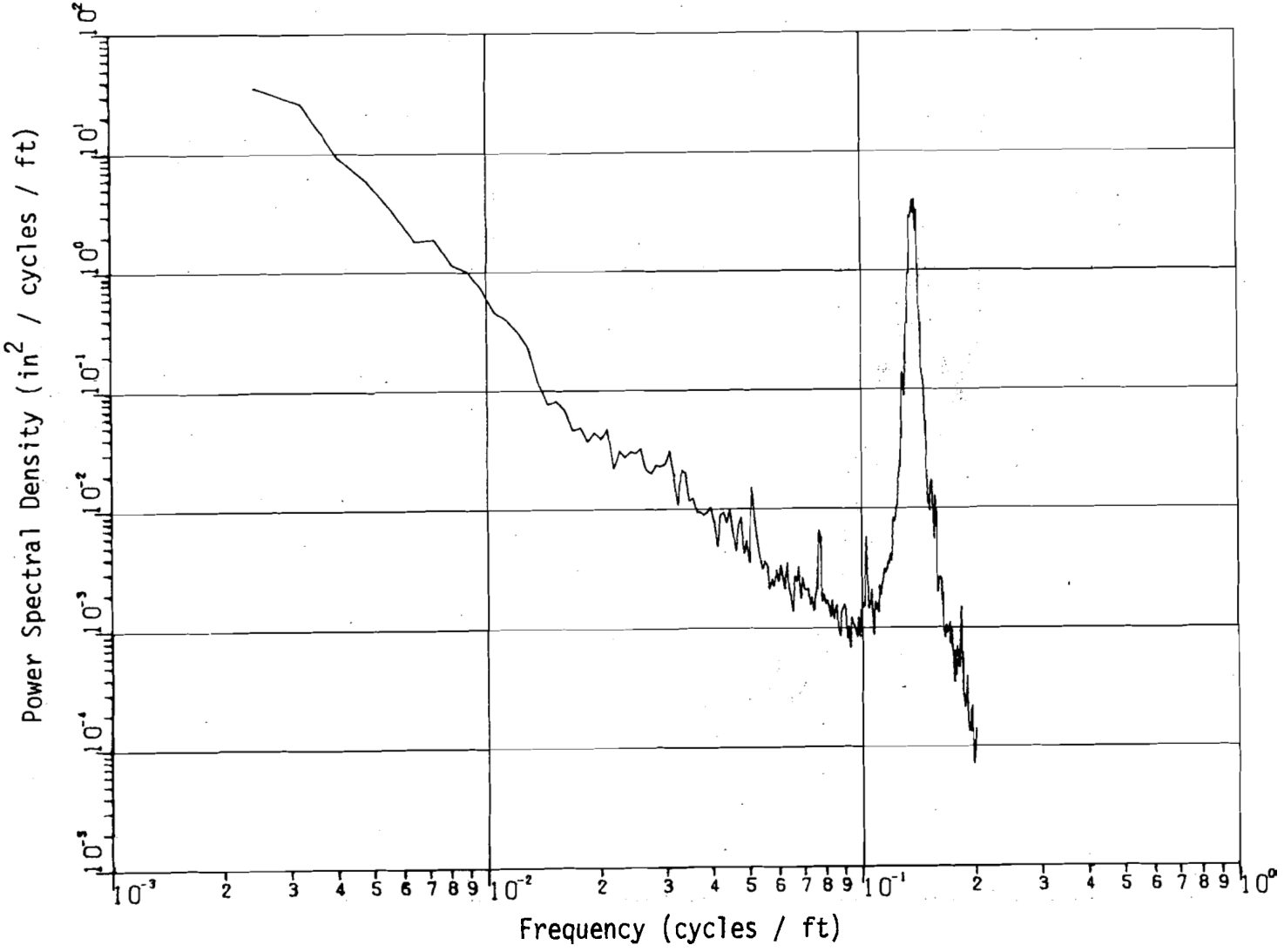

Figure 4-2 Compensated PSD of the Left Surface Measurement. CWR

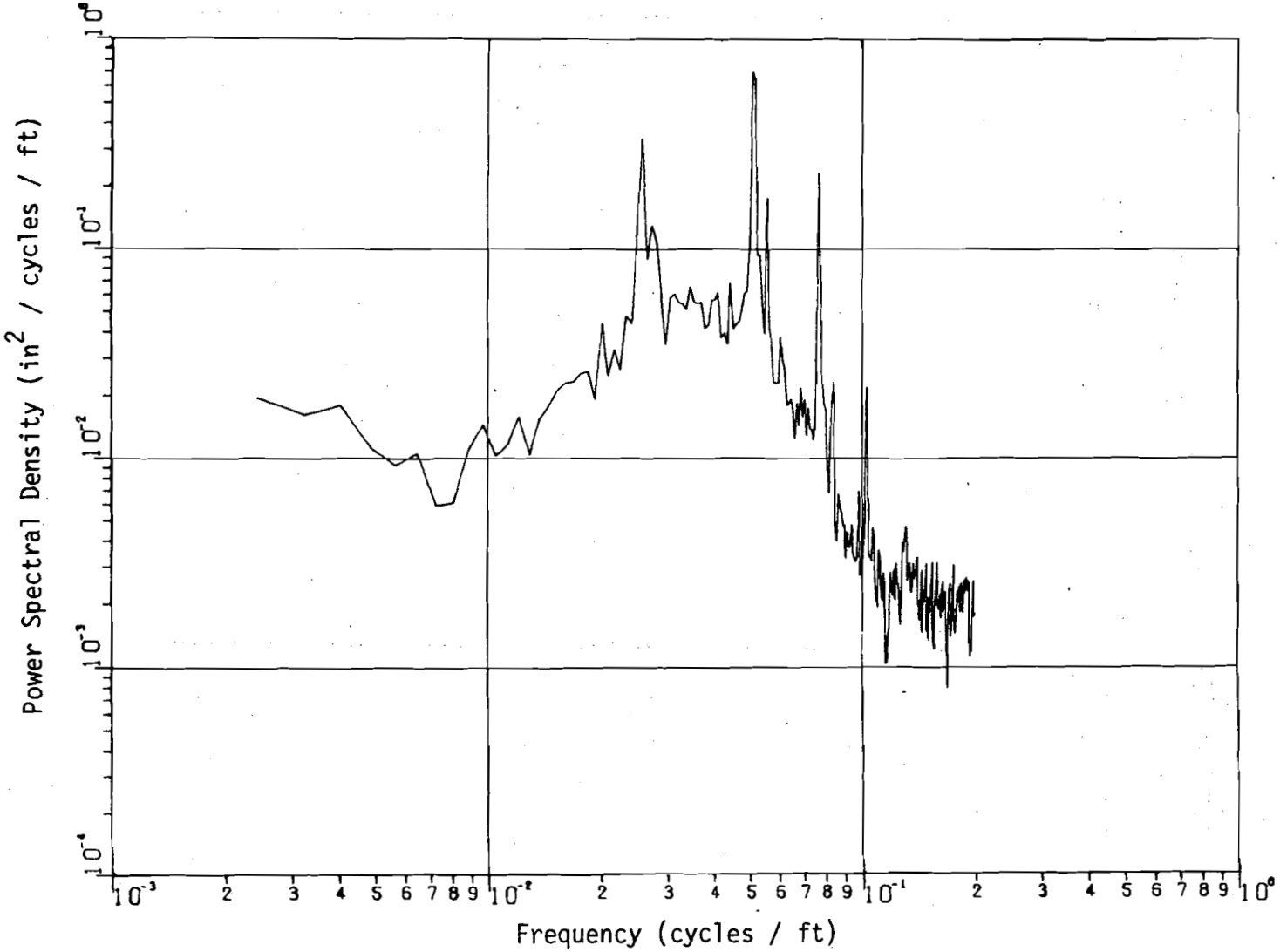

Figure 4-3 Uncompensated PSD of the Left Surface Measurement, Jointed Rail

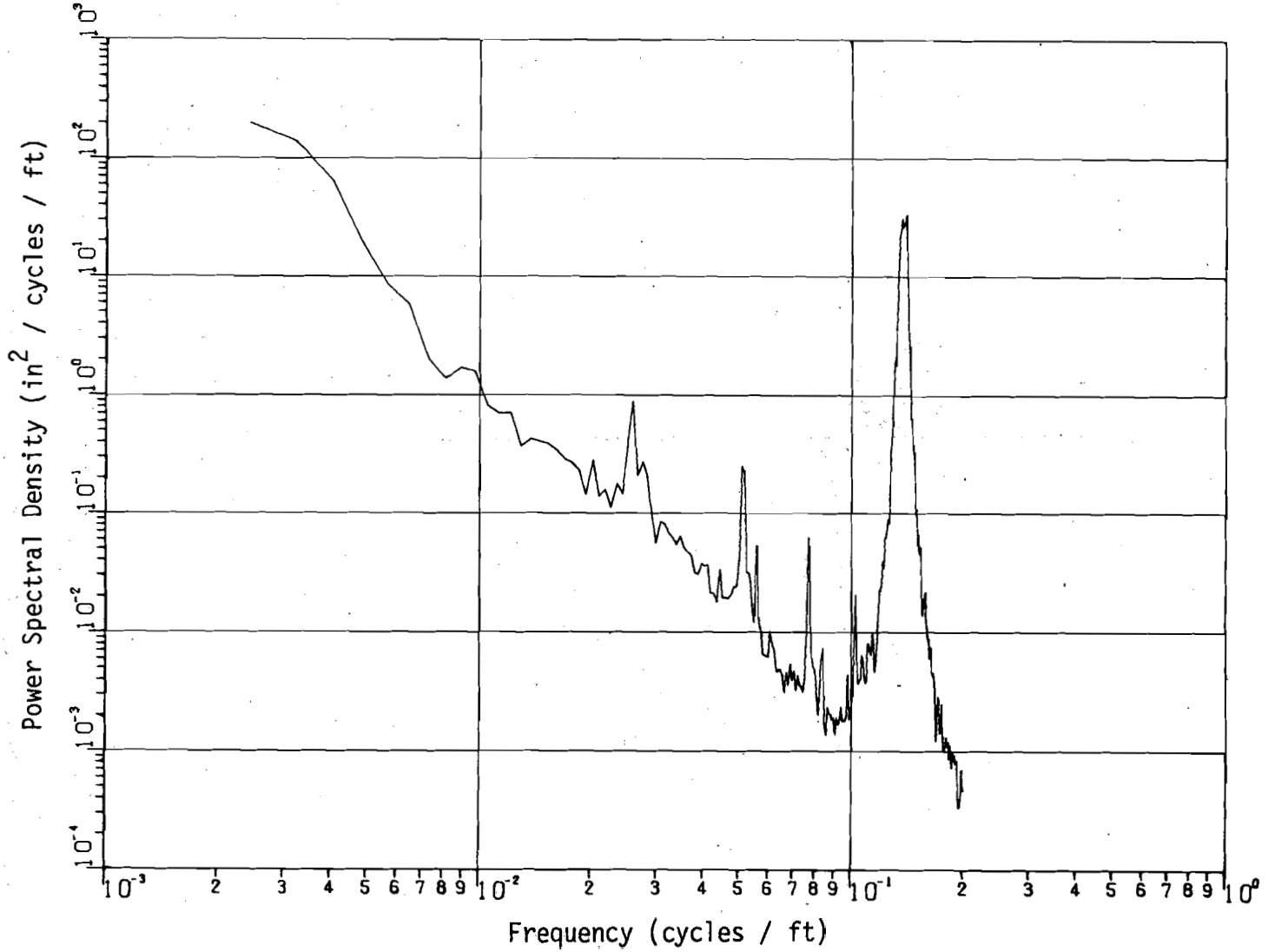

Figure 4-4 Compensated PSD of the Left Surface Measurement, Jointed Rail

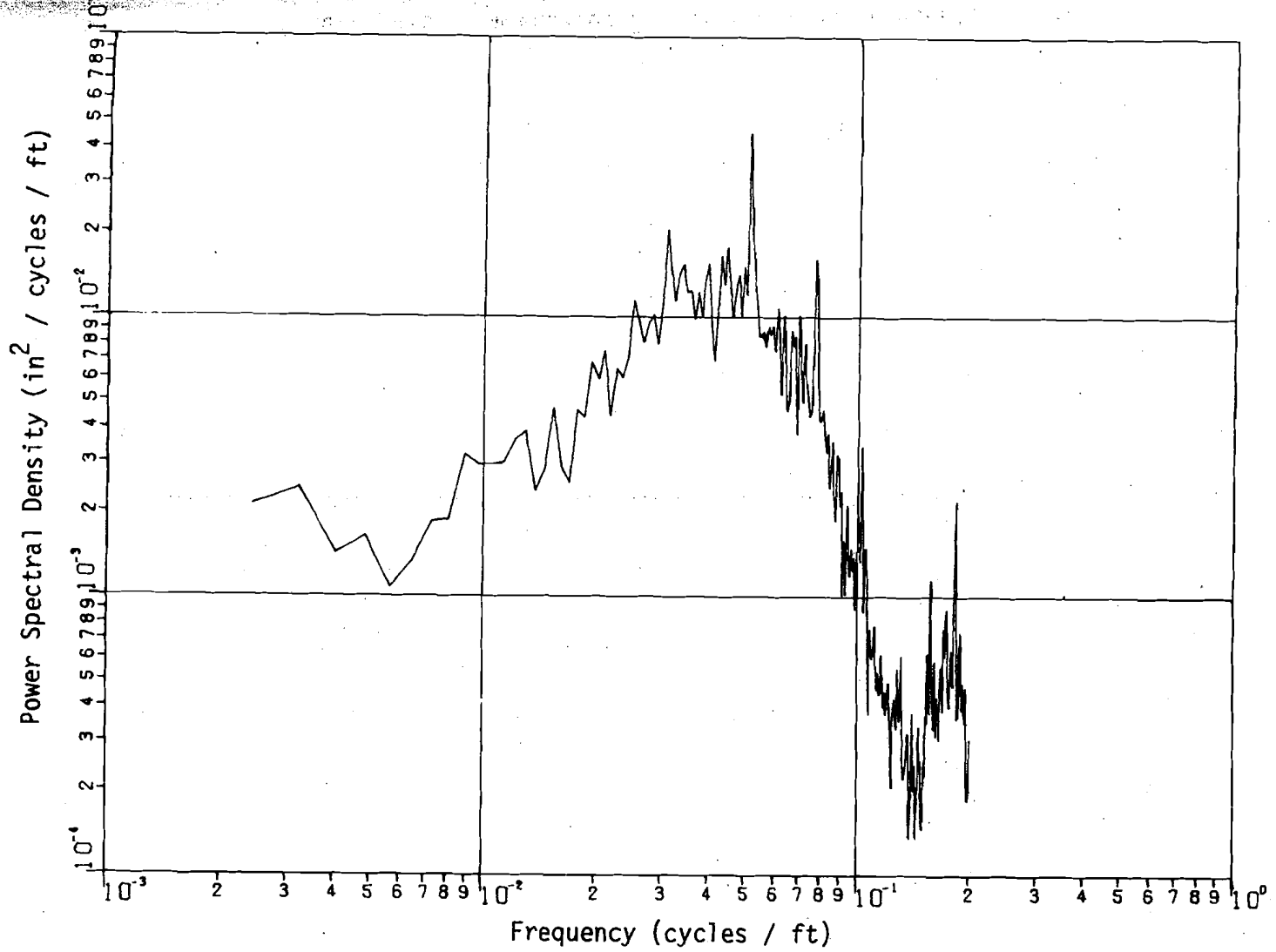

Figure 4-5 Uncompensated PSD of the Track Centerline, CWR

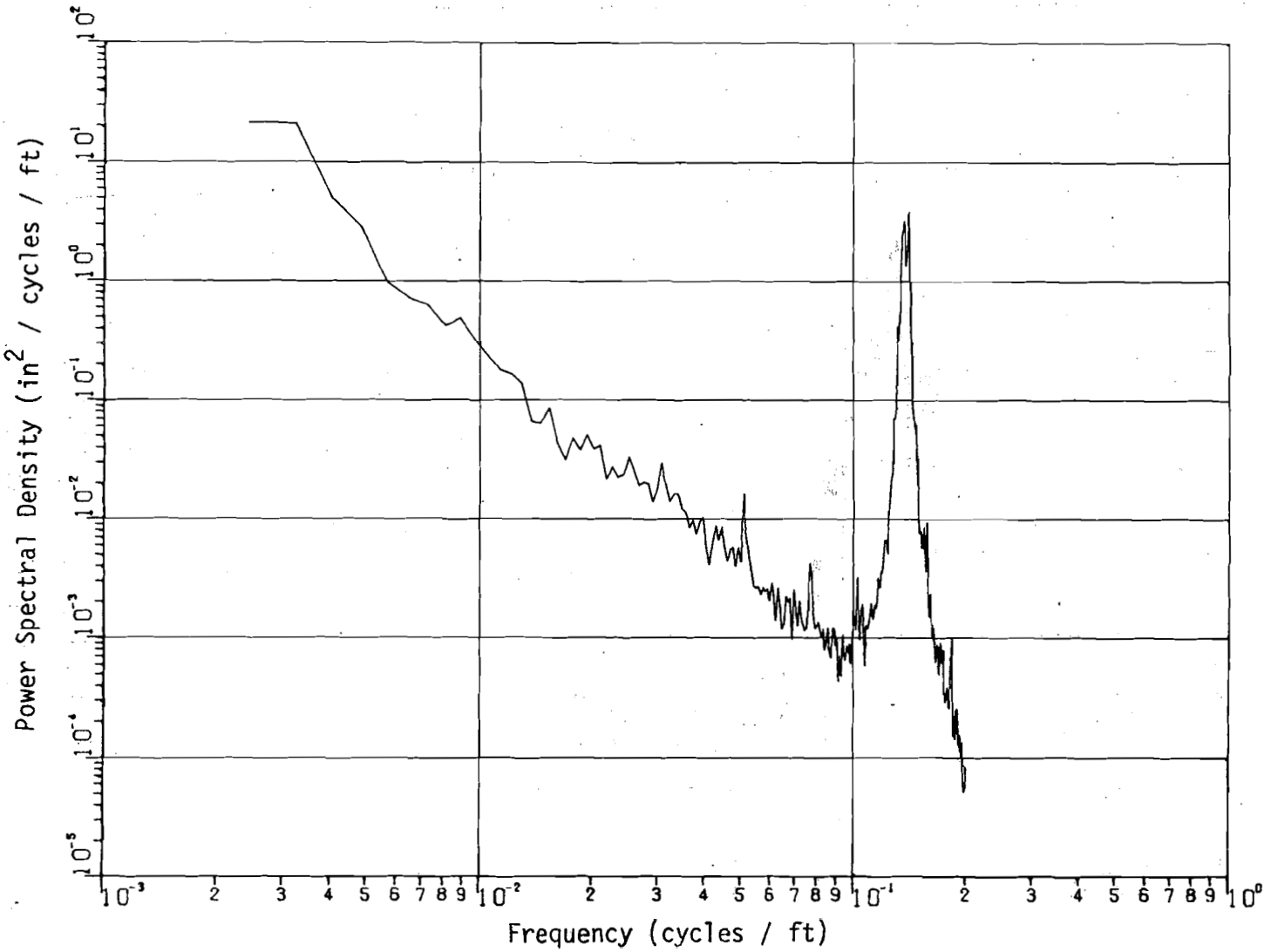

Figure 4-6 Compensated PSD of the Track Centerline, CWR

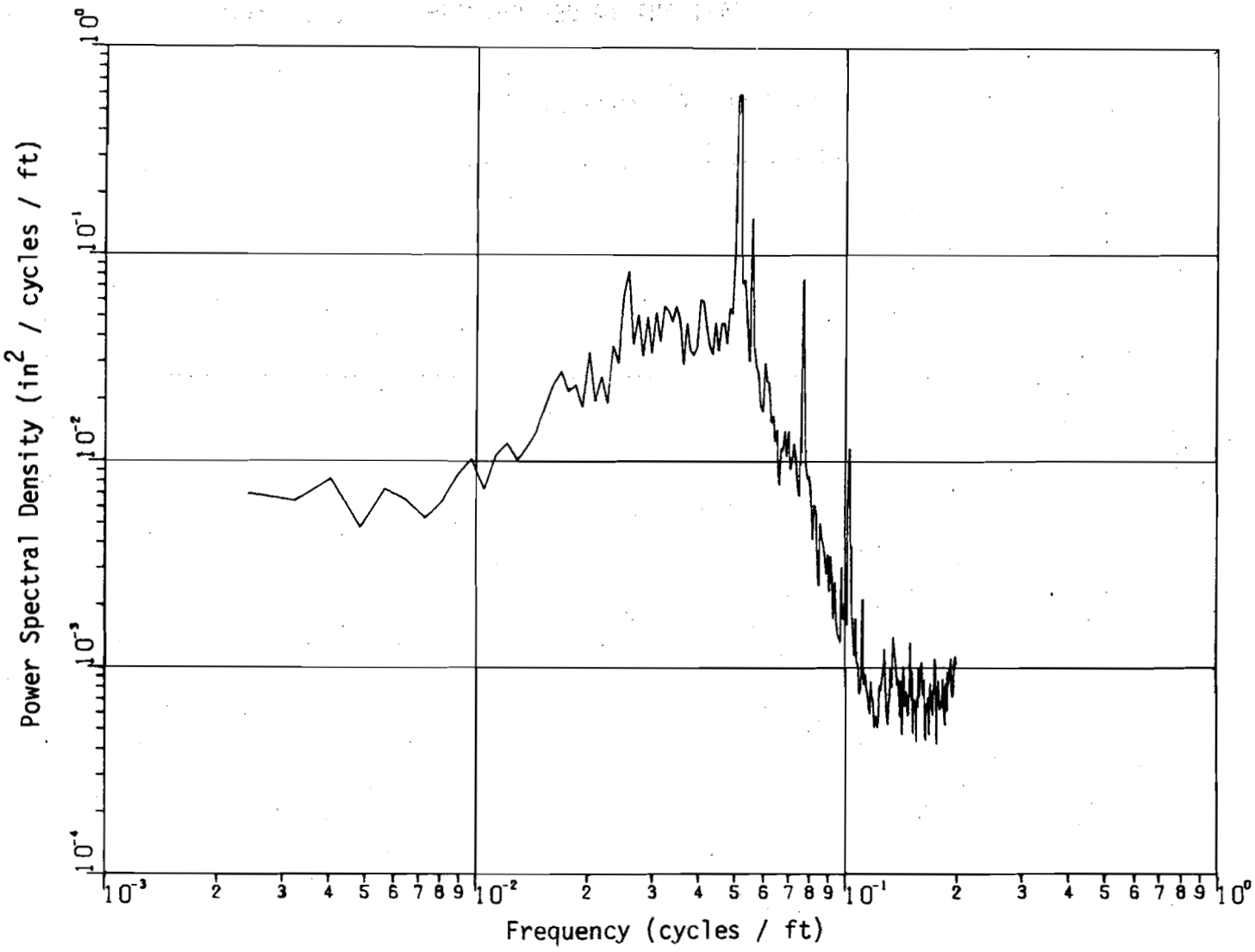

Figure 4-7 Uncompensated PSD of the Track Centerline, Jointed Rail

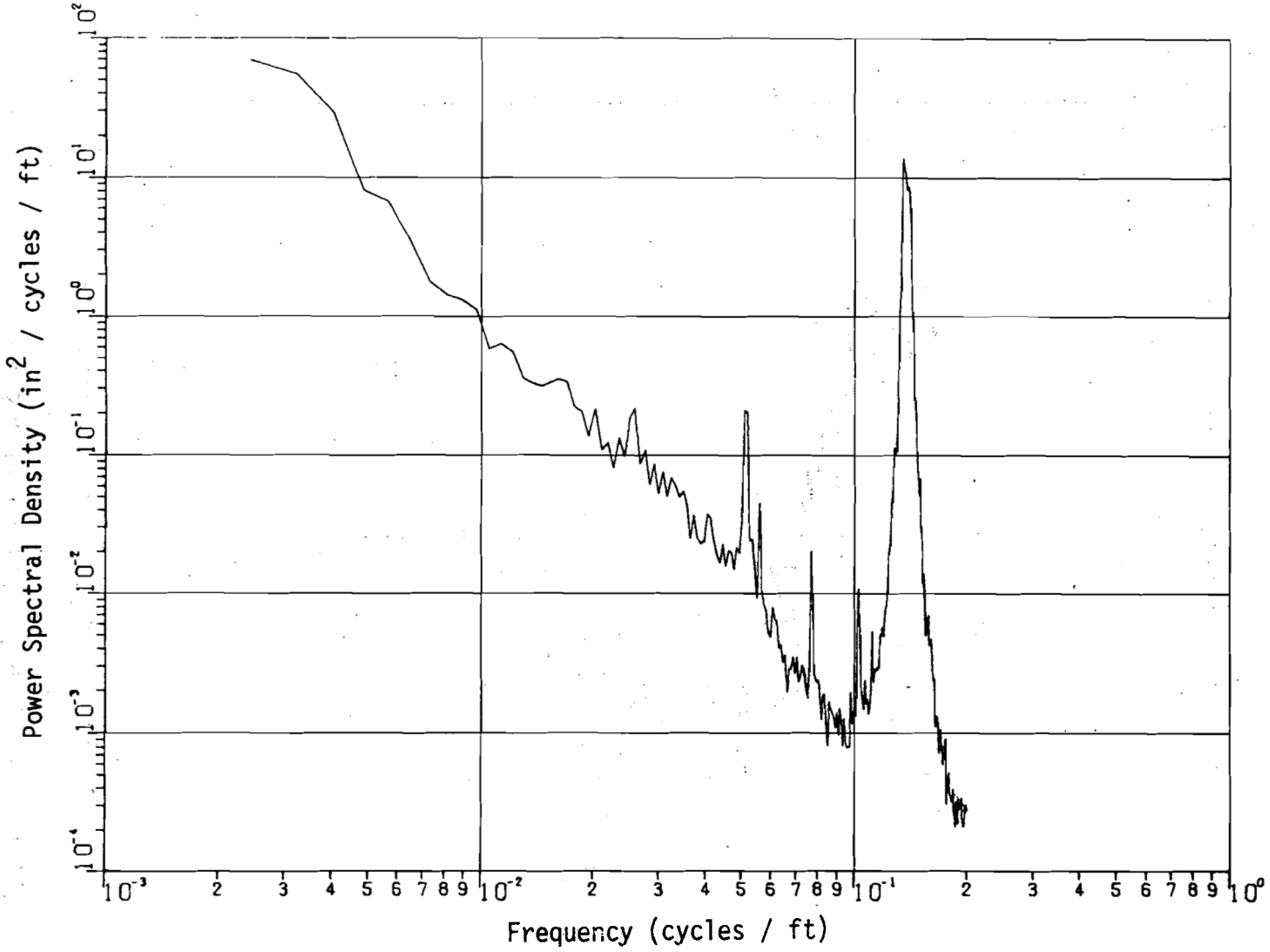

Figure 4-8 Compensated PSD of the Track Centerline, Jointed Rail

measurement data. This is because of the uncertainties associated with the compensated spectra. Specifically, the compensated spectra exhibit huge peaks at frequencies of 0.0 and 0.138 cycles/foot which contain no useful information. Any useful information to be gained by integration of the compensated spectra would be completely obscured by integration of these spurious peaks. The original chordal information, on the other hand, yields a perfectly valid relative measurement of RMS deviation. From this viewpoint, then, Table 4-1 reveals that the RMS deviations of the jointed rail are roughly twice that of the continuous welded rail.

Vehicle Response

The vehicle used in this phase of the TDOP tests is a standard 70 ton capacity mechanical refrigeration car equipped with ASF A-3 Ride Control trucks. This vehicle has been described briefly in Chapter 2.

In this report the response of the test vehicle is examined for four different vehicle/track configurations. These four configurations are defined in Table 4-2.

Table 4-2. Vehicle/Track Test Configurations and Codes

CODE	CONFIGURATION
A	Empty Car @ 58 ft/sec over CWR
B	Empty Car @ 100 ft/sec over CWR
C	Loaded Car @ 64 ft/sec over Jointed Rail
D	Loaded Car @ 100 ft/sec over CWR

The response of the vehicle is examined in terms of two response variables: the vertical acceleration of the car body center-of-gravity (c.g.) and the vertical acceleration of the car body at a point centered over the front bolster. For configurations B and D two additional response variables are monitored: the vertical accelerations of the car body at a point centered over the rear bolster and the midpoint between the rear truck sideframes. These latter variables are examined in order to isolate the truck suspension (bolster-sideframe) dynamics. All response variables are presented in terms of the corresponding power spectral density estimates computed from the experimental data. The results for configuration A are presented in this chapter. The results for the other configurations are presented in the next chapter where they are compared to the corresponding results predicted by the linear model.

The spectra for the accelerations of the car body c.g. and front end for configuration A are shown in Fig. 4-9 and Fig. 4-10 respectively. In all cases, the analog transducer signals were filtered at 20 Hz and sampled at a rate of 200 Hz. This 20 Hz filtering is readily evident in all the computed spectra of vehicle response.

A distinct feature of Fig. 4-9, the PSD of the car body c.g., is the large number of defined "dropouts". These dropouts, as discussed in Appendix B, are due to the filtering effects of the

trucks and the car body itself. The vehicle speed, combined with the wheelbase of the trucks and the distance between the front and rear truck centers, defines two fundamental frequencies given by

$$f_o = \frac{V}{2\ell} \tag{4-5}$$

where V is speed and ℓ is the prescribed distance. Any track input at either of these two fundamental frequencies or at any of the odd harmonics will be filtered out at the car body c.g. and only excite pitching of the trucks or car body. For this particular test configuration the speed is 58 ft/sec, the truck wheelbase is 5.66 feet, and the bolster separation front to rear is 45.72 feet. These parameters define fundamental frequencies of 5.12 Hz and 0.63 Hz. Since the car body c.g. is located near the geometric center, dropouts are clearly evident in the spectra at these fundamental frequencies and at all the odd harmonics.

The PSD of the acceleration of the front end is displayed in Fig. 4-10. As expected, the filtering effect of the trucks is distinctly evident at 5.1 Hz and 15.3 Hz. Note also the number of less pronounced dropouts at the odd harmonics of the fundamental frequency associated with the car body. This may be explained in terms of the separate contributions of car body pitch and bounce to the motion of the front end. Examination of Fig. 2-6 through Fig. 2-8 may be helpful in visualizing the nature of this combination. At the car body fundamental frequency and the odd harmonics no contribution to the vertical motion of the front end is made by bounce of

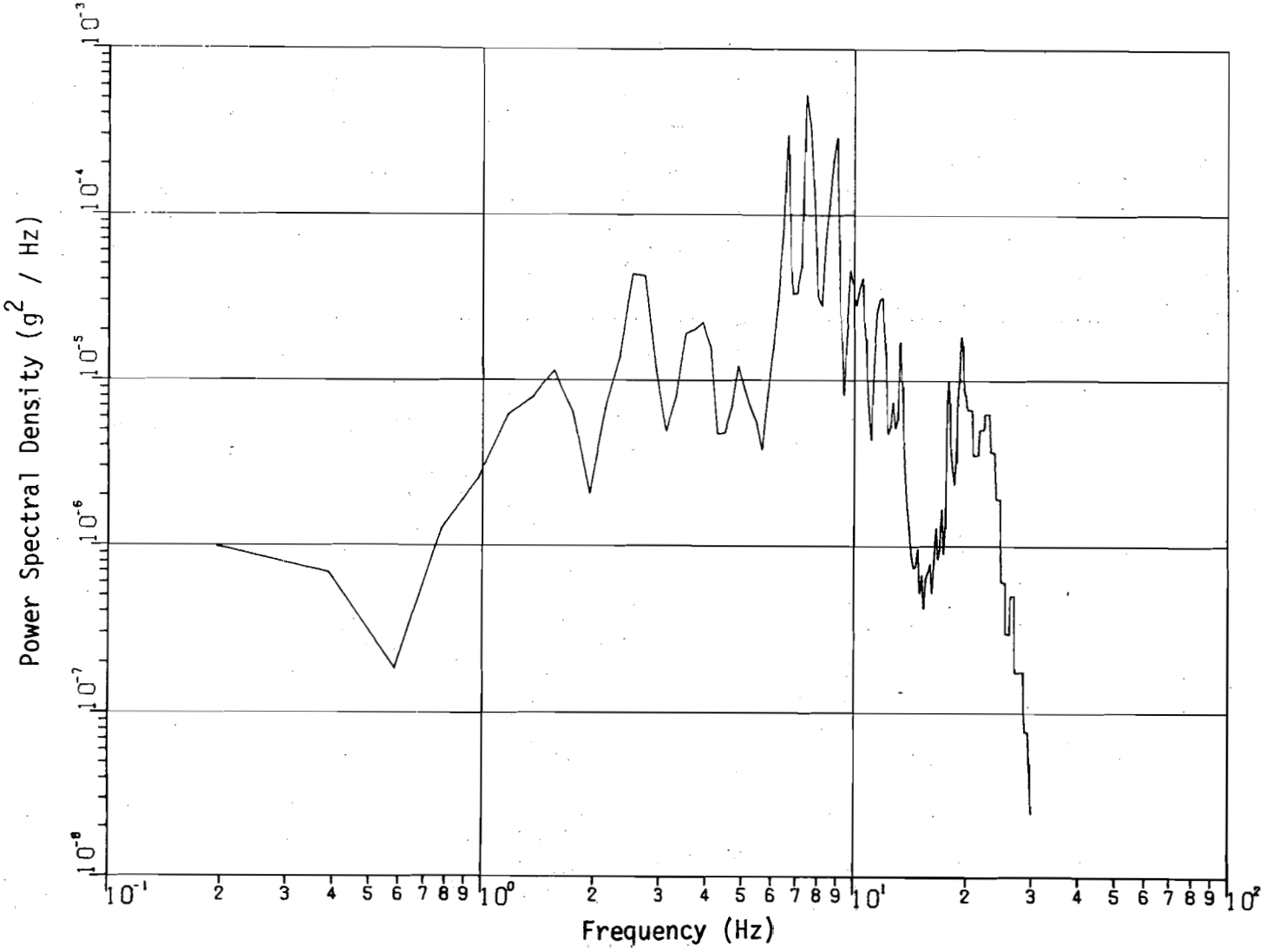

Figure 4-9 Car Body C.G. Acceleration PSD (Test Configuration A)

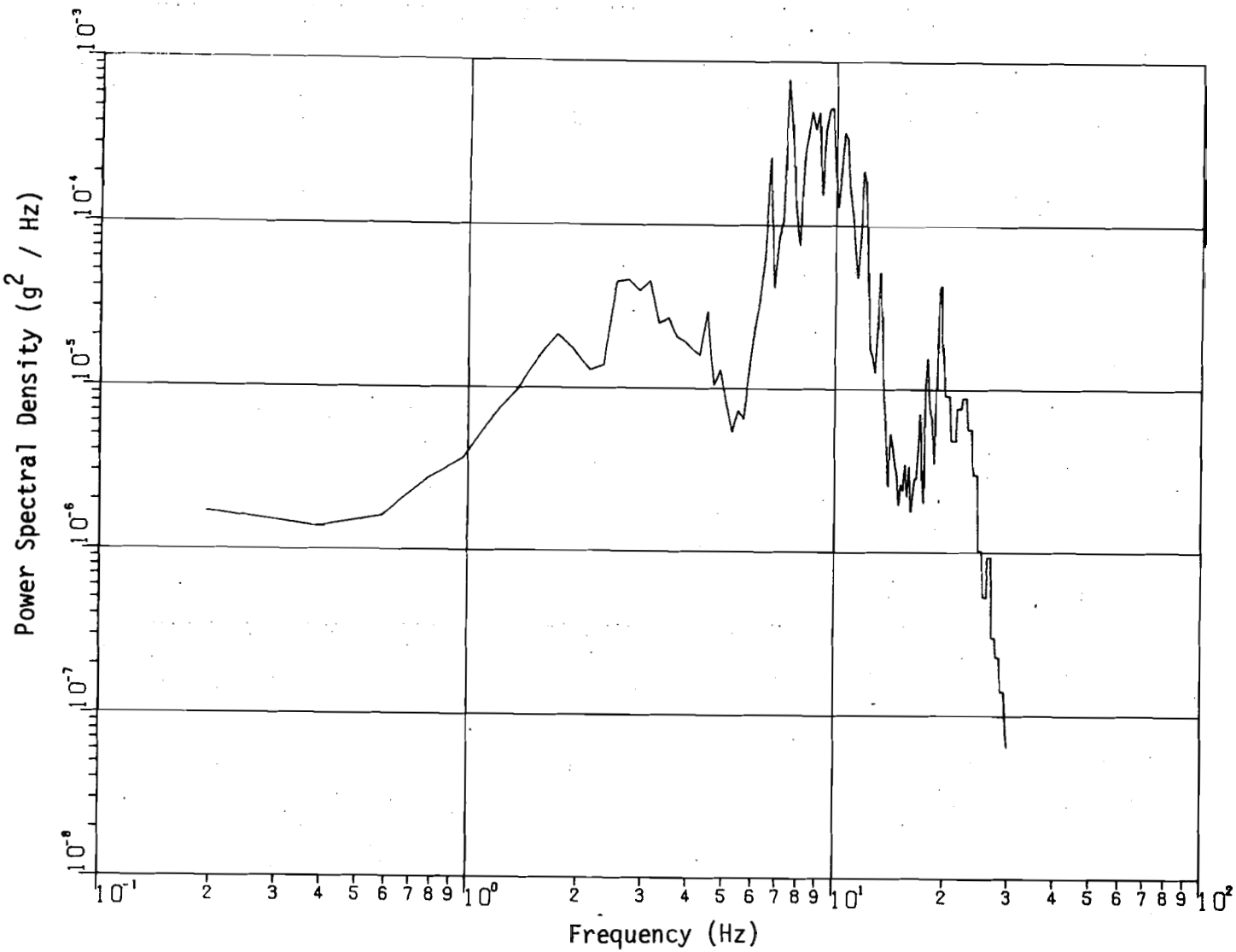

Figure 4-10 Car Body Front End Acceleration PSD (Test Configuration A)

the car body. Hence, dropouts of somewhat lesser magnitude would be expected and are apparent in Fig. 4-10.

The response of the vehicle for all configurations is summarized in Table 4-3 in terms of RMS values of acceleration. These RMS values were computed by integrating the corresponding PSD's over the indicated frequency ranges. Note that the car body front end consistently experiences higher levels of acceleration than the c.g.. This is to be expected since the c.g. of the car sees no contribution from pitch motion. Also, note that the empty vehicle exhibits higher acceleration levels than the fully loaded vehicle. This may be expected because the fully loaded vehicle induces more action in the truck suspension. Thus, the suspension more effectively filters the track input. In other words, the larger mass of the system results in a lower natural frequency and a correspondingly faster roll off in response.

Conclusion

This chapter describes the field tests that provided data for this research and lays the groundwork, in terms of experimental results, for the next chapter. The track input spectra, computed from measurements of the test track, are developed and discussed in detail. The random track irregularities yield spectra that exhibit a simple exponential relationship to frequency. Periodic track irregularities are evidenced by distinct peaks in the track spectra. Representative

vehicle response spectra are also presented and discussed. The filtering effects of pitching of the car body and trucks is clearly evident in the acceleration spectra shown. The track input and vehicle response data is summarized for all track/vehicle configurations in terms of RMS values.

Additional experimental results are presented in the next two chapters. Car body and truck acceleration spectra for different test configurations are presented in the next chapter in conjunction with results predicted by the linear model.

Table 4-3. RMS Values of Car Body Accelerations (g's) for All Configurations

CONFIGURATION	FREQUENCY RANGE (Hz)	C.G.	FRONT END
A	.2 - 1.0	.001	.002
B		.002	.003
C		.002	.004
D		.002	.003
A	1.0 - 10.	.032	.048
B		.038	.050
C		.027	.043
D		.019	.029
A	10. - 20.	.014	.033
B		.019	.038
C		.012	.012
D		.023	.028
A	.2 - 20.	.035	.058
B		.043	.063
C		.030	.045
D		.030	.040

Chapter 5

LINEAR MODEL VALIDATION

Introduction

In this chapter, the response of the linear model of Chapter 2 to the track input spectra of Chapter 4 is presented. These results, in the form of acceleration PSD's,are compared to corresponding results computed from experimental data in order to evaluate the model.

The comparison of analytical and experimental results is done in several ways. Experimental and analytical spectra and RMS levels for the car body acceleration are compared. In addition, the truck suspension performance is examined. The coherence and transfer functions of Chapter 3 are used to compute a truck suspension transfer function based on experimental data for both the empty and fully loaded vehicle. The results are compared with those predicted by the linear model. Finally, some additional experimental results relating to vehicle response are presented. These are not directly related to the linear model validation problem, but are included to demonstrate some additional aspects of the utility of spectral techniques.

Vehicle Parameters

The baseline parameters for the linear model of the S.P. refrigerator car are listed in Table 5-1. The mass properties of

the vehicle were estimated from data provided with the TDOP data tapes and from test vehicle descriptions in [3]. The mass and suspension stiffness properties of the 70-ton trucks were provided by the Harmonic Roll Series Volume 2 [8]. This reference presents the results of extensive laboratory testing of the type of truck used on the S.P. experimental test vehicle. The mass properties and spring constants come directly from this document.

The truck suspension damping is based on the computation of the expression in (2-4). The force level in the truck suspension due to the friction snubbers was obtained from laboratory measurements at various levels of sinusoidal excitation [8]. The results indicate a consistent level of 3120 lb. force per sideframe due to dry friction. The S.P. test vehicle was equipped with displacement transducers at each sideframe to monitor the relative displacement through the suspension. Examination of this data for all four test configurations revealed excursions rarely larger than 0.1 inches. When these values of friction force level and displacement combined with a frequency estimate of 2.5 Hz were used in equation (2-4), a damping value of 60,700 lb-sec/ft per truck was obtained.

The values of track structure spring rate and damping are those used by Ahlbeck et. al. in reference [6].

Model Response Computations

The linear model response is computed in terms of the power

Table 5-1 Baseline Parameters for the S.P. Refrigerator Car

PARAMETER NAME		EMPTY CAR	FULLY LOADED CAR
M_c	slugs	2233.0	6294.7
I_c	slug-ft^2	826,291.6	1,538,721.0
L_F	ft	24.57	21.76
L_R	ft	21.15	23.96
K_{FS}	lb/ft	531,600	Same
K_{RS}	lb/ft	531,600	Same
C_{FS}	lb-sec/ft	60700	Same
C_{RS}	lb-sec/ft	60700	Same
M_{FT}	slugs	247.4	Same
I_{FT}	slug-ft^2	1669.6	Same
L_{FT_1}	ft	2.83	Same
L_{FT_2}	ft	2.83	Same
K_{FT_1}	lb/ft	4.8×10^6	Same
K_{FT_2}	lb/ft	4.8×10^6	Same
C_{FT_1}	lb-sec/ft	3600	Same
C_{FT_2}	lb-sec/ft	3600	Same
M_{RT}	slugs	247.4	Same
I_{RT}	slug-ft^2	1669.6	Same
L_{RT_1}	ft	2.83	Same
L_{RT_2}	ft	2.83	Same
K_{RT_1}	lb/ft	4.8×10^6	Same
K_{RT_2}	lb/ft	4.8×10^6	Same
C_{RT_1}	lb-sec/ft	3600	Same
C_{RT_2}	lb-sec/ft	3600	Same

spectra of the acceleration of the car body center-of-gravity and the front end of the car directly above the bolster centerplate. This response is computed for three track/vehicle configurations: the (1) empty vehicle traveling at 100 ft/sec over continuous welded rail (CWR), the (2) fully loaded vehicle traveling at the same speed over the same test track, and the (3) fully loaded vehicle traveling at 64 ft/sec over jointed rail. In all cases, the corresponding spectra reduced from experimental data are presented for purposes of comparison.

The response of the model is computed using the relationship

$$P_O(f) = |H(f)|^2 P_I(f) \qquad (5\text{-}1)$$

where $P_I(f)$ is the vertical track input spectrum. This input spectrum is one of the two track spectra from Chapter 4. The frequency range of the response is limited to that of the input spectrum; in this case, a spatial frequency range of about 3.0×10^{-3} cycles/ft to 1.1×10^{-1} cycles/ft. This range translates to 0.3 Hz to 11.0 Hz at a vehicle speed of 100 ft/sec and to approximately 0.2 Hz to 7.0 Hz at a speed of 64 ft/sec. Consequently, the model response is presented only over the limited frequency range dictated by the track spectrum range and the vehicle speed. The corresponding experimental results are presented for the entire available frequency range, limited by the 20 Hz filter cutoff frequency.

Comparison of Vehicle Acceleration Results

A typical transfer function magnitude is shown in Fig. 5-1(a) for the acceleration of the front end of the fully loaded car to a displacement input. Note that this transfer function is for a heavily damped system. As mentioned previously, the relative displacement in the test truck suspension proved to be quite small, i.e., on the order of 0.1 inches. For purposes of comparison the model response is also computed for a much less heavily damped suspension. A truck suspension damping of 6070 lb-sec/ft was chosen, corresponding to an excitation level of 1.0 inches. The front end acceleration transfer function for this less heavily damped system is shown in Fig. 5-1(b). Note the lower magnitude at higher frequencies due to the lower level of damping and the associated faster roll off. Also note that the response is identical below 1 Hz.

The test vehicle response is displayed in Fig. 5-2 through Fig. 5-4 in terms of acceleration spectra. The model response for both nominal and low suspension damping is sketched over the corresponding plot of experimental results. The comparative results are summarized in Table 5-2 in terms of RMS acceleration levels. These RMS values were computed from the corresponding acceleration spectra.

Note that the response of the model in the lowest frequency range is consistently higher than the actual measured response. The

model would be expected to be most accurate at these very low frequencies which are well below the resonant frequencies of the system. This observation tends to indicate that the input spectra may be in error. At a speed of 100 ft/sec frequencies below 1.0 Hz correspond to wavelengths greater than 100 ft and such wavelengths are difficult to measure (particularly with a 14.5 ft chord). Also, the experimental spectra indicate that no significant car body dynamics are excited at these low frequencies. Based upon these observations, it appears that the track input spectra might be better described by a leveling off or even bending back over at very low frequency.

At the upper end of the frequency spectrum poor agreement again results between the model response and the actual response. A primary factor contributing to the discrepancy is probably oversimplification of the model. Modes such as car body bending as well as other higher frequency dynamics are not included in the model. It should be noted that the resonant frequencies associated with the rail spring rate and damping turned out to be higher than the experimental filter cutoff frequency of 20 Hz. The car body transfer functions were computed and revealed no significant contribution from these modes in the frequency range of interest.

Another factor to be considered is the actual resolution of the model spectra versus the experimental spectra. The resolution of the model response is a function of the analytical frequency

response which may be computed to virtually any degree of resolution. On the other hand, the resolution of the results computed from experimental data is degraded by the leakage problem discussed in Chapter 3. This is clearly apparent at the dropout frequencies where the power in adjacent frequency bands tends to "leak" and obscure the dropout in the experimental results.

One last point that must contribute to discrepancy is the inevitable presence of nonlinear effects. For example, in a particular frequency range, the friction snubbers in the truck sideframes may be sticking a large percentage of the time. This would lead to a higher level of car body response than would be predicted by the linear model since the suspension is "bound up" at these times. The presence and effects of specific nonlinearities can be quite difficult to ascertain. The deficiencies of the linear model, and the uncertainties associated with the track input spectra, are the primary causes of the discrepancies between the model and test vehicle response.

Regarding the model response, note that high damping of the truck suspension yields much better agreement with experimental results than does the lower damping in the midrange of the spectrum. In fact, in the midrange band, the highly damped linear model yields surprisingly good agreement with the actual response of the test vehicle. Examination of Table 5-2 reveals that, with proper adjustment of the truck suspension damping, the model response can

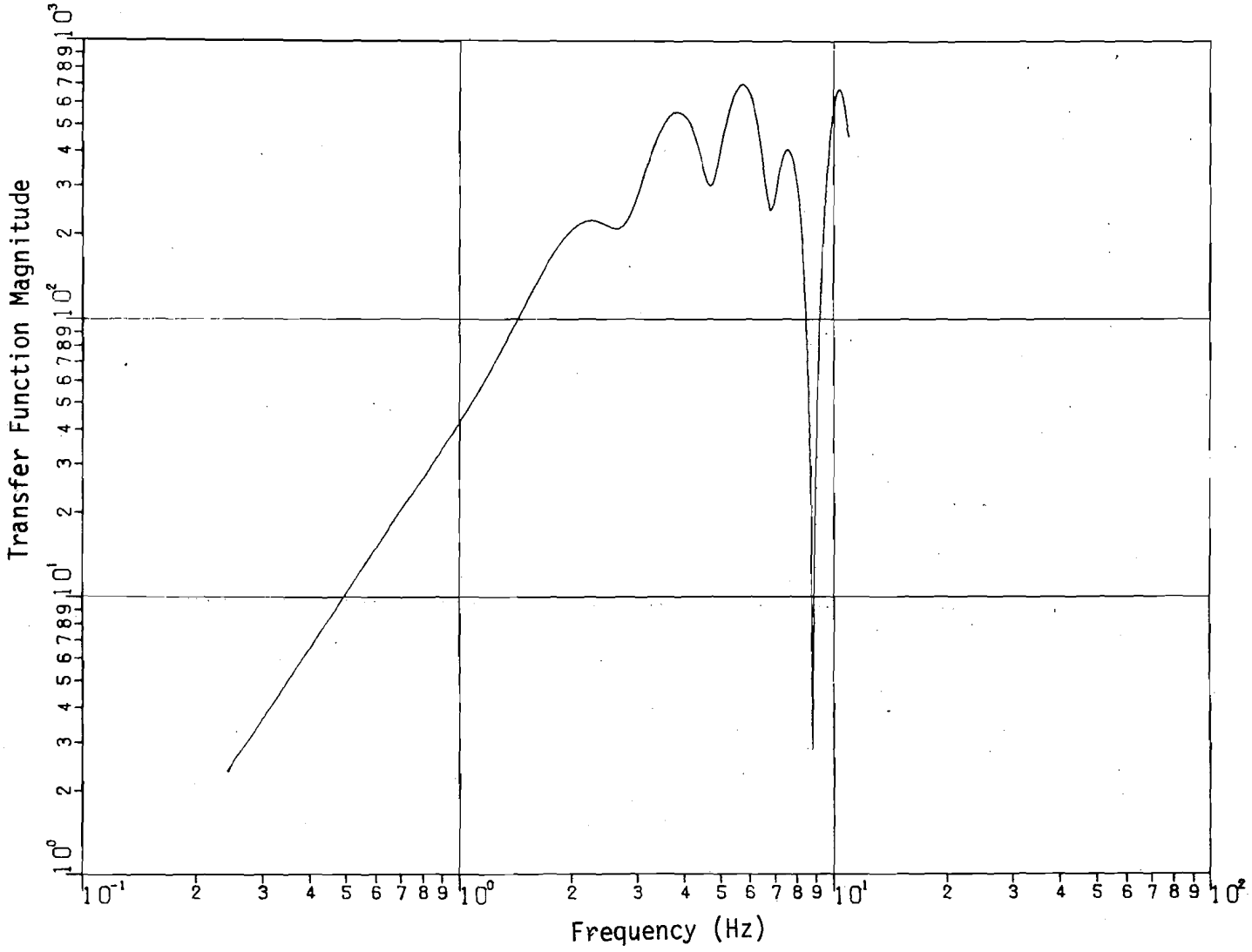

Figure 5-1 (a) Car Body Front End Transfer Function Magnitude for a Heavily Damped Truck Suspension

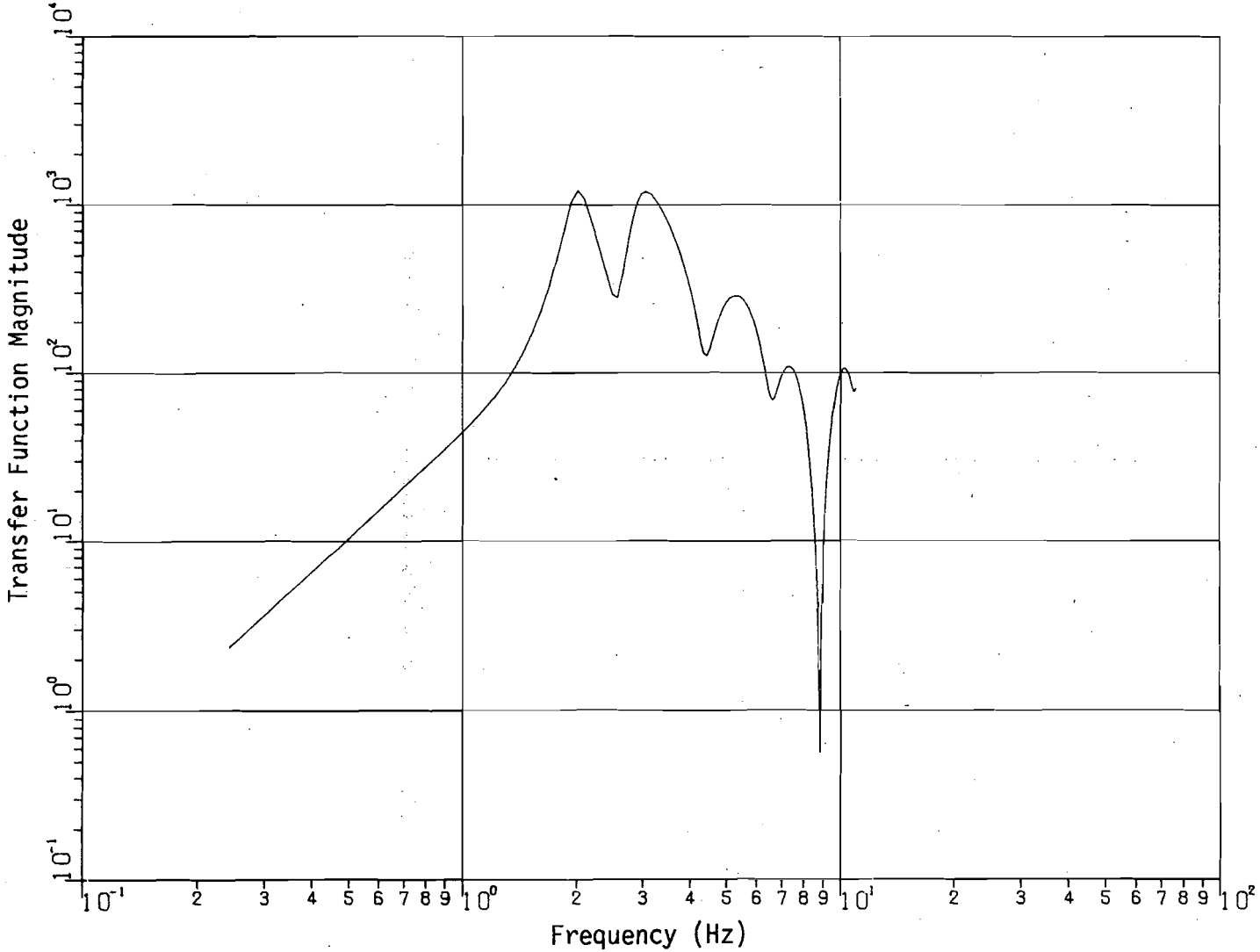

Figure 5-1 (b) Car Body Front End Transfer Function Magnitude for a Lightly Damped Truck Suspension

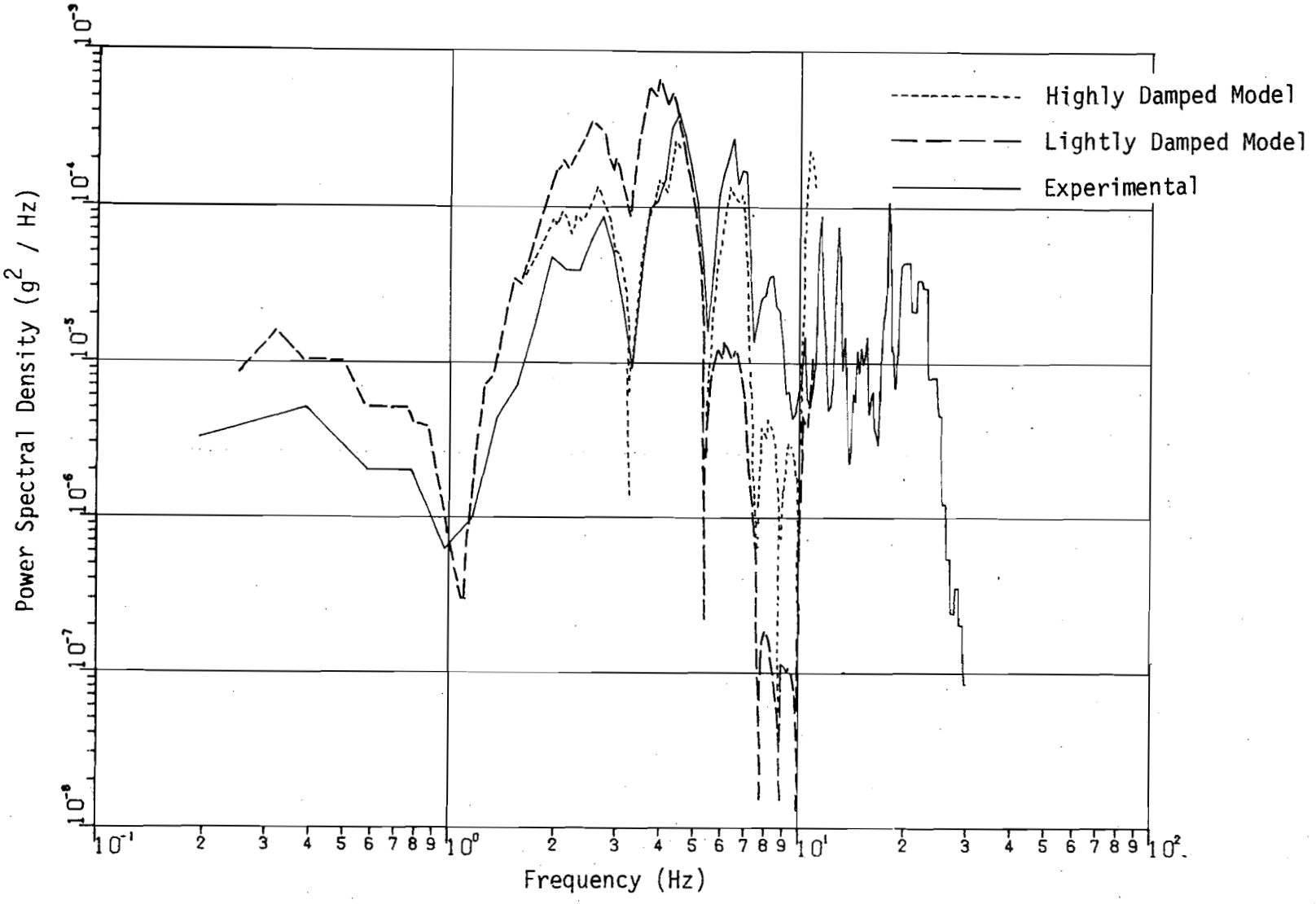

Figure 5-2 (a) Car Body C.G. Vertical Acceleration Spectra (Empty Vehicle Traveling at 100 ft/sec Over CWR)

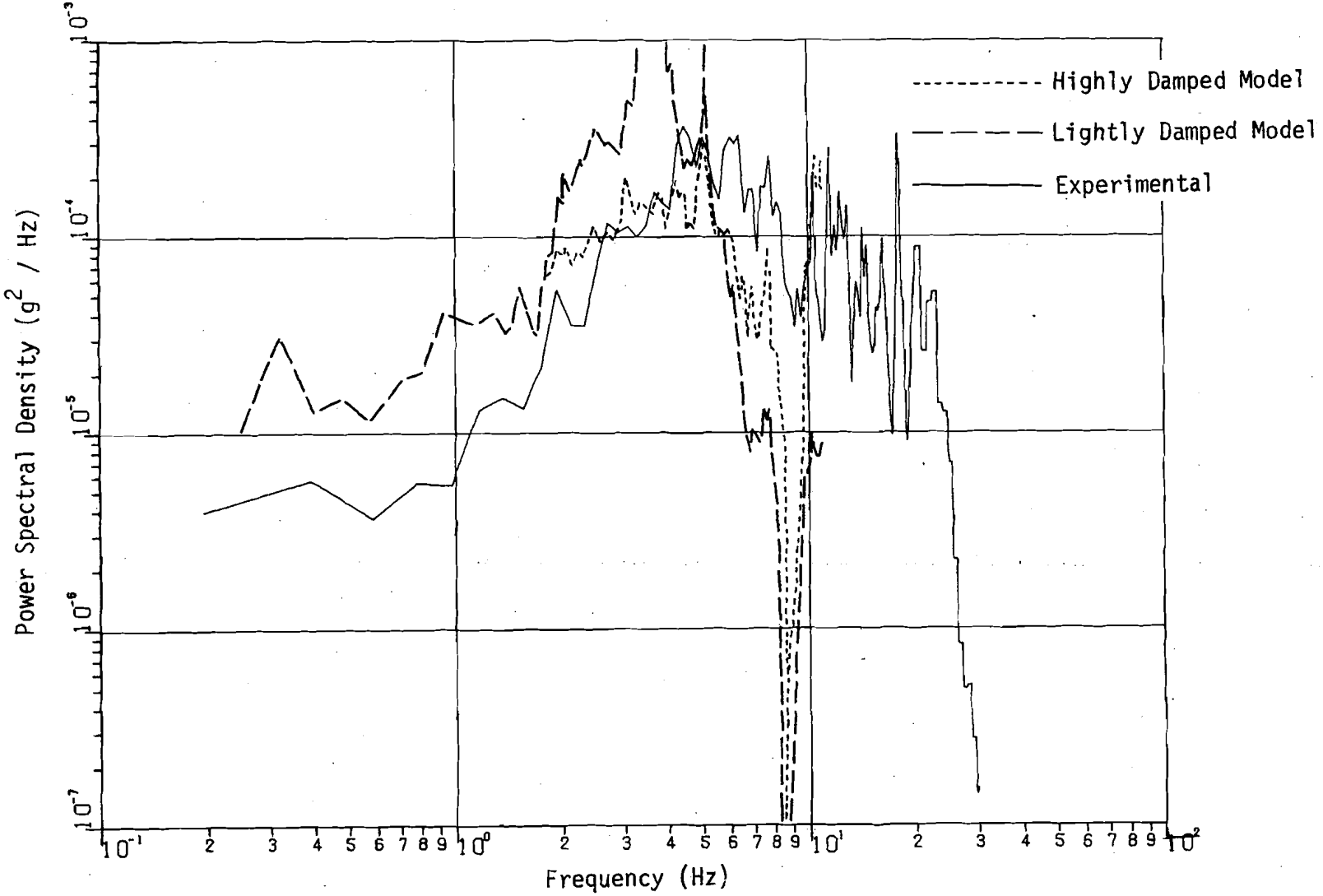

Figure 5-2 (b) Car Body Front End Vertical Acceleration Spectra (Empty Vehicle Traveling at 100 ft/sec Over CWR)

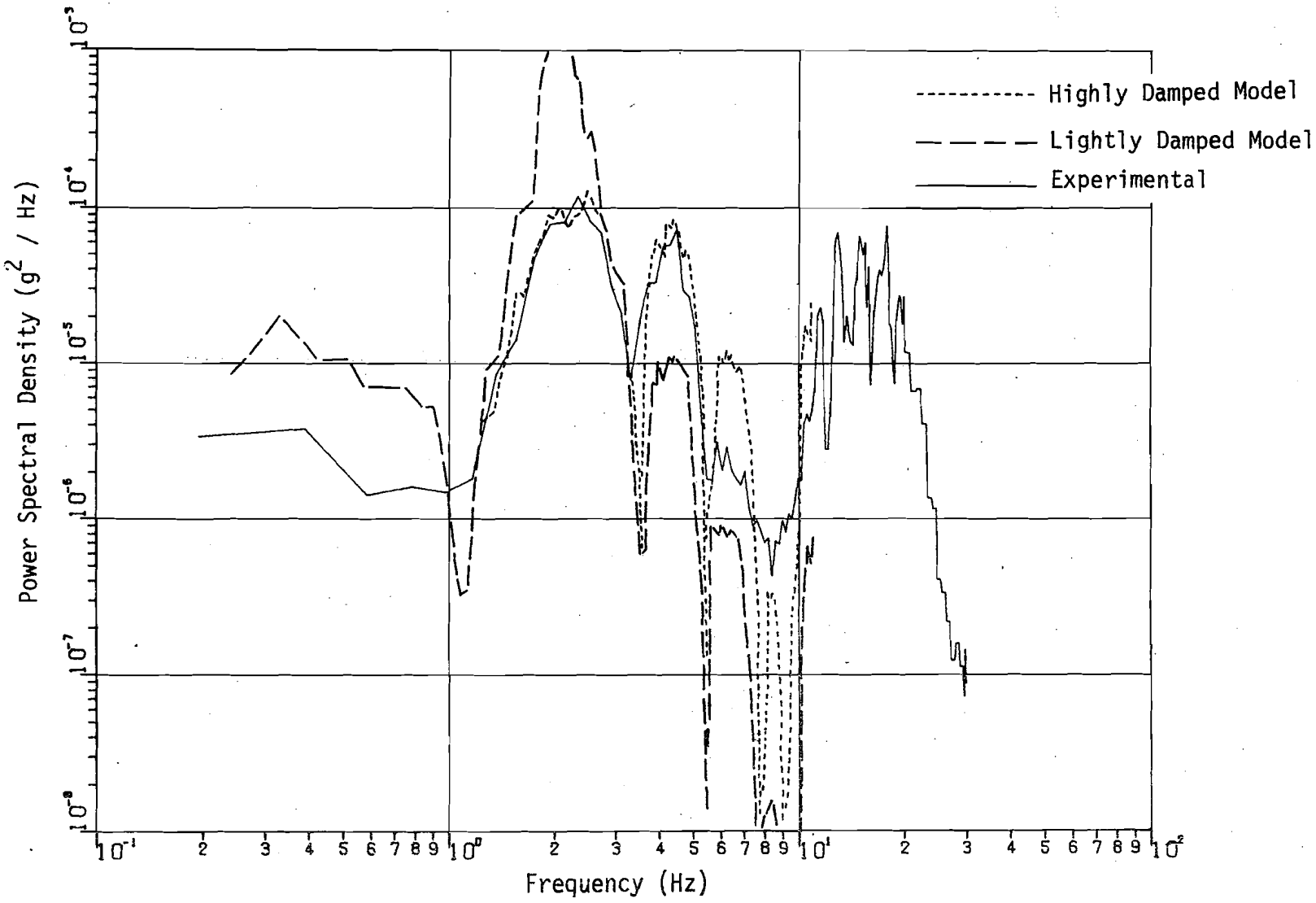

Figure 5-3 (a) Car Body C.G. Vertical Acceleration Spectra (Loaded Vehicle Traveling at 100 ft/sec Over CWR)

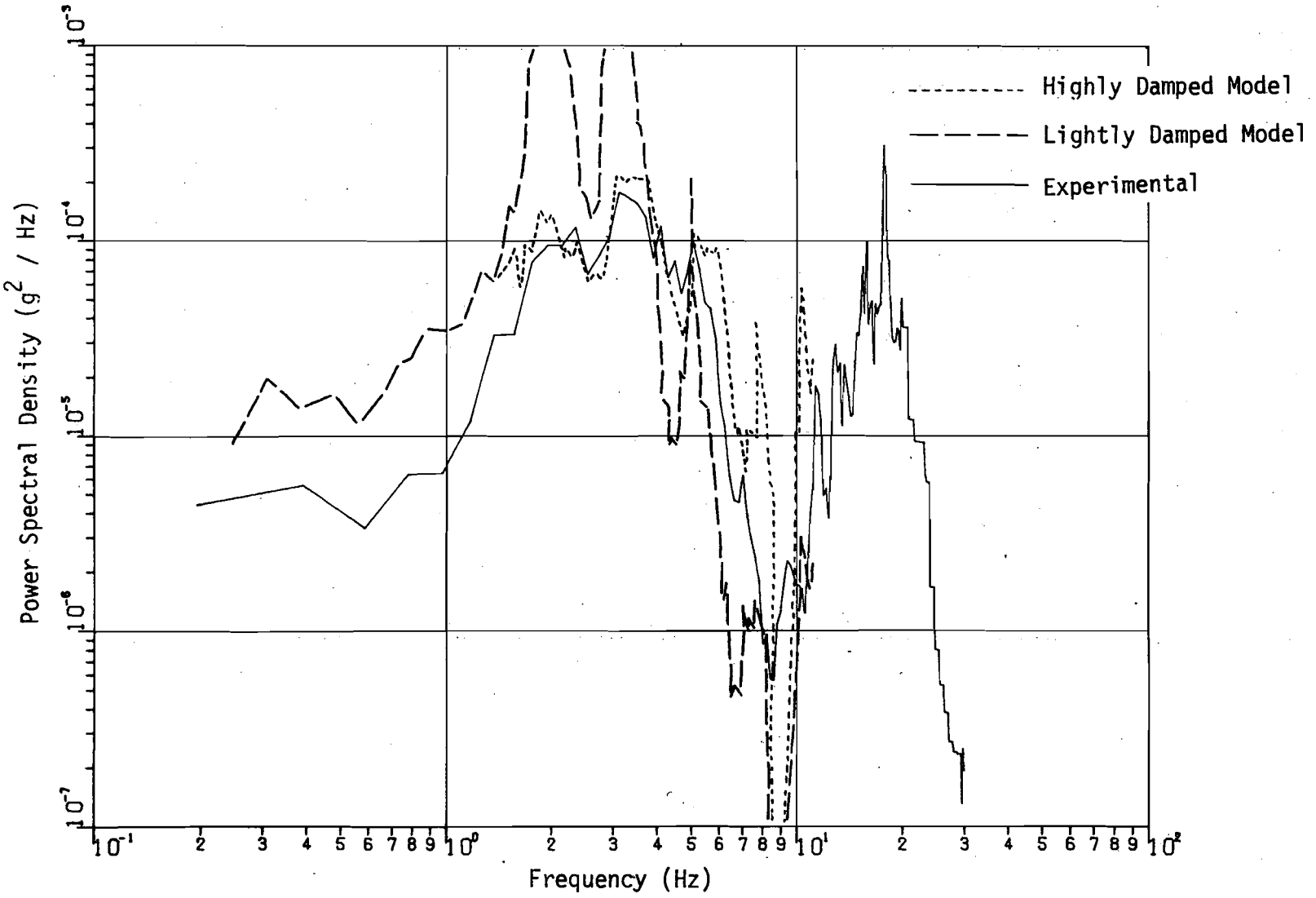

Figure 5-3 (b) Car Body Front End Vertical Acceleration Spectra (Loaded Vehicle Traveling at 100 ft/sec Over CWR)

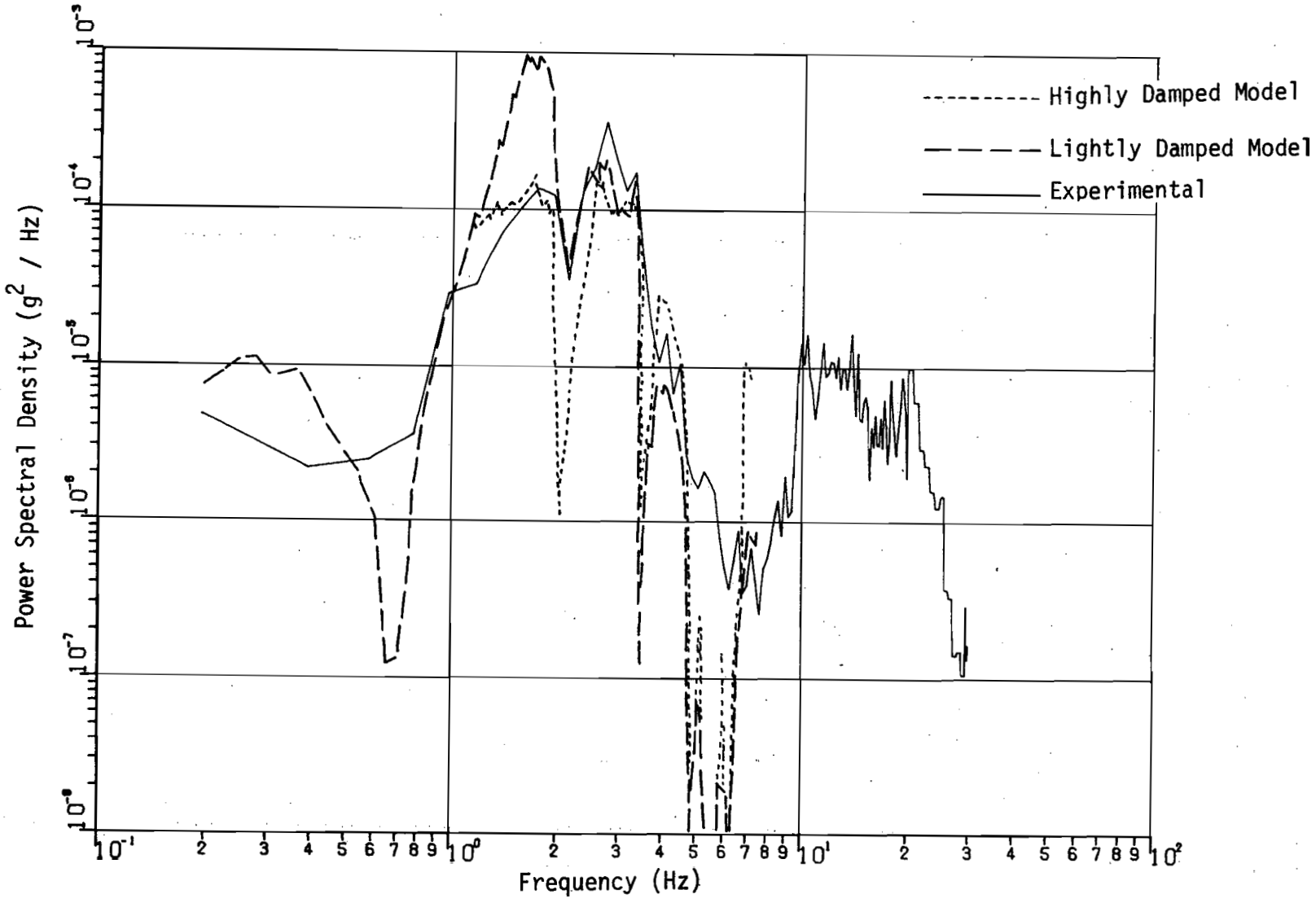

Figure 5-4 (a) Car Body C.G. Vertical Acceleration Spectra (Loaded Vehicle Traveling at 64 ft/sec Over Jointed Rail)

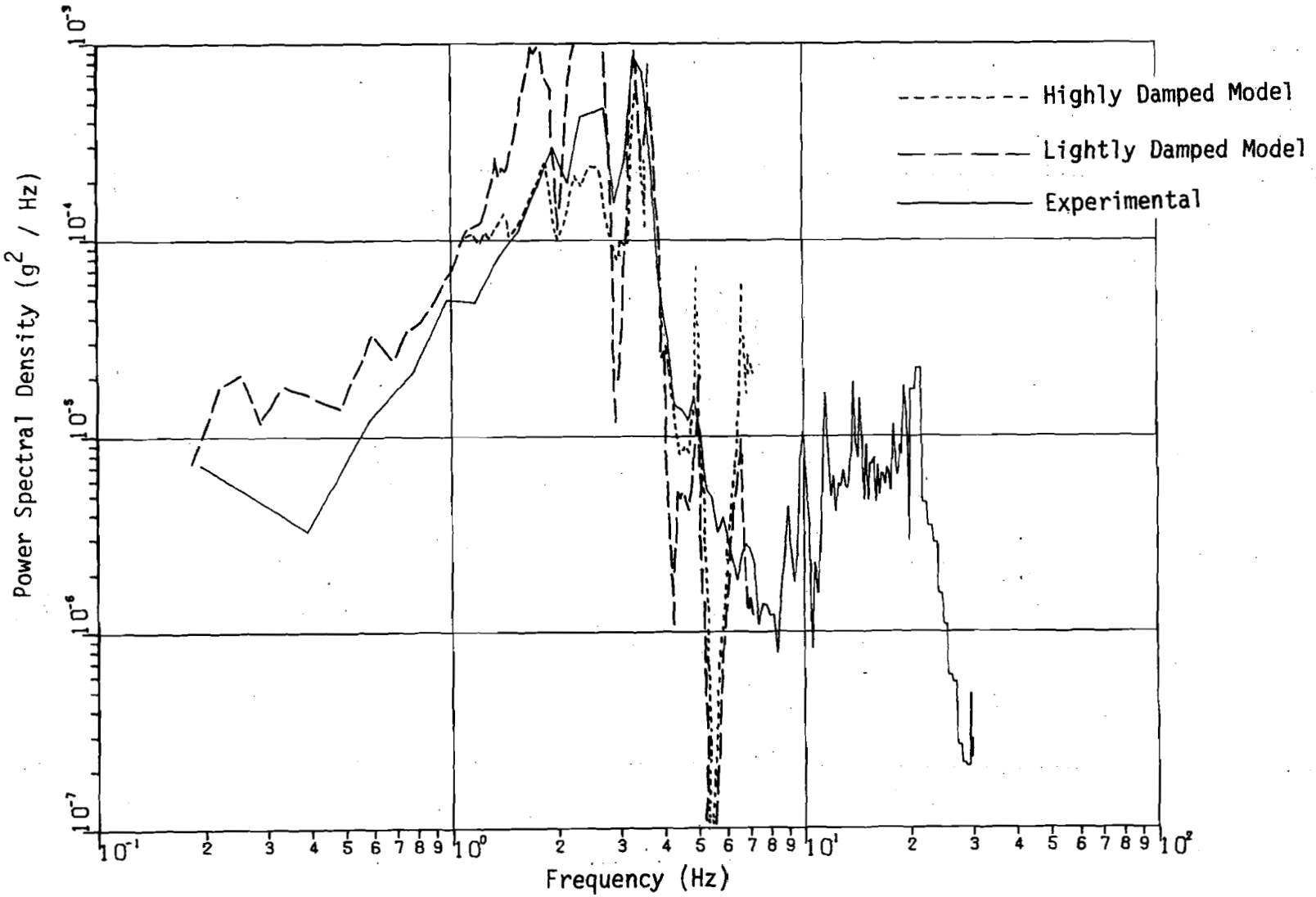

Figure 5-4 (b) Car Body Front End Vertical Acceleration Spectra (Loaded Vehicle Traveling at 64 ft/sec Over Jointed Rail)

Table 5-2 RMS Acceleration Levels (g's) for the Linear Model and Test Vehicle

TEST CONFIGURATION	FREQUENCY RANGE (Hz)	CENTER OF GRAVITY			FRONT END OVER TRUCK		
		MODEL (LOW DAMPING)	MODEL (HIGH DAMPING)	ACTUAL	MODEL (LOW DAMPING)	MODEL (HIGH DAMPING)	ACTUAL
Empty Vehicle Traveling at 100 ft/sec over CWR	0.2 - 1.0	.0033	.0033	.0021	.0062	.0061	.0025
	1.0 - 10.0	.0421	.0265	.0381	.0731	.0391	.0504
	0.2 - 10.0	.0422	.0267	.0382	.0734	.0396	.0505
Loaded Vehicle Traveling at 100 ft/sec over CWR	0.2 - 1.0	.0034	.0034	.0019	.0066	.0064	.0025
	1.0 - 10.0	.0461	.0203	.0192	.0698	.0325	.0292
	0.2 - 10.0	.0463	.0206	.0193	.0701	.0331	.0293
Loaded Vehicle Traveling at 64 ft/sec over Jointed Rail	0.2 - 1.0	.0047	.0043	.0021	.0080	.0077	.0036
	1.0 - 7.0	.0355	.0221	.0269	.0687	.0578	.0431
	0.2 - 7.0	.0359	.0225	.0270	.0692	.0583	.0432

be made to match the actual response within the limited midrange frequency band in terms of RMS accelerations.

Truck Suspension Performance

The performance of the truck suspension strongly affects the overall vehicle behavior and warrants a closer examination. All the previous results indicate that the suspension is quite stiff and may not be operating in an optimal fashion. The rear truck was equipped with an accelerometer centered on each sideframe, enabling the vertical acceleration of the rear truck center to be monitored. This truck acceleration, acting through the bolster-sideframe suspension, constitutes the vertical input to the car body rear end. Accelerometers mounted on the car body allow the vertical acceleration response at this point to be monitored. This car body acceleration may be considered the output of the rear truck suspension if negligible car body-bolster dynamics are assumed. This truck suspension input-output signal pair was examined to assess the suspension performance for the empty and fully loaded vehicle traveling at 100 ft/sec over continuous welded rail.

The input and output acceleration spectra were computed, as well as the cross spectrum, coherence, and transfer function, for both vehicle configurations. The input spectrum, coherence, and transfer function are presented in Fig. 5-5 for the empty vehicle and in Fig. 5-6 for the loaded vehicle. The truck input

and car body output RMS accelerations are summarized in Table 5-3.

In both configurations the input-output signals exhibit an extremely high level of coherence, particularly in the midrange of the spectrum. This indicates a strong correlation between the signals and should lend confidence to the transfer function computations. The marked drop in coherence near 9 Hz is due to the pitching action of the truck. Any track input at this frequency causes the truck to pitch only, with no vertical bounce of the truck center. Thus, the truck acts as a notch filter and removes information in both input and output signals. The coherence tends to fall off at low frequencies because of the very low level of response and corresponding low signal-to-noise ratio in both signals. The irregularities at higher frequencies are probably an indication of the contribution of signals other than the truck acceleration to the car body response, such as car body-bolster vibrations. Deviations from unity in the coherence can also indicate the existence of a nonlinear relationship. The truck suspension is known to be nonlinear and hence this must also be considered as a factor in the degradation of the coherence. Nevertheless, the coherence between the respective input-output signals is quite strong up to the higher frequencies and lends a good deal of confidence to the corresponding transfer functions.

The truck suspension has been modeled as a linear second order system. The transfer function may be expressed as

$$G(s) = \frac{\frac{c}{M}\left(s + \frac{k}{c}\right)}{s^2 + \frac{c}{M}s + \frac{k}{M}} \qquad (5\text{-}1)$$

where c and k represent the damping and spring rate coefficients of the truck suspension and M may be considered half the mass of the car body. Using the values from Table 5-1, the transfer function of (5-1) is sketched over the corresponding experimental transfer functions of Fig. 5-5 and Fig. 5-6.

For the empty vehicle, note that, as predicted by the analytical transfer function, the truck provides virtually no vibration isolation below 10 Hz. In fact, examination of Table 5-3 reveals that the RMS acceleration of the car body is only 20% less than that of the truck for the 0.2 to 20.0 Hz range. This may not be terribly surprising in view of the fact that the vehicle is completely empty and may be expected to induce the least amount of suspension action.

The performance of the fully loaded truck is somewhat more dramatic, as evidenced by Fig. 5-6. The suspension, when fully loaded, provides significantly more attenuation of the input acceleration than predicted by the linear model. Table 5-3 indicates an overall attenuation of the input RMS acceleration of approximately 50%.

In both vehicle configurations the analytical transfer function varies significantly from the experimentally computed transfer function. Both the analytical and experimental functions are in error to the extent that the system is nonlinear. In addition, the experimentally determined transfer function is limited by such factors as

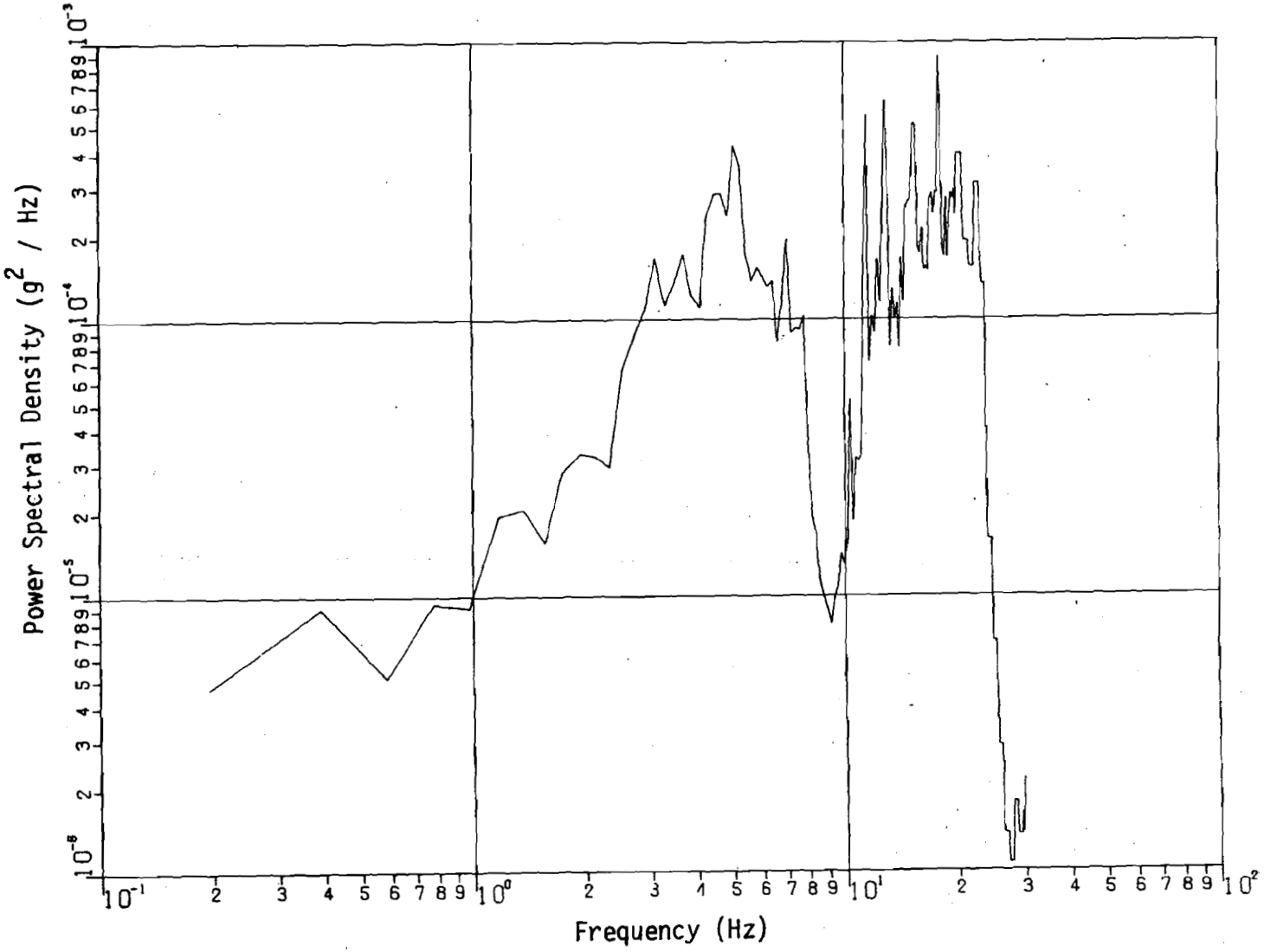

Figure 5-5 (a) Rear Truck Center Vertical Acceleration Spectrum (Empty Vehicle Traveling at 100 ft/sec Over CWR)

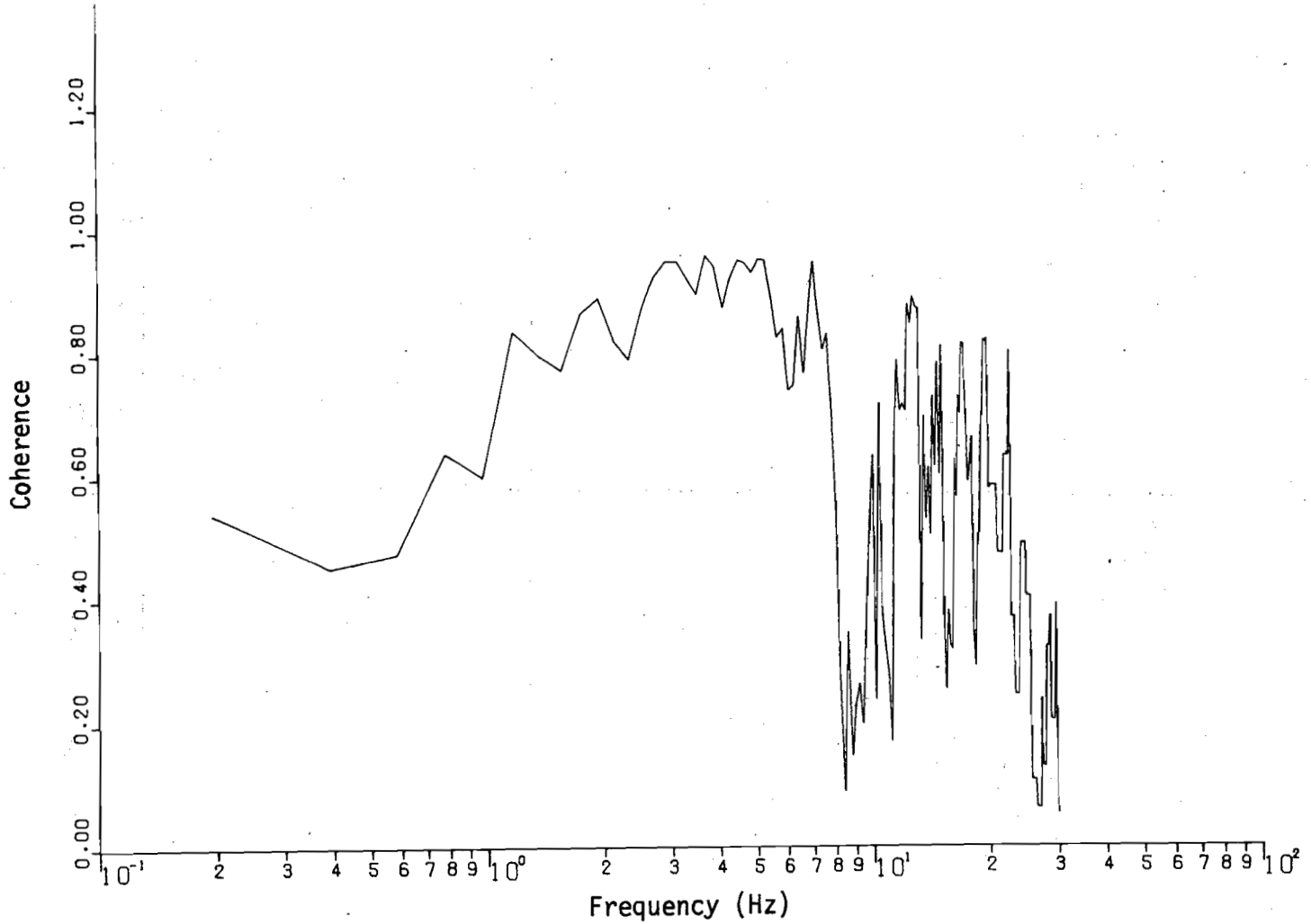

Figure 5-5 (b) Rear Truck Center - Car Body Rear End Coherence (Empty Vehicle Traveling at 100 ft/sec Over CWR)

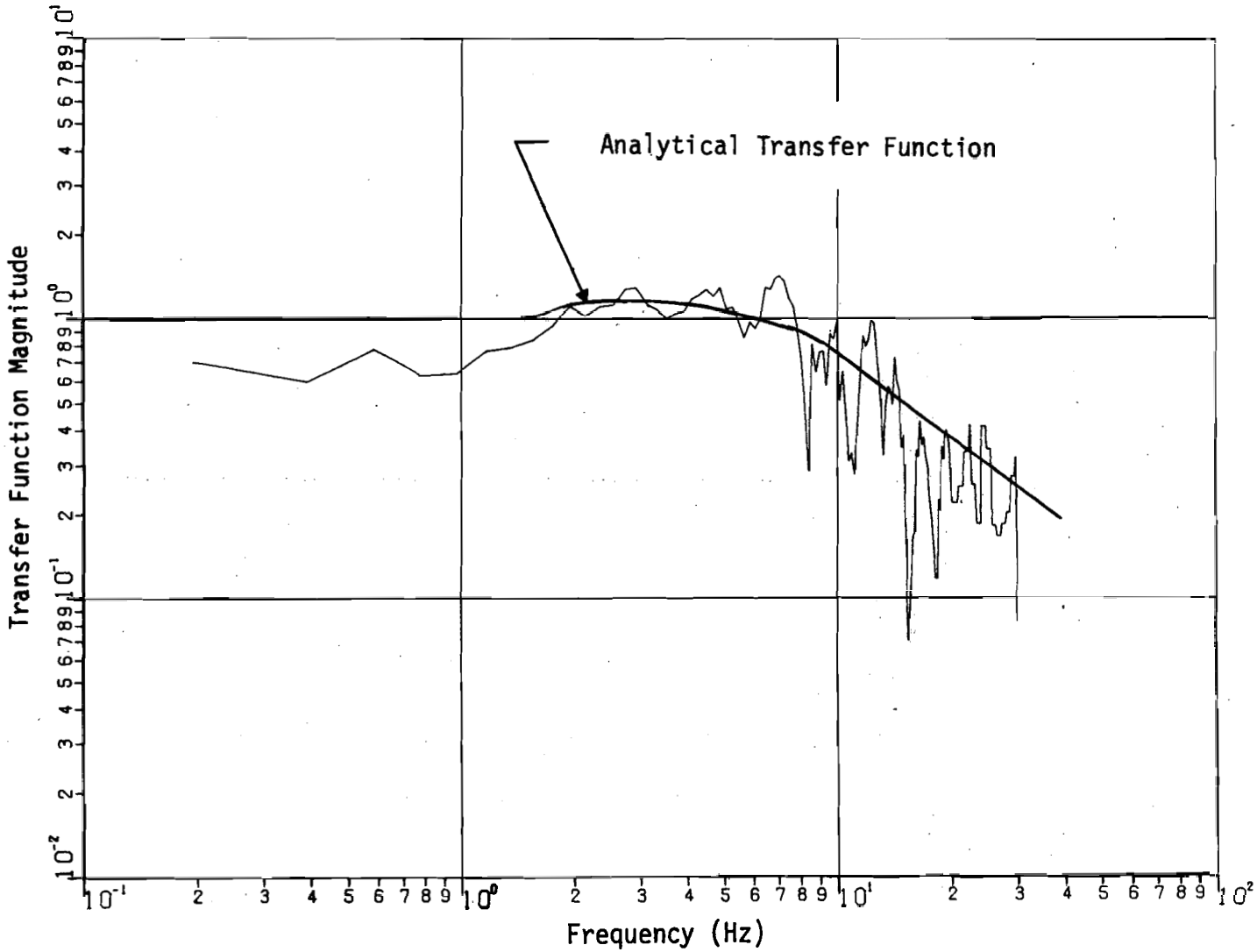

Figure 5-5 (c) Rear Truck Center - Car Body Rear End Transfer Function Magnitude (Empty Vehicle Traveling at 100 ft/sec Over CWR)

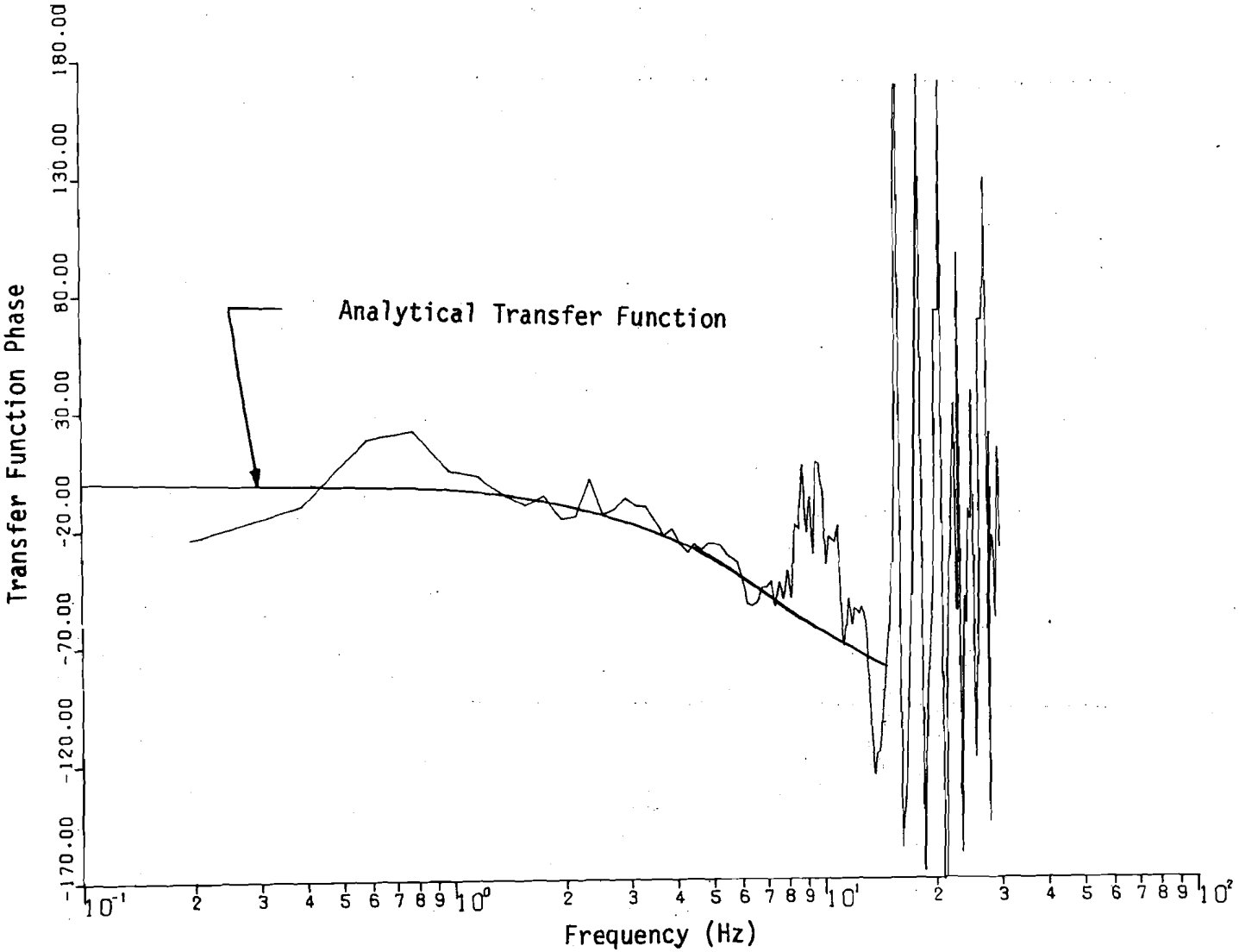

Figure 5-5 (d) Rear Truck Center - Car Body Rear End Transfer Function Phase (Empty Vehicle Traveling at 100 ft/sec Over CWR)

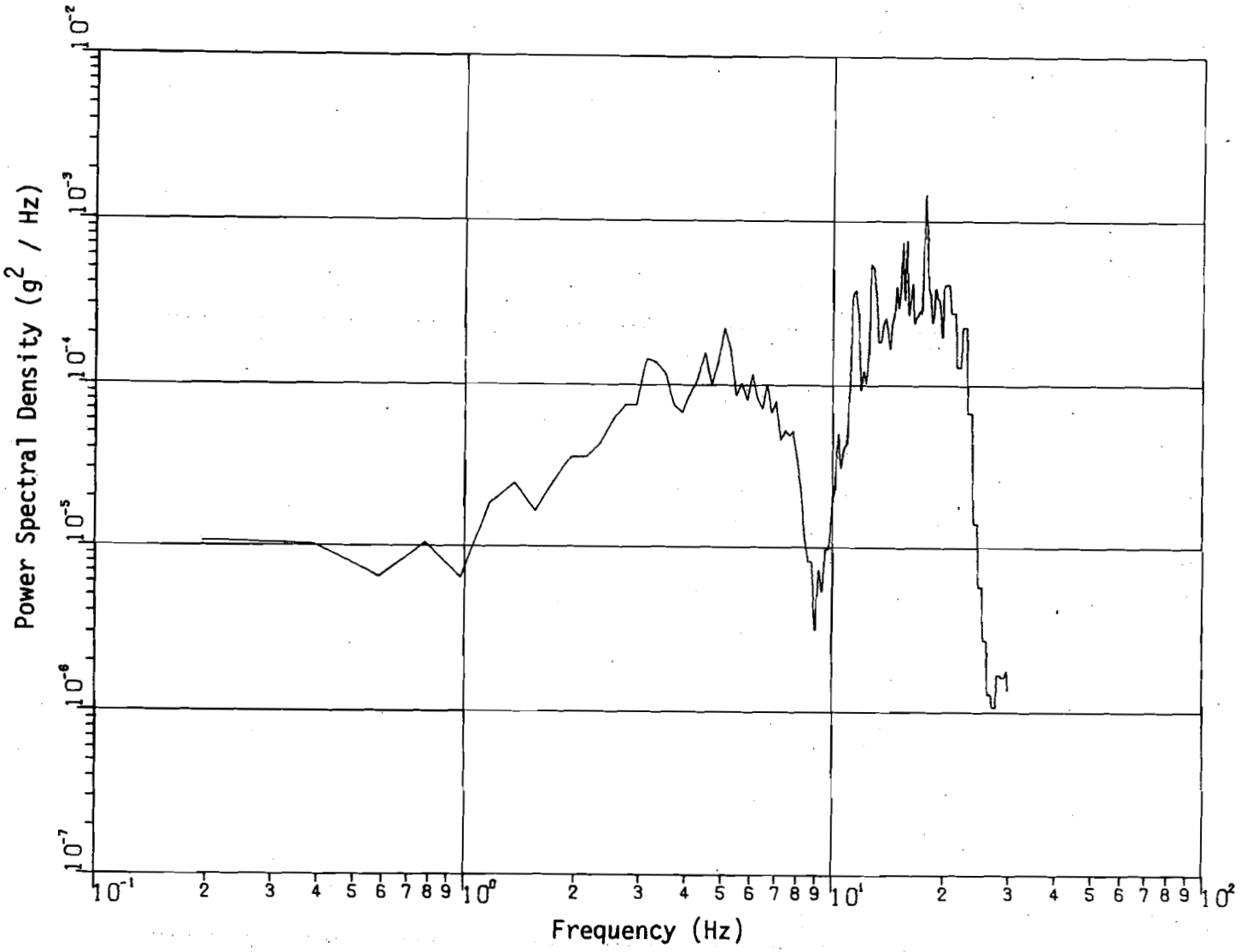

Figure 5-6 (a) Rear Truck Center Vertical Acceleration Spectrum (Loaded Vehicle Traveling at 100 ft/sec Over CWR)

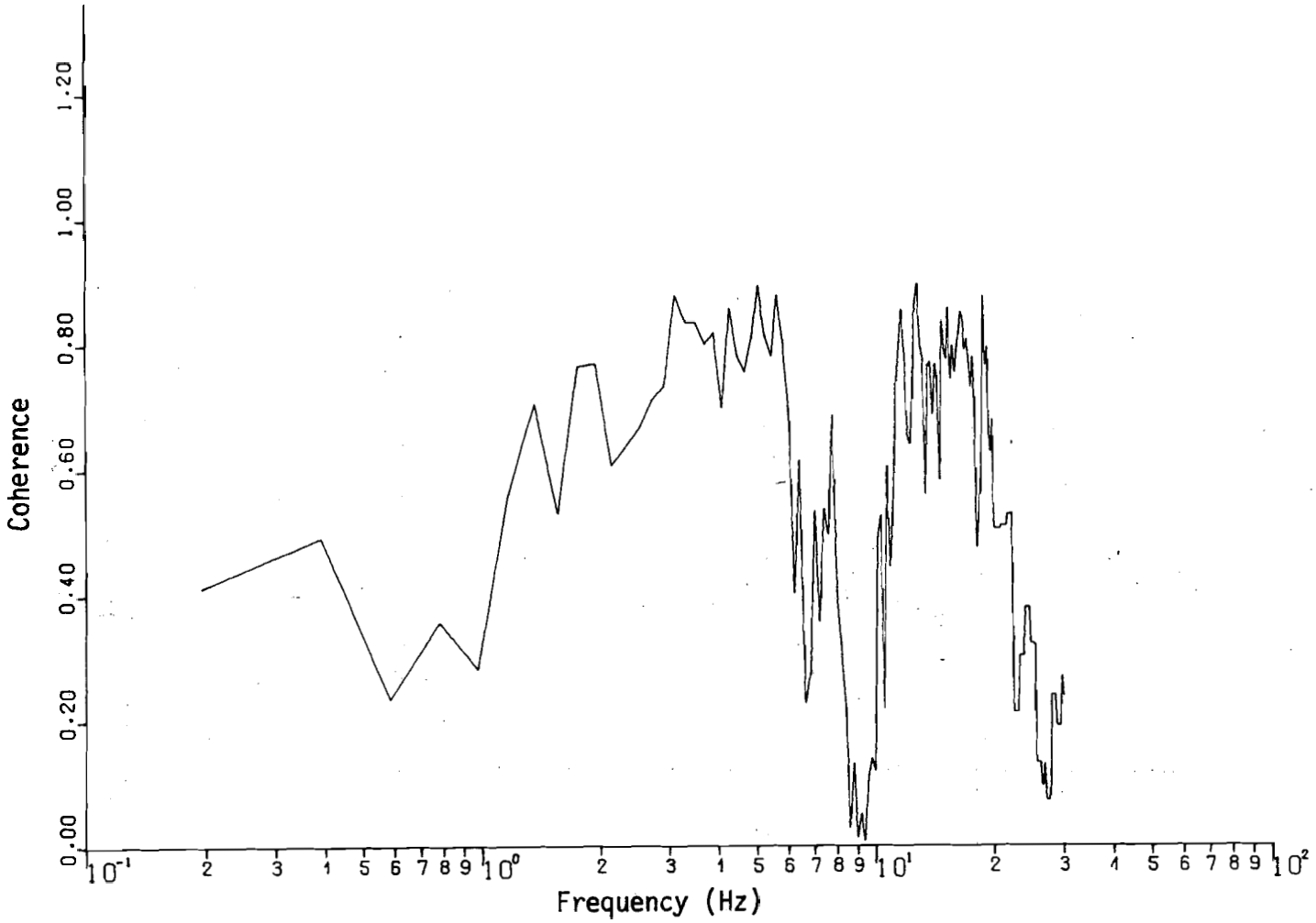

Figure 5-6 (b) Rear Truck Center - Car Body Rear End Coherence (Loaded Vehicle Traveling at 100 ft/sec Over CWR)

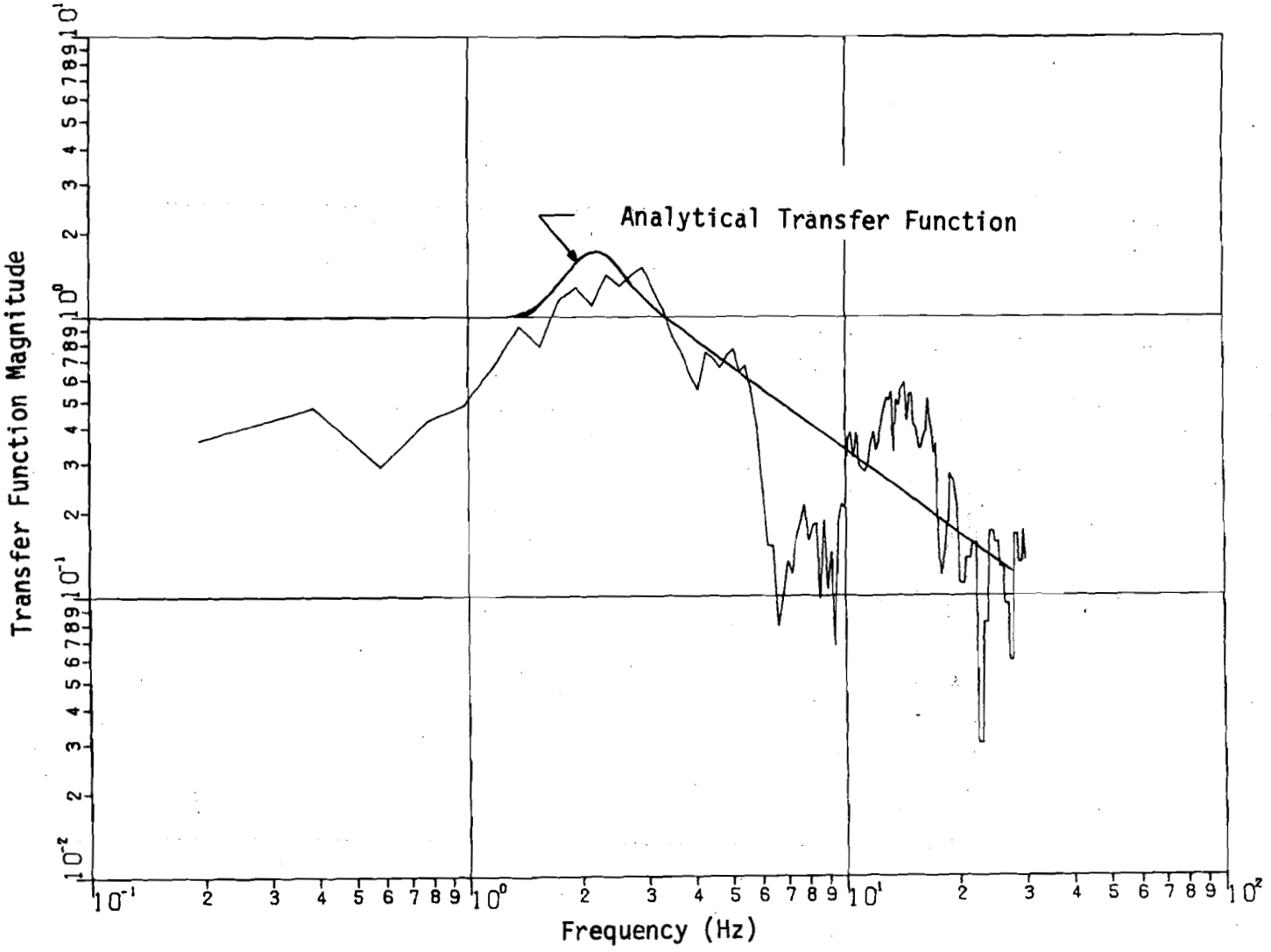

Figure 5-6 (c) Rear Truck Center - Car Body Rear End Transfer Function Magnitude (Loaded Vehicle Traveling at 100 ft/sec Over CWR)

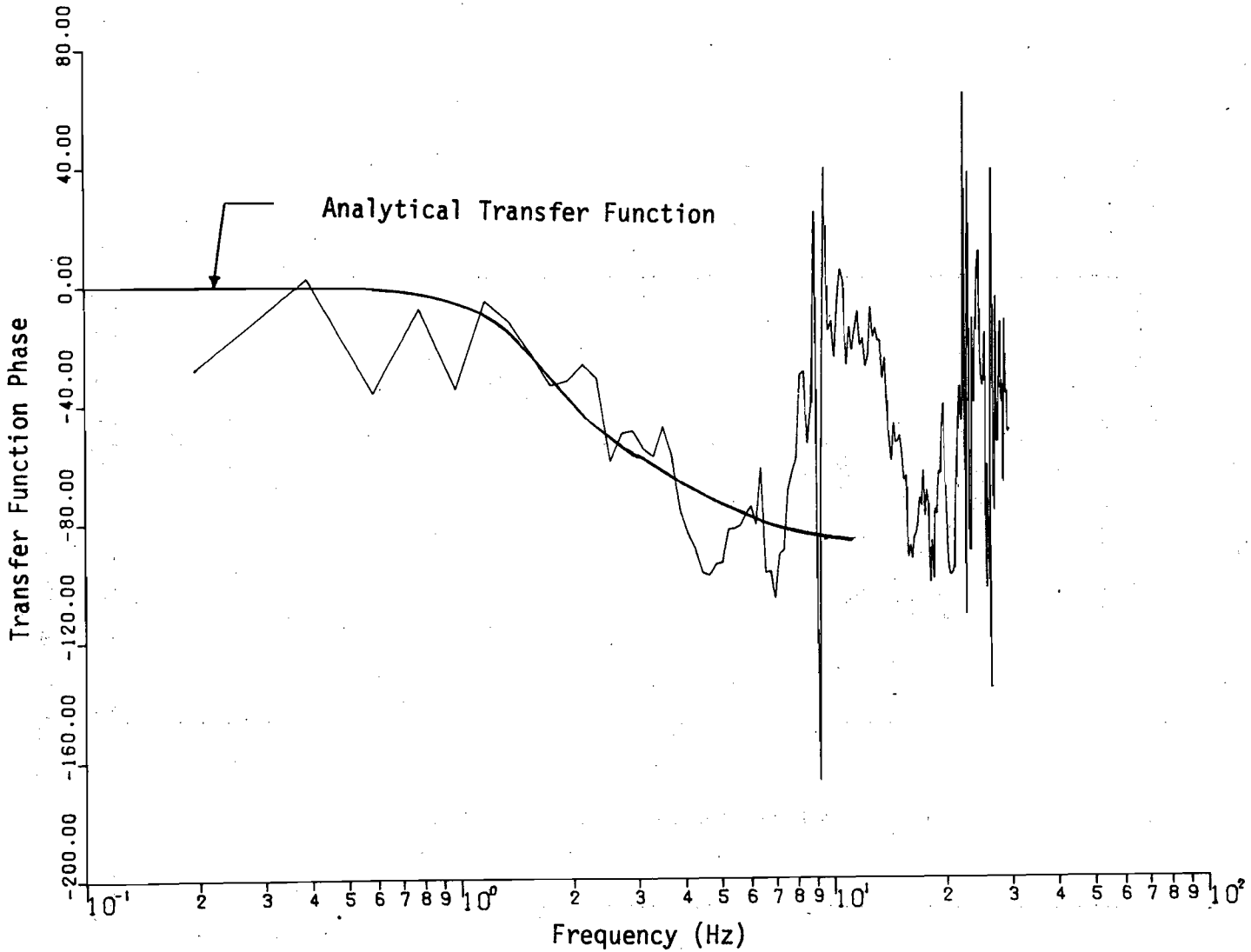

Figure 5-6 (d) Rear Truck Center - Car Body Rear End Transfer Function Phase (Loaded Vehicle Traveling at 100 ft/sec Over CWR)

Table 5-3 RMS Acceleration Levels (g's) for the Rear Truck Center and the Car Body Over the Truck

TEST CONFIGURATION	FREQUENCY RANGE (HZ)	TRUCK CENTER	CAR BODY OVER TRUCK
Empty vehicle traveling at 100 ft/sec over CWR	0.2 - 1.0	.0030	.0028
	1.0 - 10.0	.0436	.0526
	10.0 - 20.0	.0663	.0330
	0.2 - 20.0	.0794	.0622
Loaded vehicle traveling at 100 ft/sec over CWR	0.2 - 1.0	.0036	.0023
	1.0 - 10.0	.0345	.0302
	10.0 - 20.0	.0785	.0320
	0.2 - 20.0	.0858	.0440

(1) the quality of the data in terms of noise contamination and (2) the extent of the system excitation. For instance, if the input signal is deficient in a frequency band containing a system resonance, then the mode will not be excited and the resultant coherence and transfer function will be poor in this band. Hence, from a practical standpoint, this approach to system identification can be quite tenuous.

One final set of results is presented that is not directly related to the truck suspension modeling problem but demonstrates some additional interesting and useful properties of spectral functions. Due to the symmetry of the system, the input to the car body at the rear is essentially the same as the input to the front delayed in time. Based on this observation it would seem reasonable that the transfer function for the front end response to the rear end input would be quite similar to the transfer function of the rear end response to the same input. In fact, the only difference should be the time delay operator, $e^{j\omega t}$. In equation form

$$u_R(s) = e^{-sT} u_F(s) , \tag{5-2}$$

$$\frac{y_F(s)}{u_F(s)} = G(s) \tag{5-3}$$

and

$$\frac{y_F(s)}{u_R(s)} = G(s)\, e^{sT} \tag{5-4}$$

where the subscripts F and R designate front and rear, respectively. The transfer function magnitude and phase for the front end response

to the rear truck input for the empty vehicle traveling at 100 ft/sec is shown in Fig. 5-7. As expected, the corresponding transfer function magnitudes of Fig. 5-5(c) and Fig. 5-7(a) are quite similar. The corresponding phase plots, however, are radically different since the plot in Fig. 5-7(b) exhibits the phase shift due to the $e^{j\omega T}$ factor. From Fig. 5-7(b), the period of the phase rotation is approximately 2.2 Hz, which corresponds to a time delay of about 0.45 seconds. Since the vehicle is traveling at 100 ft/sec and the truck displacement front to rear is approximately 45 feet, the time delay of 0.45 seconds revealed by the transfer function phase plot appears correct. As mentioned in Chapter 3, the cross correlation can be useful in identifying a time delay in a system. For this example, the cross correlation was computed as the Fourier transform of the cross spectral density of the rear truck vertical acceleration and car body front end vertical acceleration. The result is shown in Fig. 5-7(c) which indeed reveals the expected correlation at a lag time of 0.45 seconds.

Conclusions

In this chapter the response of the linear model to the track input spectra of Chapter 4 has been examined. Within a limited frequency range the response of the model compares quite agreeably with the actual response of the test vehicle. It should be apparent that in order to obtain good agreement the input spectra must be

adequately represented as well as the system itself. An adequate representation of the track input spectra has been shown to be rather difficult to obtain. From this viewpoint the utility of spectral techniques has been demonstrated and the linear model, within limits, has been validated.

This spectral approach has also pointed to the limitations of the linear model. The examination of the truck suspension performance points to the rather significant discrepancies between the linear characteristics of the model and the actual response characteristics of the truck. It seems reasonable to assume that the primary limitations of the linear model may be attributed to the known nonlinear characteristics of the truck suspension.

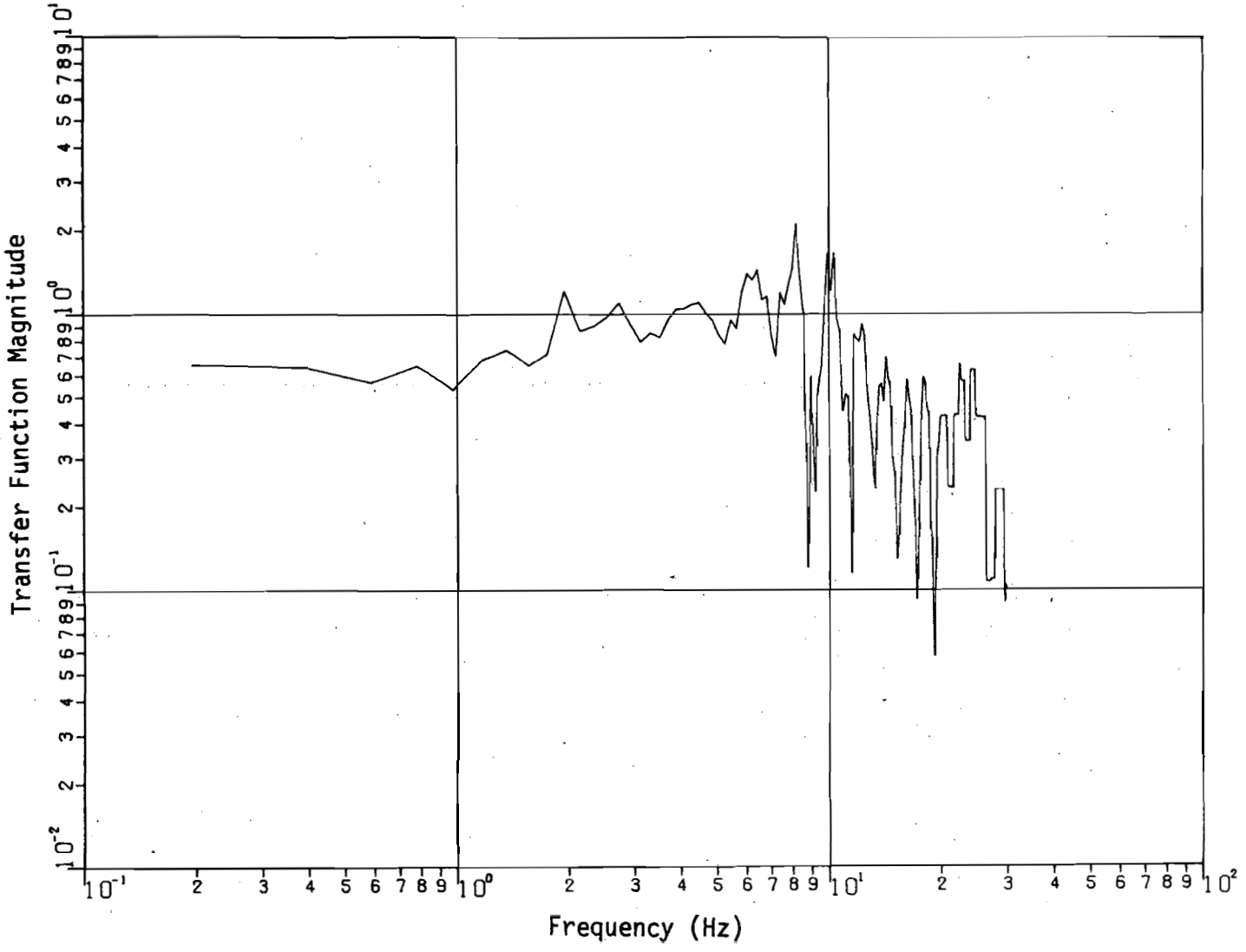

Figure 5-7 (a) Rear Truck Center - Car Body Front End Transfer Function Magnitude (Empty Vehicle Traveling at 100 ft/sec Over CWR)

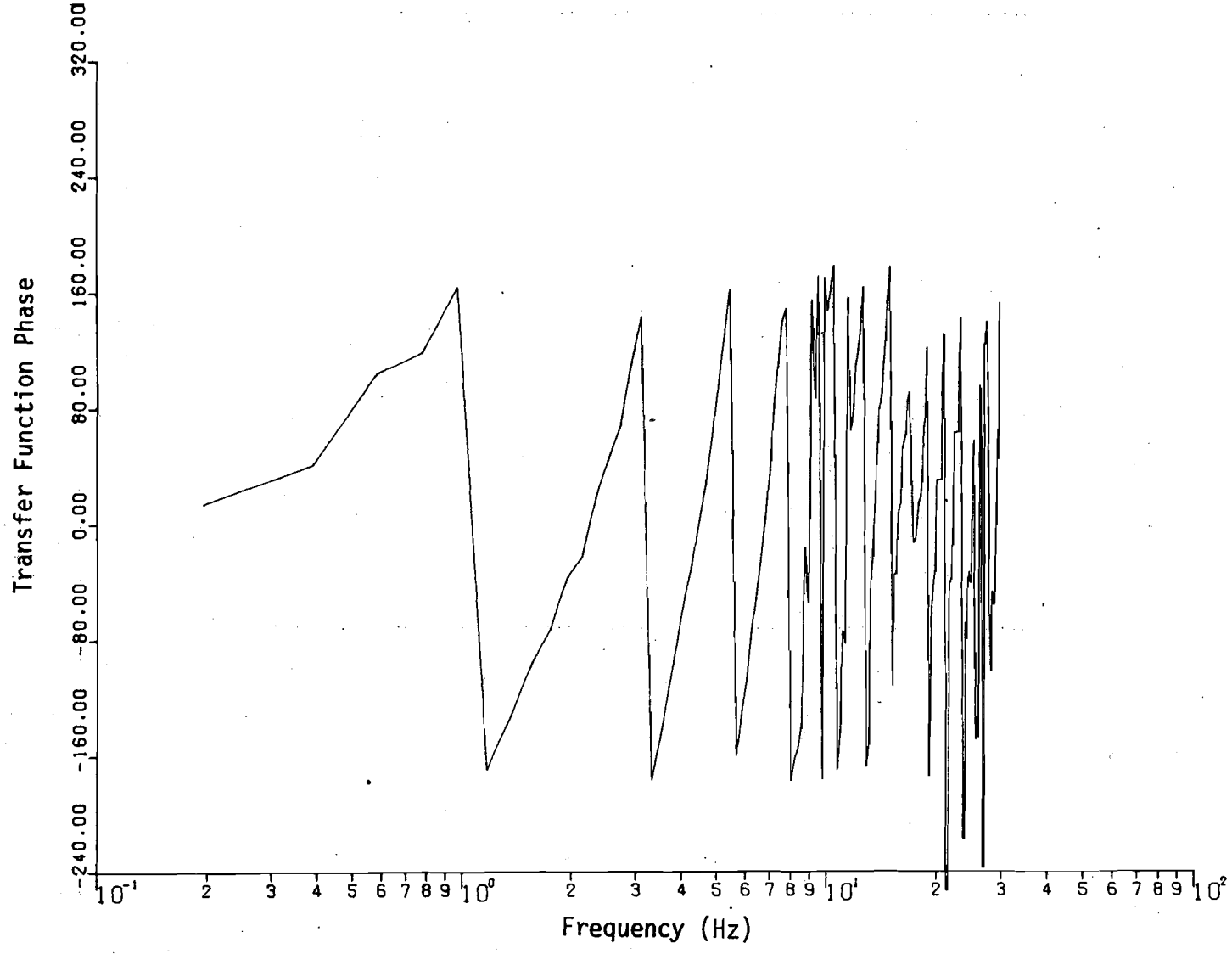

Figure 5-7 (b) Rear Truck Center - Car Body Front End Transfer Function Phase (Empty Vehicle Traveling at 100 ft/sec Over CWR)

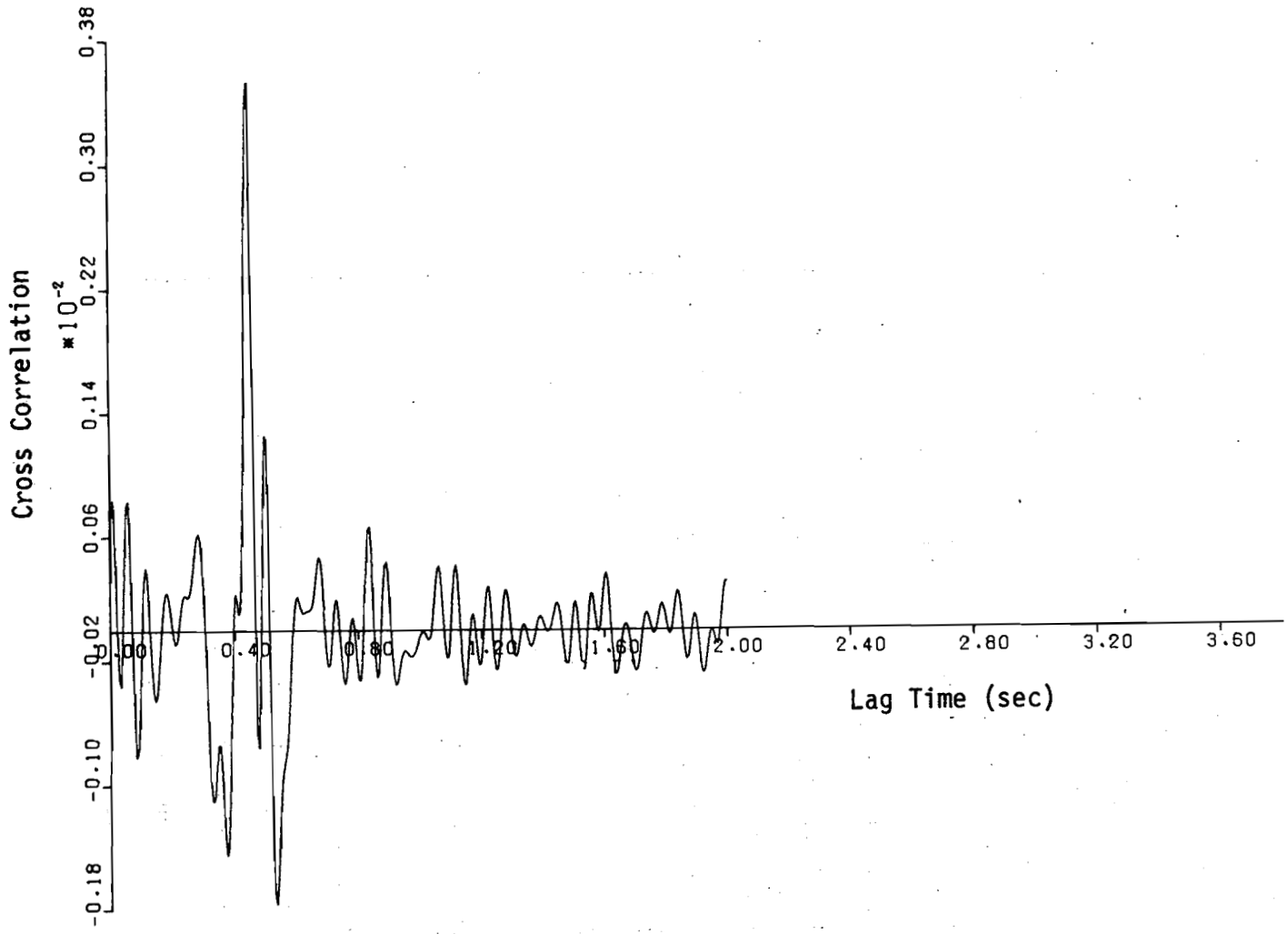

Figure 5-7(c) Rear Truck Center - Car Body Front End Cross Correlation Function (Empty Vehicle Traveling at 100 ft/sec Over CWR)

Chapter 6

CONCLUSIONS AND RECOMMENDATIONS

Conclusions

This study demonstrated that spectral analysis techniques are quite satisfactory for the validation of a linear model of the vertical dynamics of a typical freight car. The track spectra input to the linear model was computed from track geometry measurements of the pertinent sections of test track. The validity of the model was based upon a comparison of the model response spectra and the response spectra computed from vehicle acceleration measurements. The results indicate that this particular model is relatively accurate in the midrange frequency band between 1.0 Hz and 10.0 Hz. At lower frequencies, the track input spectra are not well defined because of the limitations of the track geometry measurement system. At higher frequencies, the presence of modes not included in the simple linear model results in discrepancies.

The nonlinearity of the truck suspension served to illustrate limitations of the linear model as well as certain limitations of spectral techniques. The truck suspension was isolated and analyzed using truck and car body vertical acceleration measurements. The coherence function was very useful in estimating the quality of the relationship between the signals. The relatively high level of computed coherence lent confidence to the corresponding transfer function computations. Only fair agreement resulted between the linear model of the suspension and the transfer functions computed from experimental

data. This may be attributed primarily to dry friction, the dominant nonlinear characteristic of the truck suspension. Spectral functions can only be used to identify a linear system.

Nonetheless, this surprisingly good agreement between linear theoretical analysis and experimental results demonstrates that the linear analysis provides results of sufficiently high accuracy for use in studying and solving many rail vehicle dynamic problems. This is of real practical importance, because the computer programs to implement the linear analysis are many times faster than the numerical integration techniques widely used to solve nonlinear equations of motion. Thus one can afford to make extensive use of the linear analysis in design studies, in conjunction with field tests, and in selection of components or maintenance practices.

Recommendations

The results of this study are sufficiently encouraging to recommend the spectral analysis approach to anyone considering validation of rail vehicle dynamic analyses. We are employing these same approaches in validation of rail vehicle lateral dynamic analyses with test data from the field tests conducted by the AAR and the Union Pacific Railroad.

The model validation procedure illustrated in this report reveals the limitations imposed not only by the modeling assumptions but by the experimental test procedures. The model validation process depends critically on a knowledge of the system input. In the case of the railway vehicle, alternative systems for the measurement of track geometry should be given careful consideration. In the case of vehicle

lateral dynamics, the track lateral alignment, cross-level and rail head profile variation are needed to completely characterize the track input. This data is considerably more difficult to obtain than the vertical profile information needed for the vertical dynamics study.

It is equally important that the vehicle used in any testing also be adequately characterized. In the case of the vertical dynamics problem studied here, relatively few parameters are needed. However, an understanding of rail vehicle lateral dynamics requires more extensive characterization. For example, wheel profiles, wheel and rail surface conditions, warp stiffness and friction, and centerplate friction must be known.

Special considerations involving test procedures are important if spectral analysis techniques are to be employed. For example, it is essential that time history records are of sufficient length if reliable spectra are to be computed. This was a problem with some of the TDOP data that yielded less than 100 seconds of data for some test configurations. The filtering and sampling of test signals must also be performed such that aliasing is avoided while valuable information is retained intact.

We expect that further uses for the spectral analysis approach will emerge from the lateral dynamics study that we are now conducting.

REFERENCES

1. Tsai, N. T., Law, E. H., and N. K. Cooperrider, "Research in Freight Car Dynamics," in "Overview of Freight Systems R & D," Federal Railroad Administration Report FRA/OR & D-77/58, October 1977, p. 11-34.

2. "A Comparison of Theoretical and Experimental Vehicle Behavior Using a 2 Axled Special Vehicle," Report No. 2, Question C116, Interaction Between Vehicle and Track, Utrecht, October 1972.

3. "Freight Car Truck Design Optimization: Introduction and Detailed Test Plans Series 1, 2, and 3 - Phase 1," Southern Pacific Transportation Co., U.S. Department of Transportation Report No. FRA-OR&D-75-79, June, 1975.

4. Fallon, W. F. Jr., "An Investigation of Railcar Model Validation," M.S. Thesis, Arizona State University, May 1977.

5. Fallon, W. J. Jr., "User's Manual, Random Data Analysis Programs," Report ERC-R-76010, Mechanical Engineering, Arizona State University, April 1976.

6. Ahlbeck, D. R., et al., "Comparative Analysis of Dynamics of Freight and Passenger Rail Vehicles," U.S. Department of Transportation Report No. FRA-ORD&D-74-39, March, 1974.

7. Hanson, I. C., "General Stability Analysis Computer Program," Lockheed Missiles and Space Co., Report No. LMSC 6-95-68-1, April, 1968.

8. "Harmonic Roll Series, Vol. 2: 70 Ton Truck Component Data, Physical Restraints, Mechanical Properties, Damping Characteristics," Track-Train Dynamics Program, 1974.

9. Cooley, J. W., and J. W. Tukey, "An Algorithm for the Machine Calculation of Complex Fourier Series," Mathematics of Computation, Vol. 19, No. 90, April, 1965, pp. 297-301.

10. Cooley, J. W., et al., "The Fast Fourier Transform and Its Applications," IEEE Transactions on Education, Vol. 12, No. 1, March, 1969, pp. 27-34.

11. Brigham, E. O., and R. E. Morrow, "The Fast Fourier Transform," IEEE Spectrum, December, 1967, pp. 63-70.

12. Brigham, E. O., The Fast Fourier Transform, Prentice Hall, Inc., Englewood Cliffs, New Jersey, 1974.

13. Bendat, J. S., and A. G. Piersol, Random Data: Analysis and Measurement Procedures, John Wiley and Sons, Inc., New York, 1971.

14. Welch, P. D., "The Use of the Fast Fourier Transform for the Estimation of Power Spectra: A Method Based on Time Averaging Over Short, Modified Periodograms," IEEE Transactions on Audio and Electroacoustics, Vol. AU-15, No. 2, June, 1967, pp. 70-73.

15. Richards, P. I., "Computing Reliable Power Spectra," IEEE Spectrum, January, 1967, pp. 83-90.

16. Pierce, T. G., and B. J. May, "A Study of the Stability and Dynamic Response of the Linear Induction Motor Test Vehicle," U.S. Department of Transportation Report No. FRA-RT-70-25, September, 1969.

17. Corbin, J. C., and W. H. Kaufman, "Classifying Track by PSD," Mechanics of Transportation Systems, AMD-15, ASME, 1975, pp. 1-20.

APPENDIX A

THE CHORDAL TRANSFER FUNCTION

Track irregularities in surface and lateral alignment are often measured with respect to the midpoint of a chord traveling along the track. This type of measurement differs from the deviation of the track with respect to a true, or "very straight", reference. The nature of the differentiation, i.e. the characteristic of the chordal measurement system, must be identified to assess the consequences of using chordal data. This characterization can be conveniently handled in the frequency domain by deriving the transfer function that relates the "true" deviation to the chordal deviation.

The physical situation is represented schematically in Fig. A-1 where L is the length of the chord traveling along the rail at a velocity V. The midchord deviation is represented by x_2 while x_1 and x_3 define the deviation of the chord from the "true" reference. The ratio of the midchord deviation to the true deviation may

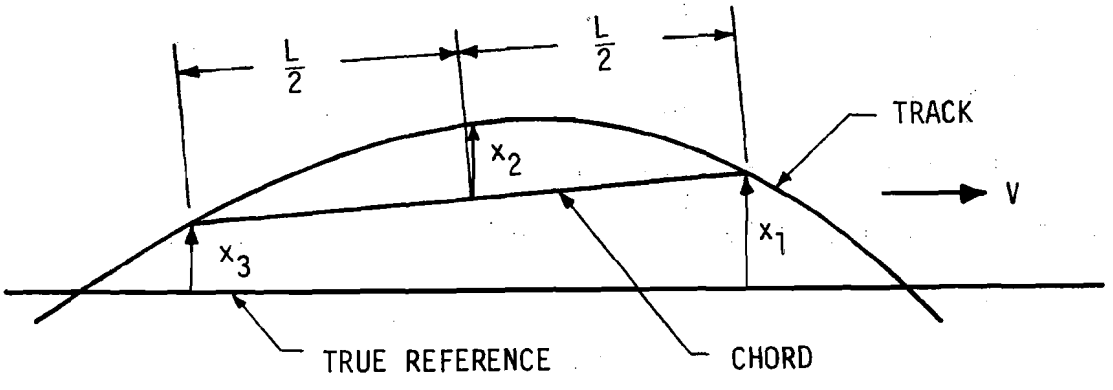

Figure A-1 Track Deviation Relative to a Chord Midpoint and a "True" Reference

be expressed as

$$G(s) = \frac{x_2(s)}{x_2(s) + \frac{x_1(s) + x_3(s)}{2}} \qquad \text{(A-1)}$$

where $T \cong L/V$ for small angular deviations of the chord with respect to the reference. Note also that

$$x_2(t) = x_1(t - T/2) - \frac{x_1(t) + x_3(t)}{2} \qquad \text{(A-2)}$$

and

$$x_3(t) = x_1(t-T) \ . \qquad \text{(A-3)}$$

Taking the Laplace transforms of (A-2) and (A-3) and substituting into (A-1) yields

$$G(s) = \frac{e^{-sT/2}\, x_1(s) - \frac{1}{2}\, x_1(s)\, [1 + e^{-sT/2}]}{e^{-sT/2}\, x_1(s)}$$

$$= 1 - \cos\,(sT/2) \ . \qquad \text{(A-4)}$$

In terms of wavelength, λ, the transfer function may be expressed

$$G(\lambda) = 1 - \cos\,(\tfrac{\pi L}{\lambda}) \qquad \text{(A-5)}$$

or in terms of spatial frequency, f,

$$G(f) = 1 - \cos\,(\pi L f) \ . \qquad \text{(A-6)}$$

This transfer function may be used to compensate spectra computed from midchord offset data. Note, however, that the chordal measurement system completely filters information at frequencies $f = 0, 2/L, 4/L, \ldots$.

APPENDIX B

THE FILTERING EFFECT OF MULTIPLE INPUTS IN A SYMMETRIC MODEL

The input to a symmetric railway vehicle model induces a pitching motion in the trucks and car body that results in a distinct filtering of the input. Consider the symmetric model of the vertical motions of a railway vehicle shown schematically in Fig. B-1.

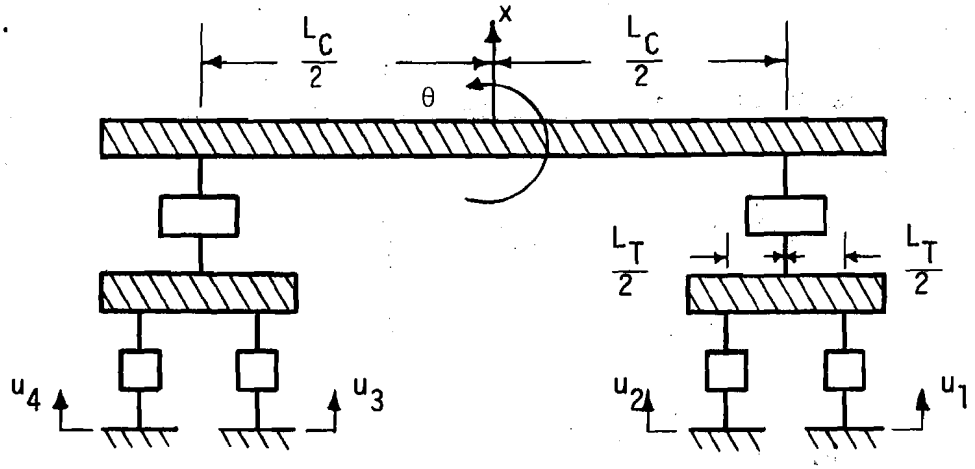

Figure B-1 Symmetric Model of the Railcar Vertical Dynamics

The blocks represent linear suspension elements. The transfer function for bounce, x and pitch, θ, for a single input may be expressed as

$$\frac{x(s)}{u_1(s)} = G_1(s) \qquad \text{(B-1}$$

and

$$\frac{\theta(s)}{u_1(s)} = G_2(s) \qquad \text{(B-2)}$$

respectively.

Under the assumption of symmetry, the transfer functions relating to the other inputs are given by

$$\frac{x(s)}{u_2(s)} = \frac{x(s)}{u_3(s)} = \frac{x(s)}{u_4(s)} = G_1(s) , \tag{B-3}$$

$$\frac{\theta(s)}{u_2(s)} = G_2(s) , \tag{B-4}$$

and

$$\frac{\theta(s)}{u_3(s)} = \frac{\theta(s)}{u_4(s)} = - G_2(s) . \tag{B-5}$$

Now, the multiple inputs may be expressed in terms of a single input, i.e.,

$$u_2(s) = e^{-sT_1} u_1(s) ,$$

$$u_3(s) = e^{-sT_2} u_1(s) ,$$

and

$$u_4(s) = e^{-s(T_1+ T_2)} u_1(s) \tag{B-6}$$

where the vehicle is traveling at a velocity V, $T_1 = L_T/V$, and $T_2 = L_c/V$. Dropping the subscript on the input, the transfer functions may now be expressed as

$$\frac{x(s)}{u(s)} = \left[1 + e^{-sT_1} + e^{-sT_2} + e^{-s(T_1+ T_2)}\right] G(s)$$

$$= (1 + e^{-sT_1})(1 + e^{-sT_2}) G_1(s) \tag{B-7}$$

and

$$\frac{\theta(s)}{u(s)} = [1 + e^{-sT_1} - e^{-sT_2} - e^{-s(T_1+T_2)}[\ G(s)$$

$$= (1 + e^{-sT_1})(1 - e^{-sT_2})\ G_2(s)\ . \qquad \text{(B-8)}$$

In this form, the filtering effect of pitching of the trucks and car body is readily identified. Regarding the transfer function magnitude, the car body bounce transfer function exhibits "dropouts" at the spatial frequencies

$$f = \frac{nV}{2L_T}\ ,\quad n = 1, 3, 5, \ldots$$

and

$$f = \frac{nV}{2L_c}\ ,\quad n = 1, 3, 5, \ldots\ . \qquad \text{(B-9)}$$

The car body pitch transfer function exhibits similar dropouts at

$$f = \frac{nV}{2L_T}\ ,\quad n = 1, 3, 5, \ldots$$

and

$$f = \frac{nV}{2L_c}\ ,\quad n = 0, 2, 4, \ldots\ . \qquad \text{(B-10)}$$

Note also that the transfer function phase abruptly shifts 180° at each dropout frequency.